

# Emerging Research in Conductive Materials for Fused Filament Fabrication: A Critical Review

Dejana Pejak Simunec\* and Antonella Sola

The progress of Industry 4.0 and the advancement of robotic design are revealing a significant gap in the capabilities of current manufacturing techniques and the selection of materials that are available in electronics. Present-day electrical systems largely rely on metals, but there is a driving need to develop new electrically conductive objects with a wide range of material properties, including expanded flexibility and softness, and with increasingly complex geometries. Electrically conductive composites can replace traditional metal-based systems. In particular, thermoplastic composites become electrically conductive with the incorporation of conductive fillers or polymers while retaining to a large extent the processability of the thermoplastic matrix. This is where fused filament fabrication (FFF), an additive manufacturing (AM) technique capable of processing a variety of thermoplastic-matrix feedstock materials, can be leveraged to create electrically conductive objects with new functionalities. While there is an increasing number of publications describing the FFF of electrical objects such as sensors and circuits, there is no comprehensive review outlining the functioning mechanisms, drawbacks, and advantages of FFF as applied to conductive materials. The present review fills this lacuna by offering a critical analysis of the specific challenges and solutions to promote FFF of electrically conductive polymers and composites.

the straightforward production of complicated geometries, bespoke parts, and lightweight structures.<sup>[2–4]</sup> This form of manufacturing can be easily integrated into smart factories as production of additively manufactured parts is a digital transfer of a computer-aided design (CAD) file into the printer. The wide range of materials available for AM has also led to the development of many different technologies that, according to ISO/ASTM 52 900, 2015,<sup>[5]</sup> can be grouped into seven main families including vat photopolymerization (photocurable resins), powder bed fusion (metal powders), and material extrusion (thermoplastic materials).

Meanwhile, the Industry 4.0-driven technological progress has led to higher requirements for connectivity and electronics, which calls for the development of new materials with improved functionality, such as flexibility, softness, and resistance to corrosion. Traditionally, electrical components would have been made with metals or metal-based materials. However, the poor flexibility of these materials limits


## 1. Introduction

In recent decades, additive manufacturing (AM) has developed from a rapid prototyping tool to a mature method of manufacturing. This is partially driven by the growth of smart factories working in an integrated system, also known as the 4th industrial revolution or “Industry 4.0.”<sup>[1]</sup> AM is a method of producing parts without specialized tooling requirements resulting in a significant decrease in waste materials and products. This approach creates 3D objects by selective deposition of material, most of the time by adding material layer upon layer, which paves the way for

pathways into areas such as cybernetics, artificial intelligence, and biomedicine, where stretchable and flexible devices are required.<sup>[6,7]</sup> In addition, there is significant room for improvement in the current methods of manufacturing conventional metal-based printed circuit boards. According to figures recently cited by Baker et al.,<sup>[8]</sup> the production of printed circuit boards according to conventional technologies is a time-consuming multistep process that generates substantial amounts of waste, with the etching step alone deemed responsible for  $1 \times 10^{12}$  L of chemical waste per year worldwide. Also, fabrication of structural and embedded electronic systems is often cumbersome with conventional processing methods posing substantial restrictions in terms of design geometry.<sup>[8]</sup> An additional drawback of conventional metal-based circuitry is that metals do offer very high electrical conductivity, but they are also likely to corrode or oxidize, unless very expensive noble metals are used like silver. The altered chemical state of reacted metals impairs the flow of electrons and, on the long term, undermines the electrical conduction in electronic devices.<sup>[8]</sup>

This is where AM can assist with enabling unprecedented design freedom, reducing cost and waste, and expanding material availability to this industry. The form of AM commonly used to produce integrated electronics is direct ink writing (DIW), which can easily produce custom integrated circuits

D. Pejak Simunec, A. Sola  
Manufacturing  
Research Way  
Clayton, Melbourne 3168, Australia  
E-mail: dejana.pejak@csiro.au

 The ORCID identification number(s) for the author(s) of this article can be found under <https://doi.org/10.1002/adem.202101476>.

© 2022 The Authors. Advanced Engineering Materials published by Wiley-VCH GmbH. This is an open access article under the terms of the Creative Commons Attribution License, which permits use, distribution and reproduction in any medium, provided the original work is properly cited.

DOI: 10.1002/adem.202101476

using UV-curable conductive ink (e.g., silver ink).<sup>[9]</sup> The issue with DIW is that it is limited to UV-curable materials that have a short shelf life and may be toxic to humans and the environment. A more environmentally friendly AM option with a larger range of materials available that are also shelf stable is fused filament fabrication (FFF—aka fused deposition modeling, FDM). This form of AM prints thermoplastics and thermoplastic composites to produce 3D parts, including novel electronics for many applications such as antistatic agents, chemical sensors, energy harvesting systems, batteries, and flexible strain sensors.<sup>[10]</sup> An advantage of FFF is that, in principle, creating a conductive feedstock material with a selection of desired properties is relatively straightforward. Conductive feedstock materials can be formulated by leveraging the intrinsic properties of conductive polymers or utilizing a conductive filler and blending these conductive elements into a thermoplastic matrix. However, the issue is that conductive thermoplastic composites for FFF have yet to “catch up” to the advancement seen in conventional conductive materials over the last 20 years. In fact, the core of the research in conductive feedstock materials for FFF began just 10 years ago, after the original patent (filed by the AM company Stratasys) on the FFF process expired in 2009. So far, key discoveries including the Nobel Prize-winning discovery of conductive polymers back in 2000<sup>[11]</sup> have not been fully applied into conductive feedstock materials for FFF. Translating conductive thermoplastics and composites from traditional manufacturing to FFF poses substantial technological challenges, especially balancing printability and conductivity. These limitations are discussed in this review paper that also proposes potential solutions inspired by innovative trends in nanotechnology. The

identification of smart approaches to maximize the electrical conductivity while retaining the ease of printing is regarded as the turnkey to enabling the full utilization of conductive polymers and fillers in FFF.

## 2. FFF Process

According to ISO/ ASTM 52 900, 2015, terminology,<sup>[5]</sup> FFF belongs to the “material extrusion” family. In order to print an object, the thermoplastic-based feedstock is heated to above its melting point (or above its glass transition temperature, if the material is completely amorphous) in the liquefier and forced to flow through a nozzle onto a build platform (**Figure 1**). The printhead is computer-controlled to release material where it is needed to obtain the desired geometry. Once deposited, the material cools and welds onto the build platform or the previous layers. The process is repeated layer upon layer until the part is complete.

During printing, the FFF printer must be capable of controlling the flow of molten material out of the liquefier through the print nozzle, whose size is generally less than 1 mm. To this aim, the feedstock filament is pushed along by rollers that use torque to force the filament into the liquefier. The filament, in its turn, acts like a piston to push the molten material out of the print nozzle. The pressure pushing the material must remain constant as well as the speed at which the nozzle moves around the build platform, so that uniform rasters of material are consistently deposited. The success of the printing ultimately is decided by the material properties and the machine parameters. If these two factors are carefully considered, controlled, and matched, a high-quality part can be produced.

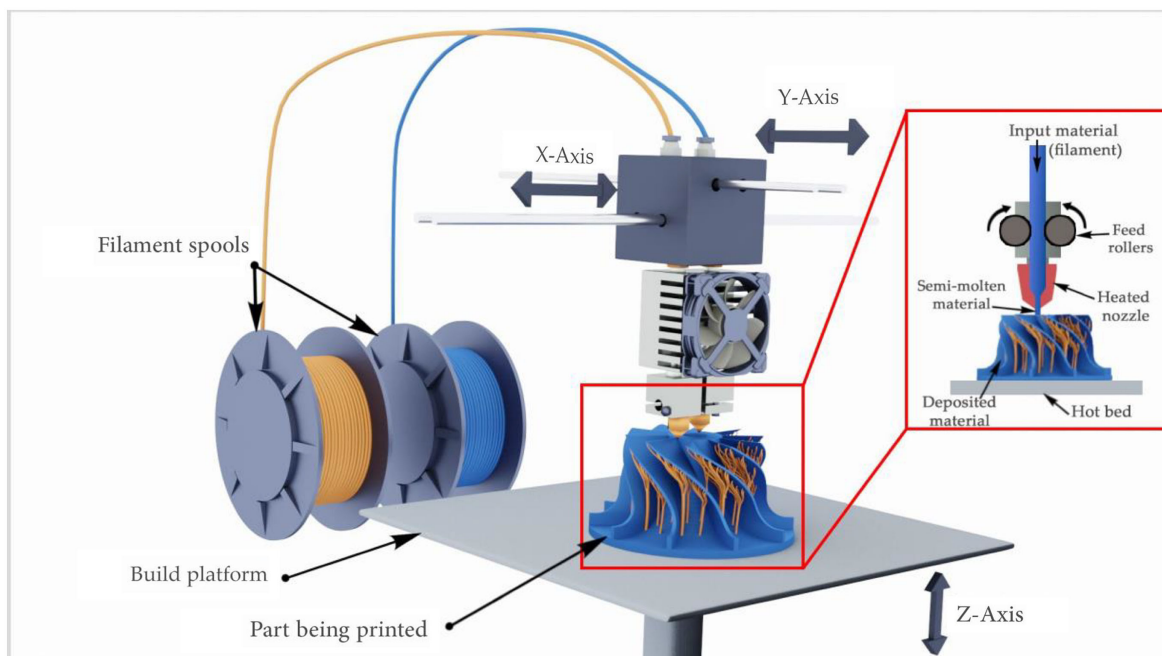


**Figure 1.** Schematic diagram of the FFF printing process on a cartesian plane (X–Y axis). Feedstock is supplied as filament, heated, and forced through a nozzle with the feed rollers onto a build platform. Once each layer is deposited, the build plate moves down along the z-axis. Reproduced with permission.<sup>[336]</sup> Copyright 2020, MDPI.

The cohesion between neighboring rasters and between subsequent layers has received different names in the literature, including “sintering,” “coalescence,” and “bonding”.<sup>[12]</sup> According to the definition introduced by Sun et al.,<sup>[13]</sup> the term healing refers to the molecular diffusion that occurs at the interface between rasters and creates a partially welded structure, while polymer sintering describes the neck growth phenomenon driven by surface tension. For polymeric materials, sintering is mainly due to viscous flow mechanisms that require a certain macromolecular chain mobility and, for this reason, sintering occurs at temperatures above the melting temperature for semicrystalline polymers, or above the glass transition temperature for amorphous ones.<sup>[12]</sup> This differs from sintering of inorganic material, which takes place below their melting temperature.<sup>[14]</sup>

An important characteristic of FFF is the anisotropy that occurs on any part that it prints. In terms of mechanical properties, once the part is printed, it does not exhibit the same level of strength or stiffness as the bulk primary material and the properties are direction dependent. This is because polymer chains align themselves in the direction of the printing, interlayer bonding between deposited layers is often poor, and voids may appear as a result of the toolpath followed by the printhead. As often observed in additively manufactured parts, the growth direction is particularly challenging.<sup>[15]</sup> Whereas minor differences are reported for parts printed parallel to the base platform, parts printed upright often feature the lowest tensile strength and improving the interfacial adhesion between layers is critical to increasing the strength in the growth direction.<sup>[16]</sup> Emerging research is demonstrating that postprocessing by thermal annealing or cold plasma treatment may be helpful to improve interlayer bonding.<sup>[17,18]</sup>

Likewise, anisotropic effects are expected to occur in electrical properties. Traditional thermoplastics used in FFF are not conductive, so conductive elements (such as fillers or conductive polymers) must be included in the thermoplastic matrix to allow the development of a percolation pathway and to change the behavior of the composite material from insulating to conductive. Shear forces acting in melt extrusion-based processes (including filament extrusion and FFF printing) are able (to an extent) to align polymer chains; similarly, they are able to preferentially orientate conductive fillers, which may cause anisotropy in electrical properties. Although this implies that the electrical conductivity of a printed object may be different along different directions, the preferential orientation of fillers is favorable for achieving conductive properties that rely on the development of a percolation pathway, as discussed in the following sections.

### 3. Percolation Theory

Percolation theory is the model that describes the network of objects within a structure and the macroscale properties that result as a response to the degree of connectivity in the system.<sup>[19]</sup> For electrically conductive composites, the percolation theory describes how electrical conduction occurs through conductive fillers.

Electrical conduction has been demonstrated to develop in two ways in conductive composites<sup>[20]</sup> 1) electron tunneling: electrons “jump” from one filler to the next one across distances through

the polymer matrix and/or; 2) direct contact of conductive fillers: electrons transfer via conductive filler pathway.

There is a minimum amount of conductive filler required for the composite to transition from insulation to conductive properties which is known as the percolation threshold. This threshold can depend on many factors, including the chemical structure of the matrix and the shape, size, distribution, and conductive properties of the conductive filler.

In particular, the volume fraction of the conductive filler plays a significant role in the percolation model, which can be described according to a power law equation (Equation (1))<sup>[21]</sup>

$$\sigma_c \approx \sigma_f (\varphi - \varphi_c)^t, \text{ where } \varphi > \varphi_c \quad (1)$$

where  $\sigma_c$  is the composite conductivity ( $\text{S cm}^{-1}$ ),  $\sigma_f$  is the filler conductivity ( $\text{S cm}^{-1}$ ),  $\varphi_c$  is the percolation threshold,  $\varphi$  is the filler volume fraction, and  $t$  is the critical exponent, which is representative of the shape (or aspect ratio) of the filler.

Experimental verifications of this equation have often resulted in deviations, particularly in the critical exponent. In fact, the critical exponent is related to the connectivity of the system,<sup>[22]</sup> but theoretical values have some discrepancy with experimentally determined values. Bauhofer and Kovacs<sup>[23]</sup> published a review article highlighting that, just in studies relating to carbon nanotube (CNT) nanocomposites, the critical exponent in the percolation theory can actually vary widely between 0.9 and 7.6 whereas theoretical values were between 1.33 and 3. It was suggested that the reason for the discrepancy is because theoretical calculations assume that the fillers are uniform and homogeneously distributed, whereas CNTs actually come in various lengths, sizes, distributions, and can easily agglomerate.

Notwithstanding the fact that Equation (1) should be applied with caution owing to these deviations observed in the critical exponent value, it is clear that one way to encourage percolation and improve electrical properties is to increase the volume fraction ( $\varphi$ ) of conductive elements. However, in terms of FFF, increasing the filler loading may result in processing difficulties, as fillers can potentially modify the viscosity of thermoplastics and may limit their printability. For example, adding a filler is expected to change the rheology and hence the flowability of the molten polymer matrix, sometimes with contradictory trends. Quite often, the addition of increasing amounts of filler results in higher viscosity,<sup>[24]</sup> but occasionally the opposite trend has been reported. In some FFF studies, the viscosity became lower as demonstrated by Gao et al.,<sup>[25]</sup> who blended polylactic acid (PLA)/carbon fibers for FFF printing and found that the repulsive interaction between carbon fibers and PLA and the alignment of carbon fibers sensibly lowered the molten viscosity in a shear flow, thus resulting in interlayer voids and poor mechanical strength in the FFF printed parts. In another study, the apparent reduction in viscosity of the low-density polyethylene (LDPE)/glass composite feedstock for FFF was simply attributed to the effect of the increased density of the composite material over the neat LDPE matrix during the melt flow index (MFI) test, which effectively “pulled down” the material faster due to gravity.<sup>[26]</sup> Despite these viscosity changes, there are several ways to balance conductivity and printability, and to reduce the dependency of conductivity on the volume fraction of the conductive elements. In fact, electrical properties are governed by

the interplay of several important factors, including 1) printing parameters and quality (Section 4); 2) electrical properties of the polymer matrix (Section 5); 3) conductive filler shape and size (Section 6); 4) distribution of conductive elements (Section 7); and 5) intrinsic conductive properties of conductive fillers and polymers (Section 8, 9, and 10).

In the following sections, these factors are explored in the context of FFF printing and the current state of the art for FFF printed composites.

## 4. Effect of Printing

### 4.1. Anisotropy

Numerous studies have already been conducted to investigate the effect of printing on the anisotropy of the mechanical properties of FFF parts,<sup>[27–29]</sup> but research into the effect of printing on conductive properties is still very limited. Another hurdle to consider is that the measurement of conductivity within FFF parts is not yet standardized and may introduce significant experimental variation between publications. At present, what emerges from the literature is that the electrical conductivity in FFF parts can be dependent on the printing direction, as the effect of printing itself will generate shear forces that are assumed to orientate conductive fillers, similar to polymeric chains. However, it is not

conclusively proven that conductive fillers (particularly with high aspect ratios) will actually orientate this way. Ecco et al.<sup>[30]</sup> found that graphene nanoplatelets (GnPs) were able to orientate in an extruded acrylonitrile butadiene styrene (ABS)-matrix FFF filament, but CNTs were not aligned (**Figure 2**), which may suggest that the size and shape of the conductive filler may influence its ability to orientate while the polymer remains in a molten state. Despite their disorientation, according to the results presented by Ecco et al.,<sup>[30]</sup> CNTs had better conductive properties than GnPs due to their improved ability to develop a percolation network through a more homogenous and randomly orientated distribution (Figure 2). Dorigato et al.<sup>[31]</sup> found that ABS/CNT nanocomposites have different conductivity values due to different printing orientations. As pointed out by Prashantha and Roger<sup>[32]</sup> for PLA/graphene FFF nanocomposites, the conductivity (measured through volume resistivity) is strongly anisotropic because different values are obtained if the measurement is taken parallel or perpendicular to the layers. Leigh et al.<sup>[33]</sup> found that a printed cube measured with probes placed perpendicular to the rasters had a higher resistance than the same cube measured parallel to the rasters, with the difference being approximately 25%. This was attributed to the defects at the raster–raster interfaces acting as discontinuities in the percolation network, whereas a complete pathway was formed parallel to the rasters. Similar results were found by Gnanasekaran

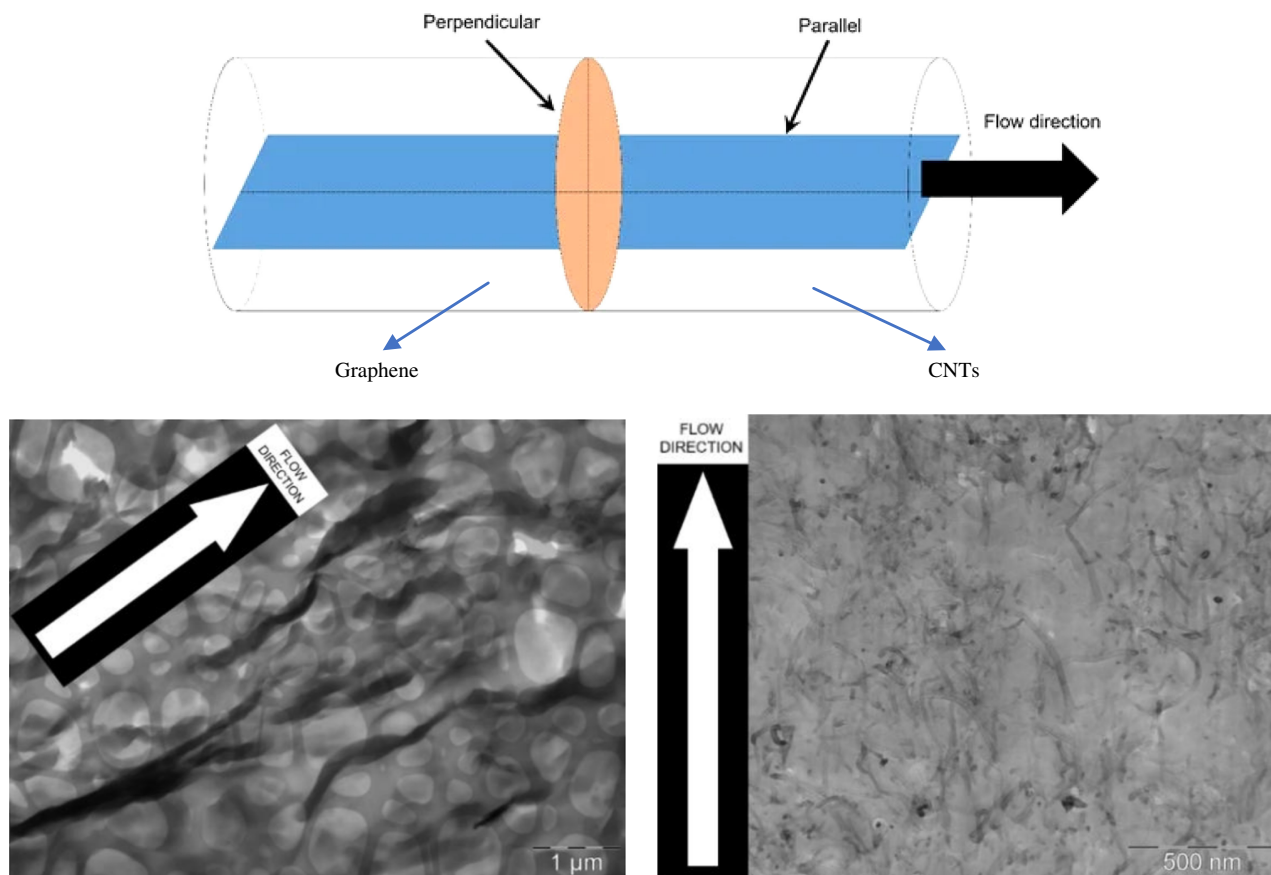


**Figure 2.** Figure shows SEM images comparing graphene and CNT filler. Reproduced (Adapted) with permission.<sup>[30]</sup> Copyright 2018, MDPI.

et al.<sup>[34]</sup> who also observed lower conductivity when measurements across many interlayer regions (such as at 45° printed raster angle) and described the interlayer region as behaving as series resistors.

Regardless of which conductive filler is chosen, there is always some degree of anisotropy imbued on a printed part and is strongly related to the thermoelectrical properties of the constituent phases.<sup>[35]</sup> Dijkshoorn et al.<sup>[36]</sup> formulated an analytical model to provide an understanding of the resistance changes and directionality due to the infill and bonding conditions in FFF parts. The electrical properties were simulated as an electrical network, which included bulk material properties (to describe the behavior of the rasters) and contact properties (to account for the interaction between neighboring rasters). In order to quantify the directionality of electrical properties in FFF parts, Dijkshoorn et al.<sup>[36]</sup> introduced a dimensionless number called “anisotropy ratio,” which was the ratio of impedivity (complex resistivity) in the horizontal and vertical directions. This definition of the anisotropy factor was consistent with the formula previously introduced by Zhang et al.,<sup>[37]</sup> who analyzed the electrical behavior of ABS–carbon black (CB) composite parts printed with a 0°/90° stacking sequence and calculated the ratio of the resistivity in the vertical direction to that in the horizontal direction. Interestingly, Zhang et al.<sup>[37]</sup> proved that the resistivity anisotropy of the printed parts could be tuned from 1.01 to 3.59 by adjusting the resistivities in different directions. Similarly, Gnanasekaran et al.<sup>[34]</sup> defined the anisotropy factor of FFF monolayers as the ratio between the conductivity in the longitudinal direction (parallel to the rasters) and the conductivity in the transverse direction (normal to the rasters) and found a value close to 7 for polybutylene terephthalate (PBT)/CNT composites at the percolation threshold. However, this anisotropy factor decreased to around 1.3 well above the percolation threshold, due to the establishment of a wider conductive network.

To prevent interlayer resistance from occurring, it is best to minimize the distance between the rasters (also known as air gap) to achieve the best possible bond between the interlayer regions as demonstrated in the piezoresistive PLA/CNT sensor developed by Mousavi et al.<sup>[38]</sup>

## 4.2. Printing Parameters

As demonstrated by the role of air gap in the research by Mousavi et al.,<sup>[38]</sup> print settings can influence conductivity in FFF composites. For example, in thermoplastic polyurethane (TPU)/CNT nanocomposites, the bed temperature of the FFF printer had little effect, but the correct setting of the print temperature was important to avoid poor extrusion of the polymer and hence encourage consistent electrical conductivity.<sup>[39]</sup> In the same nanocomposites, the layer height did not significantly affect conductivity,<sup>[40]</sup> but when CNTs were combined with a different thermoplastic (e.g., ABS/CNT), increasing the layer height resulted in a reduced conductivity.<sup>[41]</sup> So, it seems that the relevance of the layer height depends on the specific polymer matrix in use, likely as a result of the different polymer sintering and healing phenomena occurring at the interface between subsequent layers. In addition, it has been proven that

a lower infill density and a smaller layer height also influence the solvent sensing capacity of PLA/CB FFF composites, which make use of variations in resistance values to detect solvents.<sup>[42]</sup> A low infill density and a small layer height are favorable for this solvent sensing application due to better penetration of the solvent when infill is less than 100% and when numerous interlayer surfaces are present, but may not be suitable for other applications such as load-bearing and structural functions. Also, Dijkshoorn et al.<sup>[43]</sup> demonstrated how the electrical resistance of the printed part reduces by printing additional layers.

The correlation existing between printing parameters and presence of pores is another important variable. Voids are naturally introduced as a side effect of incomplete bonding of the interlayer region in FFF printed parts, but voids can also exist from print defects such as inconsistent material flow from the nozzle or incompatible printer settings. The effect of printing on the mechanical behavior of FFF printed parts is seen more clearly when void analysis is completed. For example, Ravoori et al.<sup>[44]</sup> found that the tensile strength increased rather significantly when voids were reduced from 10.8% to 1% in a FFF printed part. However, in terms of conductivity, the connection between voids and electrical properties is still unclear. Sezer et al.<sup>[45]</sup> found that the percolation threshold of printed parts can vary depending on the raster angle which, in its turn, can affect the porosity. However, in the contribution by Sezer et al.<sup>[45]</sup> voids were not analyzed and thus it is unclear if the change in the percolation threshold was due to print defects or to the raster settings themselves. In another study by Schmitz et al.<sup>[46]</sup> a loss in conductivity was generally observed after printing when compared with the compression molded samples of the same composite,<sup>[47]</sup> which was attributed to the appearance of defects and voids that prevented effective contact between deposited layers, but, again, a detailed void analysis was not completed. Advanced characterization techniques like microcomputed tomography (micro-CT) are now available to test the defect structure in printed parts.<sup>[48–50]</sup> A logical investigation of the porosity patterns that takes into account the amount, size, and placement of pores would be useful to unveil the macroscopic changes in electrical conductivity with porosity. While a systematic analysis of the correlation existing between porosity and electrical conductivity of FFF parts is still missing in the literature, it is reasonable to presume that inappropriate printing settings will negatively affect the electrical conductivity owing to the increased porosity and structural defectiveness that impair the flow of electrons.<sup>[36]</sup> Postprocessing, and especially annealing, can be a valuable tool for decreasing the porosity formed during the 3D printing process and changing the crystallinity. However, while the effect of postprocessing has been largely investigated in terms of mechanical strength and reliability,<sup>[51–53]</sup> very little is known so far in terms of electrical conductivity and additional research is certainly needed in the future. There is one preliminary investigation into the effect of annealing on FFF printed electrical properties, which had shown that resistance decreased with thermal annealing of PA6/GnPs at 80 °C. However, when these samples underwent annealing at 140 and 200 °C, electrical resistance increased<sup>[54]</sup> but it was not clear why this had occurred.

### 4.3. Printing Nozzle

Although often overlooked in the literature, the print nozzle is key to printing FFF parts with satisfactory electrical conductivity. The abrasive nature of conductive fillers like graphene or CNTs means that, over time, the print nozzle will wear out and will extrude poorly. This was verified by Gnanasekaran et al.,<sup>[34]</sup> who printed PBT nanocomposites blended with either graphene or CNTs. **Figure 3** demonstrates the significant wear suffered by the brass nozzle that is generally supplied with most commercially available FFF printers. There are several ways to mitigate this issue, especially using nozzles made of harder materials than brass, such as hardened steel or silicon carbide.

Another parameter to consider is the shape of the nozzle. Nixon and Bigio<sup>[55]</sup> found that, by using a converging die, carbon microfibers can be highly aligned within the polymer matrix, while a diverging nozzle can randomize their positions. The diverging nozzle resulted in the randomized fillers having more isotropic tensile properties due to fiber arrangement in nonaxial directions. While this is suitable to reduce anisotropy of tensile properties in FFF printed parts, it is unclear how this would impact the electrical properties.

Ultimately, also the size of the nozzle should be taken into consideration. Thaler et al.<sup>[56]</sup> found that printed ABS/CNT nanocomposites had improved conductivity when the nozzle size was increased. They rationalized that larger nozzle diameters could prevent the alignment of fillers like CNTs, which would improve the conductivity through the interlayer regions. However, Thaler et al.<sup>[56]</sup> did not verify this randomized orientation of the filler through direct observation.

## 5. Polymer Matrix

Polymers can be roughly divided into two categories: thermosets and thermoplastics. Thermoset polymers, once processed into a shape, cannot be reformed as the polymer chains have

cross-linked. In comparison, thermoplastic polymers can be formed repeatedly, but not indefinitely due to processing-induced polymeric chain degradation. The ability for thermoplastic polymers to be easily formed into shapes such as a filament and be melted again is crucial in FFF printing. This behavior is due to their molecular structure which is based on monomers covalently linked together to form polymeric chains. Upon heating, the increased mobility of the polymer chains makes it possible to form the material into the desired shape, which is then retained upon cooling. However, multiple reshaping is still possible as no crosslinking occurs between polymer chains upon heating. These macromolecule chains are one of the reasons for the aforementioned anisotropy observed in FFF printing because the extrusion and printing of the thermoplastic results in alignment of the polymer chains in a single direction.

### 5.1. Inherent Resistance of Polymer Matrix

Most thermoplastics have a very high electrical resistivity and hence they are commonly used in insulating applications such as cable and wire insulation.<sup>[57]</sup> Generally speaking, resistivity ( $\rho$ , measured in  $\Omega \cdot \text{m}$ ) is an intrinsic property of matter, as it measures the “resisting power” of a material to the flow of electricity. Electrical resistance ( $R$ , measured in  $\Omega$ ) is instead the property of a given object, as it also depends on the object's geometry through its cross-sectional area,  $A$ , and its length,  $l$ , according to Equation (2)

$$R = \rho \frac{l}{A} \quad (2)$$

Analogous considerations apply to conduction versus conductivity.

The high resistivity of thermoplastics (**Table 1**) will generally result in printed objects having high resistance. However, different polymers do have different resistivity and this is extremely

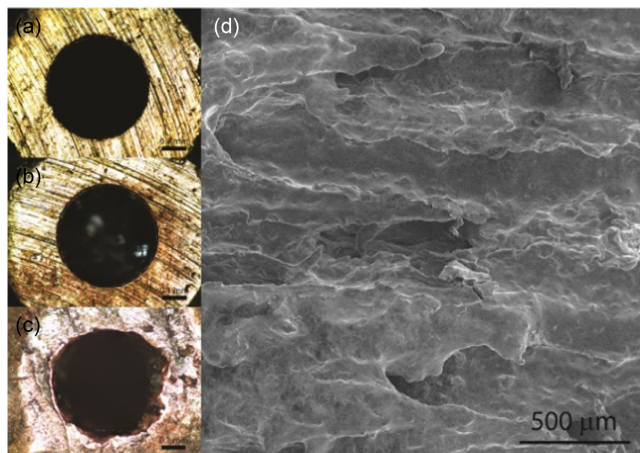


**Figure 3.** Image showing the effect of a PBT/graphene filament on an a) unused nozzle, b) nozzle after printing 10 cm PBT/graphene filament, c) nozzle after printing 1.5 m PBT/graphene filament, and d) SEM image of PBT/graphene filament after printing with abraded nozzle. Reproduced (Adapted) with permission.<sup>[34]</sup> Copyright 2017, Elsevier.

**Table 1.** List of FFF thermoplastics and their resistance values.

Thermoplastic matrix	Volumetric resistivity [ $\Omega \cdot \text{m}$ ]	Reference
Polylactic acid (PLA)	$10^{12}$	[340]
Thermoplastic polyurethane (TPU)	$10^{12} - 10^{14}$	[136]
Acrylonitrile butadiene styrene (ABS)	$10^{13}$	[341]
Polyvinyl chloride (PVC)	$10^{12}$	[342]
High impact polystyrene (HIPS)	$10^{14}$	[343]
High-density polyethylene (HDPE)	$10^{13} - 10^{16}$	[344]
Low-density polyethylene (LDPE)	$10^{13} - 10^{16}$	[344]
Polypropylene (PP)	$10^{15}$	[342]
Polyamide 6 (PA6)	$10^{10}$	[344]
Polyamide 12 (PA12)	$10^{10} - 10^{12}$	[344]
Polycarbonate (PC)	$10^{12} - 10^{14}$	[344]
Polyetherimide (PEI)	$10^{13}$	[344]
Polyether-ether-ketone (PEEK)	$10^{13} - 10^{14}$	[344]
Polyvinylidene fluoride (PVDF)	$10^{12}$	[345]

important for the obtainment of conductive composites. For example, a polymer such as polyamide 6 (PA6) having a relatively low resistivity of  $10^{10}$  ( $\Omega\cdot\text{m}$ ) will transition from insulator to conductor with a smaller number of conductive elements as compared to another thermoplastic such as polypropylene (PP) having a relatively high resistivity of  $10^{15}$  ( $\Omega\cdot\text{m}$ ) because its resistivity is inherently lower. In other words, if the same filler is used to provide conductivity, the percolation threshold will likely be lower for those polymers that have a lower inherent resistivity, such as PA6. Interestingly, there is not an obvious correlation between polarity and resistivity. PA6 is actually polar, as opposed to PP. However, other polar polymers like polyvinyl chloride (PVC) and polycarbonate (PC) have only a marginally lower resistivity than nonpolar polymers like PP or the PE variants (e.g., LDPE or high-density polyethylene [HDPE]). Although the inherent resistivity is a key factor, it is important to remark that the selection of the polymer matrix to produce FFF printable conductive composites must be balanced with other variables that significantly impact printability and conductivity, including whether the thermoplastic is semicrystalline or amorphous, its melt flow value or its mechanical properties.

## 5.2. Semicrystalline versus Amorphous

Thermoplastics, including FFF feedstock materials, come as semicrystalline or amorphous, which is dependent on their structure. In their molten form, all thermoplastics are in an amorphous state, but, upon cooling to their solid form, semicrystalline polymers will have chains fold in on themselves to form regular structures (crystalline structures) (Figure 4).<sup>[58]</sup> This does not occur for amorphous thermoplastics, whose polymer chains remain randomly arranged upon cooling. In terms of electrical conductivity, crystalline phases have sharp grain boundaries that tend to block the electrical signal, while amorphous regions typically have higher conductivity.<sup>[59]</sup> On the other hand, crystalline regions in a thermoplastic matrix can carry additional stress and increase thermal stability.<sup>[60]</sup>

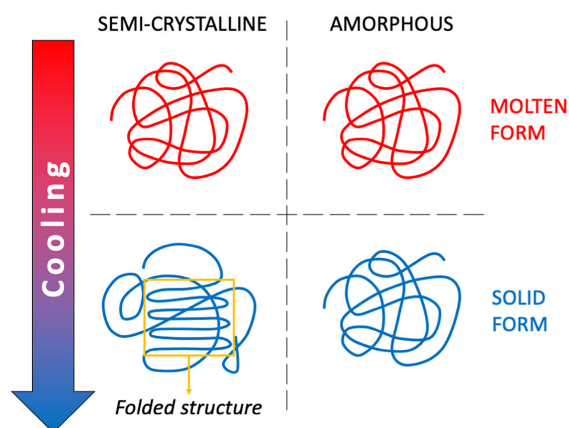


**Figure 4.** Difference between semicrystalline and amorphous thermoplastics.

The degree of crystallinity in semicrystalline polymers is largely influenced by the presence of nucleating agents and by the rate of cooling. Conductive fillers can often act as nucleating agents that encourage growth of crystals in semicrystalline thermoplastics. For example, in PP the addition of conductive fillers like graphene nanoplatelets causes nucleation and growth of crystal structures on the surface of the filler.<sup>[61]</sup> Silver nanoparticles can also promote crystallization in polyethylene terephthalate-co-polyethylene glycol (PET-PEG) thermoplastic elastomers.<sup>[62]</sup> Shmueli et al.<sup>[63]</sup> found that PP/graphene nanocomposites printed by FFF had significantly higher crystallinity (particularly at 10 wt% graphene) than unfilled PP. However, Shmueli et al.<sup>[48]</sup> did not quantify the effect of the increased crystallinity in terms of mechanical or electrical properties. The addition of CNTs to a PEEK matrix may have contradictory outcomes. Whereas uniformly distributed CNTs may serve as nucleating agents, the van der Waals force between the closely dispersed nanofillers can hinder the free movement of the polymer chains and prevent their organization in crystalline structures, thus leading to a decrease in crystallinity.<sup>[18,64–66]</sup> Additional studies would be useful to clarify the effect of crystallinity on the electrical conductivity of these promising materials.

The polymer crystallization onto the surface of conductive fillers can limit the conductivity as the lamellae create an insulating layer that prevents the flow of electrons. In order to limit the growth of insulating crystalline structures, crystallization kinetics in thermoplastics can be controlled through the rate of cooling because fast cooling limits crystal growth and because the polymer chains do not have enough time to fold into large lamellar structures. However, if properly controlled, crystallization phenomena in conductive thermoplastic composites can also become an advantage. If the rate of cooling can be reduced, Wang et al.<sup>[67]</sup> demonstrated that conductivity can be retained as larger crystals are formed in the matrix and conductive fillers like CNTs are forced back into the amorphous regions. Kalaitzidou et al.<sup>[61]</sup> compared the conductivity of compression molded PP/GnPs composites and observed that slow cooling at a rate of  $\approx 0.3$   $^{\circ}\text{C min}^{-1}$  results in a lower percolation threshold than fast cooling at a rate of  $\approx 20$   $^{\circ}\text{C min}^{-1}$ . According to Kalaitzidou et al.,<sup>[61]</sup> under slow cooling the crystallization of PP occurs at higher temperature, which promotes the growth of larger but fewer crystalline spherulites. With fewer spherulites being formed, fewer GnPs are entrapped and isolated within the center of the spherulites and hence more GnPs are still available to establish the conductive paths.

In terms of FFF, it is very difficult to control and slow down the cooling rate upon printing. Although some parameters can be manipulated to this aim, including fan settings, print temperature, and the programmed pathway of the nozzle, the rate of cooling is typically shown to be much faster than  $20$   $^{\circ}\text{C min}^{-1}$ .<sup>[64]</sup> Because the degree of crystallinity is mainly governed by the presence of nucleating agents and by the thermal history, and because the rate of cooling down cannot be significantly reduced in FFF printing, developers of FFF conductive composites should also consider other strategies to control the degree of crystallinity. For example, thermal aging is known to reduce the cold crystallization temperature of poly(L-lactide) (PLLA), which improves the ability for PLLA

to undergo nucleation.<sup>[68]</sup> An effective method to reduce crystallization is to prevent polymer chains from folding, for example, by adding a plasticizer. However, plasticizers can also influence the melt flow index, as explained in the following section.

### 5.3. Viscosity (Melt Flow)

The viscosity of a polymer is generally represented in industry as the melt flow index (MFI), which gives a measure of the propensity of the molten polymer to flow through an orifice. Viscosity plays a key role in determining the printability of a thermoplastic material and deeply influences the overall quality of the printed part<sup>[69,70]</sup> and, ultimately, the electrical conductivity. The addition of popular conductive fillers such as CNTs or graphene can rapidly increase the viscosity of the thermoplastic (also known as a rheological percolation threshold) and as a result can increase printing issues. For example, this rheological percolation threshold has been detected in the development of a PA6/graphene composite for FFF. The rapid increase in viscosity was directly attributed to dominant polymer chain entanglement, which was promoted by the increased filler loading of graphene.<sup>[71]</sup> Although high viscosity polymers and composites can be printed in FFF, they require high print temperatures and high torque motors to push the filament through the nozzle. Without optimized parameters, this can result in poor printing quality. This has been demonstrated in FFF printing of PEEK/CNT nanocomposites, which suffered from poor interlayer adhesion between deposited layers due to high viscosity and limited molecular chain mobility.<sup>[72]</sup> As previously mentioned, pores and voids are thought to impair the flow of electrons. As a consequence, although the experimental evidence in the literature is still limited, it is possible to hypothesize that print defects will impair the establishment of the percolation threshold and therefore improving the viscosity and generally improving the printability of the composite feedstock is expected to correlate to better conductivity of the FFF printed parts.

A way to decrease the viscosity to make the composite easier to print is to use plasticizers, which are typically short polymer chains that insert themselves between the macromolecular chains of the thermoplastic matrix and allow them to more easily slide past one another. This can improve the FFF processing and interlayer bonding.<sup>[73–75]</sup> Another way to potentially lower the viscosity is to decrease the amount of conductive filler. This is expected to reduce the conductivity of the filament, unless appropriate countermeasures are taken. For example, a workaround to mitigate conductivity loss is to simultaneously incorporate two conductive fillers having different particle sizes and create a multifiller composite (Section 8.4). However, if using a semicrystalline polymer, the selection of both fillers must consider the potential for nucleation (Section 5.2). This issue was discussed by Palacios et al.,<sup>[76]</sup> who blended graphene to reduce the viscosity of a polyamide 66 (PA66)/CNT nanocomposite and observed that the conductivity was significantly reduced due to extensive nucleation of the polymer matrix around the fillers, which led to the growth of an insulating crystalline layer over the fillers.

## 6. Conductive Fillers

If the polymer matrix is not intrinsically conductive (Section 10), a designer can choose to incorporate conductive fillers to induce conductivity. Conductive fillers come in a variety of sizes and shapes which can influence the percolation threshold in various ways. Also, the aggregation state plays a key role because this determines the availability of individual fillers to develop the conductive network.

### 6.1. Size

The size of the conductive filler can greatly affect the percolation threshold of thermoplastic-matrix composites. Deepa et al.<sup>[77]</sup> found that composites loaded with silver particles having a larger grain size (5  $\mu\text{m}$ ) needed a higher filler loading to become conductive (10 vol%) compared to composites with smaller particles (3.5  $\mu\text{m}$ ) that reached the percolation threshold at 7 vol%. This is because, with the same filler volume fraction, the filler size will determine the average interparticle distance, which, in turn, influences the electron transfer and, thus, the enabling of percolation. In addition, the filler size may be relevant in terms of printability. For FFF, the diameter of the nozzle imposes limitations to the size of the filler considering that the nozzle diameter on a commercially available FFF printer is generally no bigger than 1 mm. It is for these reasons that conductive fillers on a smaller scale, such as nanoscale or microscale fillers, are favorable when creating a conductive composite and their agglomeration should be carefully avoided.

### 6.2. Aspect Ratio

While working with nanoscale or microscale conductive fillers is favorable in inducing a conductive pathway, the aspect ratio of the fillers can also significantly determine the level of filler required for percolation. The aspect ratio is the measurement of the width of an object in relation to its height. In everyday life, for example, the aspect ratio is often used to describe computer monitors or televisions. The same principle can be applied to conductive fillers. For example, CNTs generally have a large aspect ratio<sup>[78]</sup> because they tend to resemble long tube shapes with a fixed diameter. Conversely, CB is nearly spherical, generally with an aspect ratio close to one (having equal height and width). If the conductive filler is changed from CNT to CB, the change in aspect ratio will affect the percolation threshold as the critical exponent in Equation (1) will change to reflect the new connectivity of the system. Besides the electrical conductivity, fillers with a high aspect ratio can also improve the tensile strength of FFF printed parts.<sup>[79]</sup>

As far as CNTs are concerned, the electrical conductivity of the composite can be significantly increased by introducing fillers with a high aspect ratio to the point that, generally, there is an inverse relationship between percolation threshold and aspect ratio.<sup>[80–82]</sup> For example, a study on TPU/CNT composites demonstrated that longer CNTs are more suitable for conductive and electromagnetic shielding applications.<sup>[83]</sup> However, Schilling et al.<sup>[84]</sup> caution that using this inverse percolation-to-aspect ratio relationship in modeling applications may be misleading, as

rod-like particles below 1000 aspect ratio do not strictly adhere to this rule. This is supported by Sethi et al.<sup>[85]</sup> who suggest that, as compared to the aspect ratio, length is a better unit of measurement to characterize CNTs, as it appears to strongly correlate to the percolation threshold, especially if the CNTs are in a “wavy” rather than straight form which will reduce their effective length.<sup>[86]</sup>

Different considerations may apply to other fillers with a different shape. In the case of fillers with a platelet shape, such as graphene,<sup>[78]</sup> this shape can be easily orientated during FFF printing<sup>[87]</sup> or during filament extrusion. For example, it was shown that graphene had better orientation than CNTs in an extruded ABS filament for FFF.<sup>[30]</sup> The effect of this strong orientation is to facilitate the development of the percolation threshold along the extrusion direction, which can be achieved at lower filler loadings when the graphene aspect ratio is increased.<sup>[78,88,89]</sup>

Generally speaking, the main reason for using fillers with a high aspect ratio (or filler length) is to minimize the average distance between the individual fillers to enable percolation either through direct contact of the fillers or through the electron tunneling phenomenon. This is illustrated in **Figure 5** and demonstrates that, with equal volume fraction and distribution, fillers with high aspect ratio have shorter interparticle distances, so electrons can tunnel or flow more easily between them (described visually as red arrows).<sup>[90]</sup>

When developing a new conductive material for FFF, the aim is often to balance conductivity and printability with standard equipment, so consideration of the size and shape of the conductive filler is important.

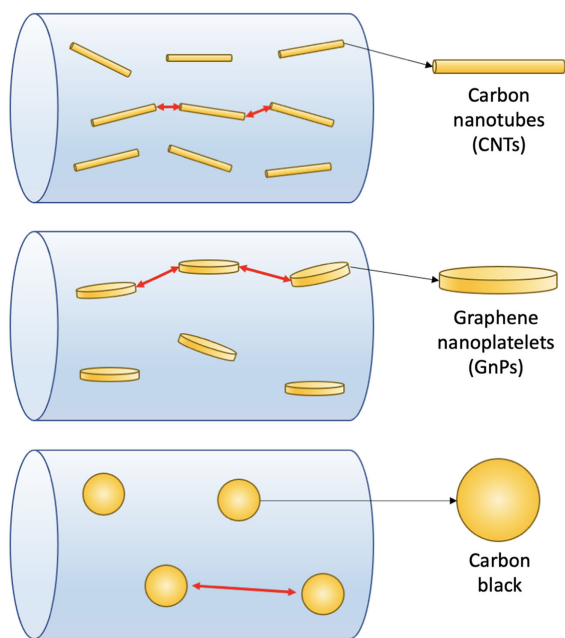


**Figure 5.** FFF filaments produced with fillers having different geometries, but with equal dispersion and volume fraction.

## 7. Conductive Element Distribution

In this section, the effect of the filler distribution on percolation in conductive composites and printed parts is discussed, as well as the main techniques that make it possible to control the filler distribution.

One of the most challenging issues when producing conductive composites is to prevent agglomeration of conductive fillers. When conductive fillers agglomerate, they effectively increase their size and/or reduce their aspect ratio, which will increase the percolation threshold and will require higher filler loadings to achieve conductivity. For FFF in particular, agglomeration is a problematic event not only because of the potential increase of the percolation threshold, but also because of the increased likelihood of clogging the print nozzle.<sup>[91]</sup> Clogging due to agglomeration of spherical fillers like CB has been modeled by Beran et al.,<sup>[92]</sup> who created a mathematical approximation of the printability of the thermoplastic composite based on factors such as viscosity, nozzle geometry, and filler type.

In terms of electrical conductivity, when agglomeration occurs as illustrated in **Figure 6**, it is obvious that the average distance between the conductive agglomerates is increased as compared to nonagglomerated systems (Figure 5). With this in mind, there are several ways to encourage the breakdown of agglomerates and improve the distribution of conductive elements in a thermoplastic matrix, which can be applied when manufacturing FFF feedstock in order to obtain conductive parts with the lowest filler loading possible.

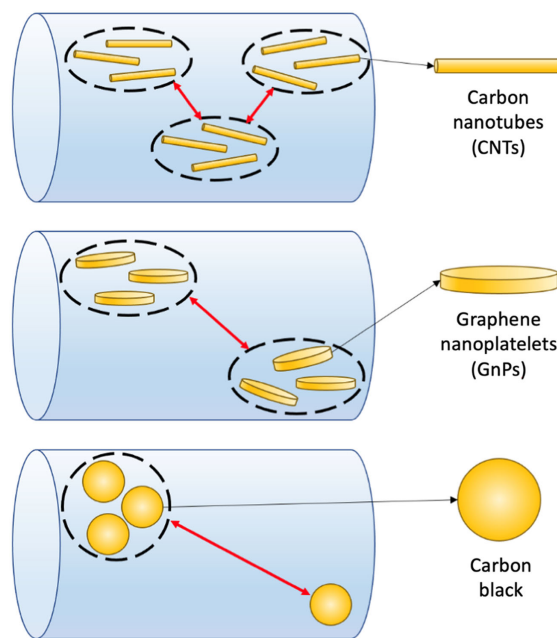


**Figure 6.** FFF filaments produced with CNTs, CB, and graphene with agglomeration and equal wt%.

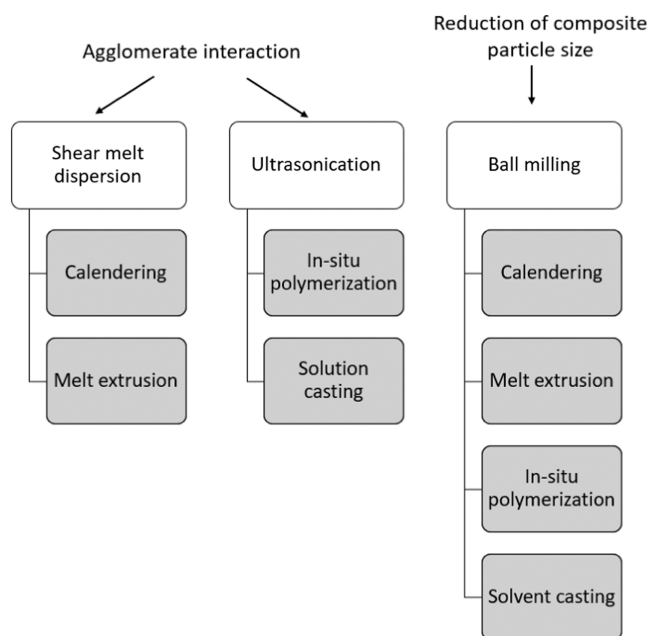


**Figure 7.** Relationship between the various approaches to assist in filler dispersion (either breakdown of agglomerate interactions or particle size reduction) and their relationship to various production methods for conductive thermoplastic composites (calendering, melt extrusion, in situ polymerization, and solvent casting).

## 7.1. Pathways to Production of Uniformly Distributed Conductive Nanocomposites

To produce conductive composites for FFF, one way is to enable the percolation threshold by ensuring the conductive fillers are uniformly distributed and are close enough to each other to induce one or both percolation mechanisms. Also, as previously mentioned, it is important to break down potential filler agglomerates. There are several popular methods to assist in dispersion of conductive fillers, including shear melt dispersion, ultrasonication, and ball milling (Figure 7). The first two methods specifically interact with the conductive filler agglomerates and provide energy in various forms to overcome the van de Waals forces which hold the agglomerates together. Ball milling is used instead to reduce the particle size of the polymer or filler, thus improving the homogenization of the system, and can be used in a variety of applications. These techniques have various levels of feasibility in FFF and may be useful to prepare the raw materials for the extrusion process because the composite must be developed as a filament to be printable by FFF. There are some material extrusion printers which can print pastes<sup>[93]</sup> or pellets (also known as fused granular fabrication or FGF),<sup>[94,95]</sup> but these technologies are limited and not as common as the filament standard for FFF printing.

Conductive thermoplastic composites can be fabricated in a variety of ways. Common methods to produce (conductive) composites with thermoplastic matrices include calendering, melt extrusion, in situ polymerization, and solution casting. These composites' manufacturing methods may utilize either shear

melt dispersion or ultrasonic dispersion as the main mechanism to induce a homogenous distribution within the thermoplastic matrix and can benefit from ball milling to adjust the size of the polymer and filler before mixing (Figure 7).

Considering that filaments are the main form of feedstock used in FFF, this requires the crucial step of producing the filament through an extruder. Also, very tight tolerances apply to the filament's cross section, which must be round with specific diameters ( $1.75$  or  $2.85 \text{ mm} \pm 0.1 \text{ mm}$ ). Filament extruders use melt-mixing to compound thermoplastic matrix and fillers; however, using techniques such as ball milling or ultrasonication can provide an initial preblend or precompounding step to imbue the filler into the thermoplastic matrix. This can be useful to improve the filler dispersion (unless selective distribution is sought after as discussed in Section 7.2) and plays a key role in enabling the conductive properties of the composite feedstock for FFF.

### 7.1.1. Shear Melt Dispersion

The basic mechanism of shear melt dispersion is to effectively disperse fillers through a thermoplastic matrix when the matrix is in a molten state and shear forces are applied to the composite. This dispersion method is popular in industry because of its low cost and simplicity<sup>[96]</sup> and can be done in an internal mixer or in an extruder.<sup>[97]</sup> Manufacture of composites via shear melt dispersion mechanisms can be achieved through the action of hot rollers (such as calendering) or through the rotation of a screw configuration (melt extrusion). In both cases, the final aim is to reduce the size of the agglomerates and disperse the filler into the thermoplastic melt to create a homogenous structure.

According to the modeling of multiwalled CNT agglomerates in high viscosity polymer melt, homogenous distribution could only be achieved using shear melt dispersion.<sup>[98]</sup> In one experimental study, agglomerates of CNTs in a PC matrix were reduced via rupture and/or erosion mechanisms. Interestingly, both mechanisms were active at low mixing speeds, while the rupture mechanism dominated at high mixing speeds.<sup>[99]</sup> Other studies observed rupture mechanisms when CB was dispersed into molten PE<sup>[100]</sup> and both rupture and/or erosion mechanisms for CB under shear flow in liquid media such as water.<sup>[101]</sup> The rupture mechanism describes a whole large agglomerate breaking off into smaller agglomerates, whereas erosion occurs when individual conductive fillers break off from an agglomerate.<sup>[102]</sup> Filler distribution by erosion is slow, but gentler on the filler. This results in less damage, which is very advantageous for conductive fillers with high aspect ratio, for example, CNTs. Conversely, filler distribution by rupture is fast, but may damage the fillers, so both mechanisms have their advantages and disadvantages.

A key criterion that governs the effectiveness of shear melt dispersion is to ensure the selected thermoplastic has a suitable viscosity to enable it to hold its shape while under molten conditions (represented as "melt strength"). It is known that increasing the shear forces will improve dispersion because agglomerates are reduced; however, this will also reduce the length of polymer chains. When this occurs, the molecular weight distribution drops (depending on the severity of the shear forces), and this will reduce the viscosity and the melt strength of

the polymer. This is also expected to negatively impact the final mechanical properties in FFF prints.<sup>[103]</sup>

The following sections discuss the two main methods for producing conductive composites which use the shear melt dispersion method, namely, calendaring and melt extrusion.

**Calendering:** The process of calendaring involves pushing a polymer or polymer-matrix composite through a number of heated rollers to obtain a film or sheet. Conductive composites can be produced via calendaring with thermoplastics<sup>[104]</sup> or with thermosets like epoxy.<sup>[105]</sup>

Similar to what happens in extrusion processes, calendaring is able to align conductive fillers such as CNTs<sup>[104]</sup> and graphene<sup>[106]</sup> through shear stresses. Li et al.<sup>[107]</sup> demonstrated the effectiveness of calendaring to align CNTs into a HDPE/polyoxyethylene (PEO) blend to produce anisotropic conductive composites. Tang et al.<sup>[108]</sup> used shear forces generated through calendaring to improve the dispersion of CB into high impact polystyrene (HIPS). Although this ability may be regarded as an advantage when producing conductive composites, there is still a limited number of publications on the use of calendaring to produce electrically conductive thermoplastic composites.

In terms of applicability to FFF, an additional step would be required because calendaring produces composites in a sheet or film form. This calendared feedstock would have to be pelletized or granulated and then melt extruded because FFF printers receive a filament as the standard feedstock configuration. In this regard, although calendaring can be an interesting option for pre-mixing in order to achieve an improved dispersion, it would be more time efficient to simply use extrusion because extrusion can melt-mix and create the filament in a single step.

**Melt Extrusion:** For the specific production of FFF feedstock, shear melt dispersion is preferentially done via melt extrusion through a single screw or twin-screw extruder. In both types of extruder, the feedstock (in pellet or powder form) is forced through a heated screw (or screws for twin-screw extruders) at a set speed and temperature.<sup>[109]</sup> The polymer (or composite) exits the extruder via a die with a specific diameter to match the filament requirements for FFF printers. For blending composites or multiple polymers together, a twin-screw extruder is recommended as it provides higher shear to allow for better dispersion, whereas a single screw extruder provides less shear and is not recommended for mixing (unless the screw has mixing sections).<sup>[110]</sup>

As discussed in Section 7.1.1, the shear melt dispersion method is an effective way of breaking up agglomerated fillers, but can potentially reduce the molecular weight of the polymer matrix. It is therefore not recommended to run multiple extrusion cycles of the same thermoplastic composite to improve dispersion or subject the composite to extremely high shear. A way around this issue is to produce a “masterbatch” composite with a high filler loading and then dilute this to the desired filler loading with additional pellets of the same thermoplastic matrix used to produce the initial masterbatch. This way, the damage to the molecular structure of the polymer matrix is mitigated because the dilution polymer has minimal interaction with the extruder and therefore the composite can achieve the desired filler loading, have good dispersion, and retain its mechanical properties. Masterbatch methods are also effective to create large volumes of composite material with a good filler distribution, which is

particularly important in FFF where commercially available filaments are sold in 300 g to 2 kg spools. To improve the dispersion of the masterbatch, it is a good practice to start with a low viscosity grade of the thermoplastic and dilute this with the same thermoplastic with a higher viscosity.<sup>[111–113]</sup>

In melt extrusion, mixing conditions can strongly affect the dispersion and the deagglomeration mechanisms, and thus the percolation threshold of conductive composites.<sup>[114]</sup> Studies have demonstrated the importance of the mixing speed and temperature to achieve a homogenous filler distribution and ultimately to maximize the electrical conductivity of the composite, with the best conductivity values being commonly associated to higher temperatures and higher mixing speeds.<sup>[115]</sup> For example, McClory et al.<sup>[116]</sup> found that increasing the screw speed in an extruder significantly improves dispersion of CNTs in HIPS.

In addition to mixing speed and temperature, the polymer viscosity (or melt flow) is the main factor which influences the dispersion of conductive elements and determines how well the shear forces can break agglomerates apart in the molten thermoplastic matrix. Polymers with high melt flow (or low viscosity) values are typically recommended in this regard.<sup>[117]</sup> On the other hand, polymers with low melt flow (or high viscosity) are able to be easily extruded into a filament of a specific diameter (within the tolerance of the FFF printer) and are likely to retain their shape after they exit the die. The identification of the right viscosity depends therefore on a trade-off between filler dispersion and extrudability/printability and will require some trial and error. A common practice in industry is to combine plasticizers or copolymers<sup>[118]</sup> to balance ease of extrusion (high viscosity) with shear-induced disaggregation of conductive elements (low viscosity).

### 7.1.2. Ultrasonication

Ultrasonication uses ultrasonic waves to overcome the van der Waals forces holding filler aggregates in a liquid medium (Figure 8). A key parameter in sonication is the energy that must be delivered into the solution to break the filler aggregates. In their review article concerning the dispersion of CNTs, Huang and Terentjev<sup>[98]</sup> pointed out that CNTs with various aspect ratios have different binding energies holding the aggregates together. The choice of the dispersion method must take into account the energy provided to the suspension, as the dispersion method

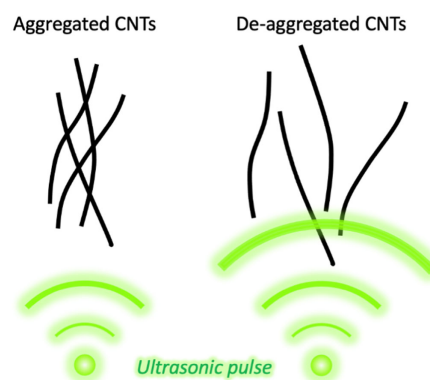


**Figure 8.** Ultrasonication of CNTs.

must overcome the energy that binds aggregates together (binding energy) and remain below the energy that would cause fracture of the CNTs (fracture resistance). Ultrasonication is well suited to provide enough energy to overcome the binding energy while remaining below the fracture resistance limit for single-walled CNTs with an aspect ratio around 10. This changes when the aspect ratio increases to above 1000, as ultrasonication is not able to match the binding energy anymore and shear mixing is recommended instead. Besides energy, time is another important variable because ultrasonication has also been shown to damage conductive fillers if the sonication time is too long.<sup>[119,120]</sup> Accordingly, processing parameters must be finely tuned to achieve an efficient deagglomeration without excessive damage.

Ultrasonication is recommended to assist in those applications that require the filler to be immersed in a liquid for subsequent processing, such as *in situ* polymerization or solution casting. Both these techniques rely in fact on liquid media to disperse the filler, which is ideal for ultrasonication.

***In Situ Polymerization:*** When applied to conductive materials, *in situ* polymerization creates conductive composites by directly polymerizing a polymer from its constituent monomers in the presence of a conductive filler (Section 10). As with solution casting, *in situ* polymerization composites are typically prepared in organic solvents, which makes it possible to ultrasonicate the system for enhanced dispersion. However, when the two methods are compared, conductive composites prepared with *in situ* polymerization often have higher conductivity than solution cast composites. This was demonstrated by Sohba et al.<sup>[121]</sup> who created a TPU/polyaniline (PANI)/CNT nanocomposite and found that, as a result of *in situ* polymerization of PANI, CNTs had reduced aggregation, better dispersion, and improved interaction with the TPU matrix. In particular, it was found that, if the polymerization of PANI was conducted in a TPU solution in the presence of CNTs, PANI was able to polymerize around and create a coating onto the CNT surface, which prevented agglomeration and improved dispersion. This ultimately led to a better conductivity than it was observed when CNTs were added at a later stage (*ex situ*), after polymerization had taken place.<sup>[122]</sup>

*In situ* polymerization is done by mixing the filler with a polymer precursor (prepolymers or monomers) and uses heat or radiation to begin the polymerization process.<sup>[123]</sup> However, *in situ* polymerization is a highly exothermic reaction that can be hardly controlled in large production levels because increased temperatures reduce the rate of polymerization.<sup>[124]</sup> In addition, the production rate is relatively low as compared to the requirements for the industrial scale-up of filament extrusion for FFF. Also, the obtained composites may need additional purification steps if they are to be used in melt processing such as extrusion, compression molding, or injection molding because, if any residual solvent is present, this would rapidly evaporate as a gas and produce bubbles in the thermoplastic. Oftentimes, *in situ* polymerization results in high viscosity polymers,<sup>[125]</sup> which makes printing more difficult. These drawbacks impart severe limitations to the uptake of this method in the production of FFF feedstock.

***Solution Casting:*** Solution casting is a method that produces thermoplastic composites by dissolving the thermoplastic matrix into an organic solvent and dispersing the filler into this polymer

solution. Once the filler becomes uniformly dispersed, the solvent is allowed to evaporate, leaving behind the thermoplastic-matrix composite. Organic solvents generally capable of dissolving polymers include dimethylformamide (DMF), tetrahydrofuran (THF), or chloroform. The filler can be dispersed either through mechanical mixing (stirring) or through ultrasonication. Controlling the rheology of the polymer/filler dispersion is important because the mixture becomes increasingly more viscous as solvent evaporates, which may change how well stirring or ultrasonication can disperse the filler. Therefore, solvent casting may require some trials to optimize the filler dispersion in the polymer solution and (similar to *in situ* polymerization) would also require an additional step to remove all traces of chemicals before producing an FFF filament through melt extrusion.

***Solution Mixing versus Melt Blending:*** For the obtainment of FFF conductive composites, in principle, solution casting may be used to enhance the conductivity of the final composite by acting as a preliminary mixing step to improve the filler dispersion. For example, Sandhu et al.<sup>[126]</sup> found that, if an ABS/graphene nanocomposite was initially solvent cast and then melt extruded, this method led to better dispersion than simply melt compounding upon extruding alone. However, the study did not provide details about the solution mixing and casting steps.

However, the results reported in the literature are ambiguous. For example, Talwar et al.<sup>[127]</sup> found that melt extrusion was a better method of dispersing CNTs within a PLA matrix than solution casting. On the other hand, Thaler et al.<sup>[56]</sup> discovered that, at low filler loadings, solution cast ABS/CNT composites had higher conductivity than melt compounded counterparts. Then, once the filler loading was increased, the conductivity of the melt compounded composite easily surpassed the solution cast one. Therefore, it appears that solution casting can achieve better distribution at lower filler loadings, but upon increasing the filler loading, melt extrusion may provide better dispersion. Similarly, Dal Lago et al.<sup>[128]</sup> found that PLA/graphene composites with a relatively low filler loading (0.5–1 wt%) had a lower percolation threshold if produced by solution casting because the same composites produced by melt compounding did not achieve a good dispersion. Analogous results were also reported in polyvinylidene fluoride (PVDF)/CNT composites,<sup>[129]</sup> with solvent mixing leading to improved distribution below 5 wt% of filler concentration as a consequence of melt compounding being unable to overcome the forces holding conductive agglomerates together. In the study by Spinelli et al.,<sup>[130]</sup> both methods resulted in comparable values of conductivity in PLA/graphene composites. According to the results presented by Spinelli et al.,<sup>[130]</sup> the aspect ratio of the graphene filler was more important than the mixing strategy. However, when graphene was replaced with CNTs in another study, the composites prepared by melt extrusion had better conductivity than the solution cast counterparts,<sup>[131]</sup> which suggests that the relative effectiveness of different compounding methods may be affected by the filler composition and aspect ratio.

Even if solution casting can be included as an initial blending step before melt extrusion, its suitability for large-scale production of FFF feedstock is limited as the process is generally done on a laboratory scale and most solvents used to dissolve thermoplastics are toxic. In addition, evaporation of the solvent would

require a safe transport of the released gases, which may be difficult or not convenient to do on an industrial scale. However, one way to mitigate these issues and effectively incorporate solution casting into the production of FFF composites is to use solution casting for the obtainment of a masterbatch for subsequent melt extrusion. A solvent cast masterbatch can help to obtain a homogeneously distributed FFF printable composite, as demonstrated in the production of ABS and 1.0 wt% graphene composites, which were successfully printed if using the solution cast masterbatch method, but could not be printed if using the melt extrusion masterbatch method.<sup>[132]</sup> However, an important consideration is that, depending on the final filler loading, even the production of a masterbatch may exceed the viability of solvent casting, although the production volume would be relatively low in view of the subsequent dilution of the masterbatch with neat polymer by melt compounding. In other words, solution cast masterbatches (which are typically done on a laboratory scale) may not meet the industrial requirements for larger volumes required to produce FFF filament.

### 7.1.3. Size Reduction of Thermoplastic Particles—Ball Milling

In principle, ball milling is a method of breaking up polymer particles with collisions from ball bearings inside a reactor that is constantly moving. The polymer particles inside are trapped between the colliding bearings and fractured. Eventually the polymer particles are broken down to a fine powder (as shown in **Figure 9**).<sup>[133]</sup> The effectiveness of ball milling is largely influenced by the mechanical properties of the polymer particles which can be highly ductile, brittle, or a combination of both properties depending on the environmental conditions. For thermoplastics in particular, the glass transition temperature is crucial because the polymer behaves as a glassy polymer and becomes relatively brittle at any point below this temperature,<sup>[134]</sup> whereas the behavior is substantially rubbery, and hence unsuitable for ball milling, above this temperature. This may represent a challenge in FFF, as several thermoplastics that are currently used as feedstock materials have a very low glass transition temperature which can be further reduced in the presence of moisture.<sup>[135]</sup> This is the case, for example, of TPU, whose glass transition temperature approximately ranges between  $-8$  and

$-48$  °C.<sup>[136]</sup> Keeping the milling chamber at this temperature often requires the usage of liquid nitrogen and is unavoidably energy consuming.

Although comminution is the most common application of ball milling, this technique can also be effective to obtain polymer blends with controlled morphology. For example, Pontes et al.<sup>[137]</sup> prepared PVDF/PANI powder blends by mixing the two constituents together in a ball miller and compared this method to the same blend produced via the *in situ* polymerization. They found that, once each blend was compression molded, when the level of PANI was above 43 wt% the PVDF/PANI samples prepared after ball milling had higher electrical conductivity than the counterparts prepared after *in situ* polymerization. This was attributed to the presence of PANI located preferentially between the PVDF particles at high PANI levels as a result of the ball milling-induced distribution of PANI powder around the PVDF particles.

Ball milling may be practical for reducing the particle size of polymer powders and for promoting mixing, and therefore can assist with all the production methods mentioned above, especially with melt compounding. Dweiri et al.<sup>[138]</sup> observed that PP-matrix composites produced by melt compounding with a combination of fillers including graphene, CB, and CNTs had improved conductivities if all the constituents were initially ball milled together. Similarly, a reduction in percolation threshold was observed in PEI/GnP composites with the additional step of ball milling followed by melt extrusion, compared to only melt extrusion.<sup>[139]</sup>

In regard to its applicability in calendering, based on the available literature, which is very rare, it is not possible to conclude with absolute certainty that ball milling will improve the composite production method. However, given the suitability in melt compounding methods, ball milling is likely to have analogous beneficial effects in calendering. In solution casting, ball milling may assist with dissolving the polymer into the solvent, as smaller polymer particles will need shorter time to completely dissolve.

As far as FFF printing is concerned, one study used ball milling<sup>[140]</sup> to prepare a FFF printable composite consisting of aluminum plastic packaging waste and graphite. Another FFF study using ball milling was in the creation of FFF printable linear low-density polyethylene (LLDPE)/GnP composites.<sup>[141]</sup> However, in both cases, the research goal was to investigate thermal conductivity and not electrical conductivity, so the relationship between ball milling and electrical properties of conductive composites is untested in FFF.

A potential drawback is that ball milling may damage brittle particles, including conductive fillers, with a high aspect ratio. For example, ball milling has been shown to shorten the length of CNTs with increasing milling time.<sup>[142]</sup> However, the potential damage caused by ball milling can be positively utilized to pre-treat CNTs and to introduce controlled defects on their surface before subsequent processing, such as coating them with silver.<sup>[143]</sup> This technique, although very promising to functionalize and improve the effect of CNTs, has not been demonstrated in any FFF conductive composite development and this deserves attention in future research.

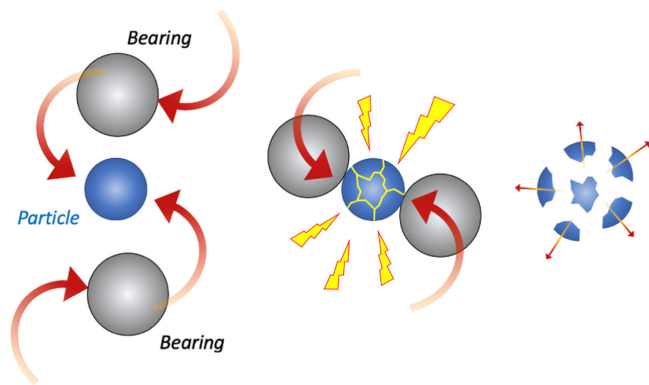


**Figure 9.** Schematic process of ball milling process on a polymer particle.

#### 7.1.4. Concluding Remarks

In terms of comparing the available techniques, which induce either aggregate breakdown or particle size reduction to distribute filler elements through the thermoplastic matrix, there is no clear answer as to which approach should be preferred. The choice largely depends on the specific materials in use and is also highly dependent on the resources (and limitations) of the composite developer in terms of potential for scale-up, time invested, and need of balancing conductivity and printability of the composite. However, it is important to note that, to produce feedstock for FFF printing, the material must be extruded into a filament through an extruder, whose functioning mechanisms rely on melt compounding. If the polymer is in a form that is compatible with a filament extruder (dry pellets or powder), quite often melt compounding in the extruder is the easiest way to mix matrix and filler and to produce the filament at the same time. Any other dispersion method can be used but may require additional steps such as purification or drying before extruding the filament. Also, the viability of the process for scaling up to large volume production must be carefully considered. These factors are summarized in Table 2.

The dispersion methods discussed in this section can also be combined as seen in Yan et al.,<sup>[144]</sup> who manufactured a cocontinuous structure by first using ultrasonication to coat CNTs onto PE particles followed by shear blending into a PC matrix. This caused the conductive filler to selectively migrate between the interfaces of the two polymer matrices as a form of selective localization. This can be targeted to reduce the percolation threshold and is seen in some nanocomposites that contain semicrystalline polymers (Section 5.2).

#### 7.2. Selective Localization—Nonuniform Dispersion

In the section above, various dispersion methods have been presented to uniformly distribute filler elements, including conductive ones, through a thermoplastic matrix. However, when conductive fillers come into play, in order to reduce the percolation threshold, it may be preferable to intentionally localize conductive elements in a certain region of the thermoplastic matrix

in order to induce the so-called “double percolation.”<sup>[145]</sup> When immiscible thermoplastic polymers are melt blended, they can form a cocontinuous structure or a “sea-island” structure of one phase surrounded by a sea of another phase (Figure 10). This is due to the arrangement of the phases resulting from unfavorable mixing entropies and is highly dependent on the phase composition of the blend. Upon being dispersed in an immiscible polymer blend, some conductive fillers selectively migrate into a polymeric phase (or to the polymer–polymer interface) due to the differences in interfacial tension.<sup>[146]</sup> This can be achieved through careful selection of polymer blends to ensure that the phase containing conductive filler is continuous and the percolation threshold is usually lower than in a single polymer matrix. This phenomenon is known as double percolation.

In the example by Zhou et al.,<sup>[147]</sup> this behavior was investigated with a blend of PS and PMMA melt blended together with CNTs. The localization of CNTs in either PS or PMMA was predicted with the wetting coefficient  $\omega$  (based on Young's equation) according to Equation (3)<sup>[148]</sup>

$$\omega = \frac{\gamma_{(\text{filler-polymer B})} - \gamma_{(\text{filler-polymer A})}}{\gamma_{(\text{polymer A-polymer B})}} \quad (3)$$

where  $\gamma_{(\text{polymer A-polymer B})}$ ,  $\gamma_{(\text{filler-polymer A})}$ , and  $\gamma_{(\text{filler-polymer B})}$  are the interfacial energies between the polymers A and B, between the filler and polymer A, and between the filler and polymer B, respectively. Depending on the value of  $\omega$ , a filler (such as CNTs) will be predicted to localize either (visualized in Figure 10): 1) within polymer A (if  $\omega > 1$ ); 2) within polymer B (if  $\omega < -1$ ); and 3) within the interface between polymer A and B ( $-1 < \omega < 1$ ).

Double percolation, where conductive fillers are exclusively located in one phase of a polymer blend (or at the interface between them), is thus an effective method to enable percolation threshold at relatively low filler loadings.<sup>[149–151]</sup> Figure 11 demonstrates how selective localization can assist in reducing the percolation threshold as the conductive fillers (shown here as elongated structures) preferentially migrate to one phase of the thermoplastic blend. Under selective localization, the distance between the fillers is reduced and percolation can occur

**Table 2.** Limitations of each dispersion method in FFF nanocomposite production.

Dispersion mechanism	Dispersion method	Composite production method	Limitations to FFF nanocomposites
Aggregate interaction	Shear melt dispersion	Calendaring	Output is generally a film or sheet, additional step required to transform into pellets for filament extrusion (not generally used for FFF feedstock production)
		Melt extrusion	Good dispersion requires high shear which can damage the thermoplastic molecular structure
	Ultrasonication	In situ polymerization	Method produces lab-scale amounts, requires significant scale-up, purification, and drying steps, is exothermic, and requires precise temperature control
		Solution casting	Requires removal of liquid medium or nonsolvent (purification and drying step), difficult to scale up, solvents are normally toxic
Particle size reduction		Ball milling	Can damage conductive fillers, <sup>[346]</sup> may require low-temperature control if polymer has low glass transition temperature

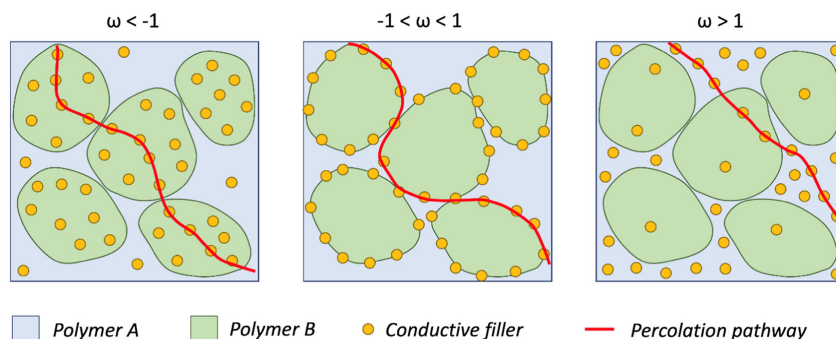


**Figure 10.** Diagram showing the effect of the wetting coefficient calculated in Equation (2) on the selective localization of a conductive filler and the resulting development of the percolation pathway. It is important to note that in a “sea island” structure such as the one depicted here, some filler must be present in both polymer phases to connect the fillers to create conductivity.

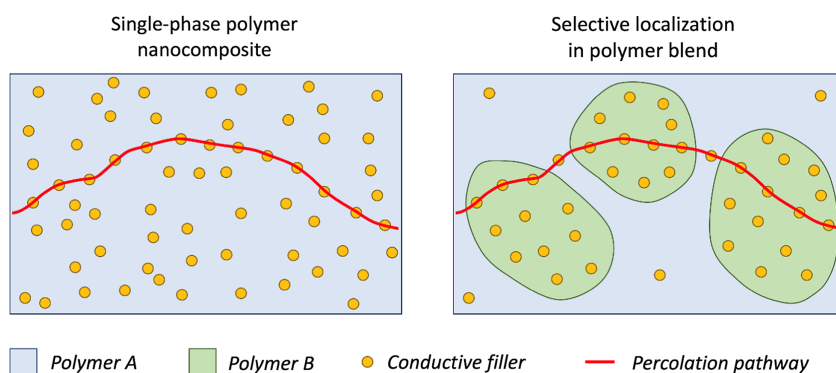


**Figure 11.** Selective localization in two separate thermoplastic blends with the percolation pathway shown in red. To enable percolation however, some of the fillers must exist in both phases (white and gray areas).

(shown as the red dotted line). As a result, lower percolation thresholds can be achieved than in single phase polymer nanocomposites.<sup>[152–154]</sup>

A comprehensive review article recently published by Pang et al.<sup>[155]</sup> offers a detailed scrutiny on the development of ultralow percolation thermoplastics with carbon-based fillers and highlights the wide range of production methods that can be applied to this aim. A simple way to induce double percolation via selective localization is to blend a high viscosity polymer A with an immiscible low viscosity polymer B. Viscosity is strongly related to interfacial energy, as interfacial energy is proportional to the viscosity of the polymer in a zero-shear state<sup>[156]</sup> (i.e., when no shear forces are applied onto the polymer melt). So, blending a high viscosity polymer A with an immiscible low viscosity polymer B will lead to an overall reduction of viscosity of the polymer blend and will also encourage selective localization due to the difference in interfacial energies.

Cayla et al.<sup>[157]</sup> demonstrated that interfacial tension differences between polymers can be exploited to guide CNT localization. When polycaprolactone (PCL) was blended with either polyamide 12 (PA12) or PP, CNTs were shown to preferentially migrate to PCL. A similar result was also seen with CNTs added into a PCL/PLA blend where the filler selectively localized within PCL.<sup>[158,159]</sup> Other examples of selective localization in immiscible polymers include HDPE/poly(methyl-methacrylate) (PMMA)

(with a CB filler) and PMMA/PP (CB filler),<sup>[159]</sup> PLLA/PCL (CNT filler),<sup>[160]</sup> and PC/PVDF (CNT filler).<sup>[161]</sup> Similarly, the selective migration of filler has led to reduced percolation thresholds in SEBS (styrene/ethylene-butylene/styrene)/PA6/CNT blends,<sup>[162]</sup> and in PA(6/12)/poly(ethylene-co-methyl acrylate (EMA)/CNT blends.<sup>[163]</sup>

Occasionally, selective localization can also be achieved with miscible polymers, provided that they have different viscosities. For example, one study used a mixture of low and high viscosity PLLA to produce a PLLA matrix with CNTs only located in the low viscosity PLLA region, which resulted in a very low percolation threshold of 0.019 vol%.<sup>[164]</sup>

Although the greatest part of the literature is focused on carbonaceous fillers, selective localization has also been induced using other (noncarbonaceous) fillers such as metal particles, like nickel,<sup>[165]</sup> and copper nanowires,<sup>[166]</sup> and extended to conductive polymers, like PANI.<sup>[167]</sup>

As previously mentioned, it is important to note that, for conductivity to occur, it is necessary that the fillers are connected, which means they must be located in a continuous phase or on a continuous polymer–polymer interface.<sup>[168]</sup> Intuitively, the relative proportions of each polymer in the blend can influence the final morphology. Liu et al.<sup>[169]</sup> discovered that increasing the amount of PA6 can significantly change the morphology of a PA6:ABS blend from cocontinuous (at 50:50 (PA6:ABS) wt%)

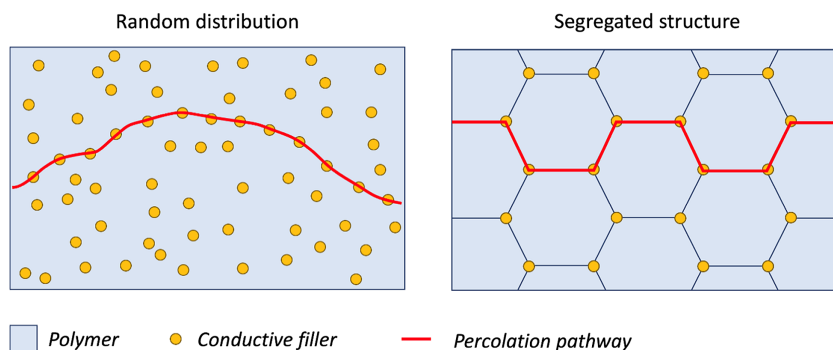


**Figure 12.** Illustration of the difference in distribution of conductive fillers (black) in a random (left) and segregated network (right).

to “sea-island” (at 70:30 (PA6:ABS) wt%). In both cases, CNTs will preferentially migrate to PA6.

Besides the polymer blend strategy, the percolation threshold can be governed through the intentional arrangement of conductive fillers to create segregated networks<sup>[155]</sup> as illustrated in **Figure 12**. Various techniques that use an initial premixing step to produce conductive composites with a segregated network have been recently developed. For instance, Pang et al.<sup>[155]</sup> obtained a segregated structure by simply coating CB over polymer pellets and then compression molding them to form hexagonal structures. Zhang et al.<sup>[170]</sup> formed ultralow percolation nanocomposites (with 0.08 wt% CNTs) by blending PE with CNTs and then coating this mixture onto PP pellets. In another example, isopropyl alcohol was used to disperse GnPs, which was followed by the addition of PP powder and ultrasonication for 1 h.<sup>[171]</sup> The organic solvent was allowed to evaporate and this resulted in complete coverage of PP particles with GnPs. These coated particles were then either compression or injection molded to produce conductive thermoplastic composites. Due to the segregated structure, the percolation threshold was significantly lower in these premixed samples (5 vol%) compared to samples simply melt blended in a compounder (7 vol%). Basically, the technique, developed by Drzal’s group,<sup>[172]</sup> uses ultrasonication as a dispersion method to produce a uniform filler’s coating on the polymer particles that ultimately produces the selective localization of the filler. This method is very effective, as the coating process takes only 1 h. Also, isopropyl alcohol is more environmentally friendly than the greatest part of organic solvents commonly used in situ polymerization or in solution casting. A similar example is the coating of CNTs and GnPs onto PLA which was used by Shi et al.<sup>[173]</sup> to produce FFF filaments. In this case, only deionized water was employed as a liquid medium and the dispersion was ultrasonicated for 3 h.<sup>[173]</sup> Based on these pilot investigations, it is likely that ultrasonication was essential to distribute the fillers. However, additional research would be useful to exactly define the role of ultrasonication in the coating process and to finely tune the ultrasonication parameters.

In terms of AM, one example of selective localization being specifically exploited in FFF is described in the study by Eutionnat-Diffo et al.<sup>[174]</sup> who combined LDPE- and PP-based elastomer (PBE) polymers with a mixture of Ketjenblack (a form of CB) and CNTs. CNTs were mainly located at the interface of the LDPE/PBE phases while Ketjenblack (KB) was located both in the LDPE phase and at the LDPE/PBE interfaces. The filaments

produced using the composite material had a maximum conductivity of  $\approx 1000 \text{ S cm}^{-1}$  using LDPE/PBE in an 80:20 ratio with 10 wt% KB and 2.5 wt% CNTs. However, it is important to note that this study used a FFF printer that processes pellets as feedstock rather than a filament (which is the standard in commodity FFF printers), so it is unclear whether this composite feedstock might be suitable for printing from a filament. A survey of the literature suggests that it is more common to observe selective localization in selective laser sintering (SLS) than in FFF because conductive fillers such as CNTs<sup>[175]</sup> or CB<sup>[176]</sup> can be easily coated onto the surface of the polymer powders used as feedstock in SLS. In this regard, it is important to remark that the literature clearly demonstrates that it is possible to melt blend composites having a double percolation structure; however, it is still unclear whether selective localization may be effectively combined with melt extrusion. In future research, it would be relevant to understand whether double percolation can be obtained and even controlled through melt extrusion, as this would open new possibilities to achieve ultralow percolation thresholds in FFF. A rare example in which selective localization was used to reduce filler dependency and percolation threshold in FFF was demonstrated by Shi et al.,<sup>[177]</sup> who solvent mixed PCL and CNTs in DMF and then dipped a PLA filament into this suspension to obtain a coating of PCL/CNTs. After printing, this filament resulted in the selective localization of CNTs within the interlayer regions of the printed parts, which substantially increased the conductivity from  $2.42 \times 10^{-9} \text{ S m}^{-1}$  for conventional PLA/CNT composite parts to  $3.28 \times 10^{-1} \text{ S m}^{-1}$ . Aside from this example, to the best of our knowledge, there are no other published studies which intentionally create this structure in FFF printed parts starting from the filament itself. Although it is possible to melt blend composites having a double percolation structure, it is unclear if melt extrusion has the same effect given the different processing methods. This might open new possibilities to achieve ultralow percolation thresholds in FFF which have not yet been properly explored.

## 8. Carbonaceous Fillers

Carbon-based fillers are a popular choice to imbue thermoplastics with conductive properties. They are stable at the processing temperatures typically required to extrude FFF filaments and are relatively affordable. However, carbonaceous fillers have a high

tendency to aggregate. A way to mitigate aggregation of carbon-based fillers is to lower the interparticle attractive forces by either covalent or noncovalent functionalization. This section presents the most popular carbonaceous fillers currently used in the literature to obtain FFF conductive filaments, with a focus on CNTs, graphene, and CB, and summarizes the corresponding strategies for mitigating their aggregation. Continuous carbon fibers in conductive applications for FFF printing are also discussed.

### 8.1. CNTs

CNTs are widespread to produce nanocomposite feedstocks for FFF due to their high aspect ratio and good conductive properties. At the end of September 2021, a Scopus search using fused deposition modeling/FDM or fused filament fabrication/FFF and carbon nanotubes as keywords returned over 140 articles, including several review articles summarizing work on CNT composites.<sup>[178,179]</sup> In the review articles written by Bauhofer and Kovacs,<sup>[23]</sup> the major issues encountered when printing CNT composites by FFF are discussed along with their potential solutions.

One of the main hurdles observed in the production of CNT composites in FFF is the strong tendency to agglomerate of CNTs, particularly at high filler loading. Fillers with high aspect ratios are prone to agglomerate due to the strong van de Waals forces acting between them. Mora et al.<sup>[180]</sup> created a predictive percolation model of CNTs in a thermoplastic matrix that takes into account both terms of agglomeration ( $\zeta$ ) and segregation ( $\chi$ )

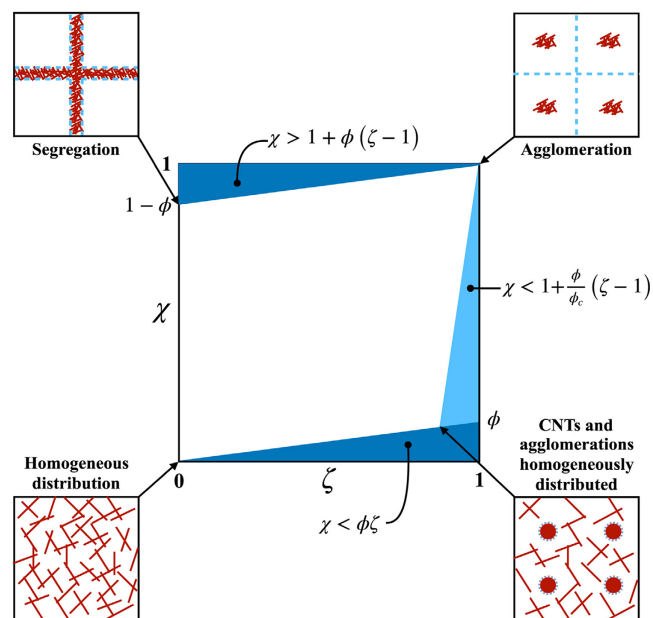


**Figure 13.** Model parameters representing CNT in various microstructures including: homogeneous distribution ( $\zeta = 0$ ,  $\chi = 0$ ), segregation ( $\zeta = 0$ ,  $\chi = 1 - \phi$ ), agglomeration ( $\zeta = 1$ ,  $\chi = 1$ ) of CNTs, and homogeneous distribution of agglomerates and CNTs. Light blue and dark blue areas correspond to parts of the domain that do not reach percolation or do not have practical applicability. Reproduced (Adapted) with permission.<sup>[180]</sup> Copyright 2020, Elsevier.

(**Figure 13**). This model was validated against PLA- and HDPE-matrix composites and supported the conclusion that the percolation threshold is different for different matrixes (PLA—0.23 vol%, HDPE—0.18 vol%). This model was successfully extended to other thermoplastic matrixes to determine the tendency for CNT agglomeration ( $\zeta$ ) and segregation ( $\chi$ ).

In addition, it is often reported that the melt viscosity of the composite increases at high filler loading. Thermoplastic-matrix composites with high viscosity are difficult to print due to the pressures generated in the print nozzle. In particular, when CNTs are used in FFF (such as in PVDF/CNT filaments), the composite can be difficult to extrude when the CNT content is above 10 wt% and can require modifications to the printer (e.g., higher torque to provide additional pressure and force the molten feedstock to flow through the print nozzle).<sup>[181]</sup> Analogously, technical issues have been reported with the extrusion of the filament because, above 15 wt% of CNTs, the composite may break during winding.<sup>[181]</sup>

Some researchers have mitigated this issue upon printing by increasing the nozzle size<sup>[182]</sup> or the print temperature,<sup>[183]</sup> but this limits the capability of FFF technology to print fine structures, may cause degradation of the thermoplastic polymer, and leads to poor-quality printed parts due to structural defects.<sup>[79]</sup> A way to reduce this “filler dependency” is to use CNTs with larger aspect ratios because this is known to lower the percolation threshold (Section 3), although this may also increase the tendency to agglomerate (Section 7).

In addition to choosing a suitable distribution method as already discussed in Section 7.1, it is possible to improve the dispersion by increasing the compatibility of CNTs with thermoplastic polymer matrixes either by adding chemical charges on the walls (covalent bonding) or by reducing the effect of the van de Waals forces acting between the CNTs (noncovalent bonding) as summarized by Feng et al.<sup>[184]</sup> The basic principles of the two functionalization approaches are discussed in the following sections.

#### 8.1.1. Covalent Functionalization

A very common type of covalent functionalization of CNTs is obtained when chemical side groups are permanently attached to the side walls by immersing CNTs into an acid. Although this type of treatment may cause permanent damage to CNTs, the appended side groups enable increased compatibility with thermoplastics.<sup>[185]</sup> For example, CNT dispersion in thermoplastics such as TPU<sup>[186]</sup> is improved due to the compatible hydrogen bonding that is induced through covalent functionalization. The same approach can also be extended to other thermoplastics

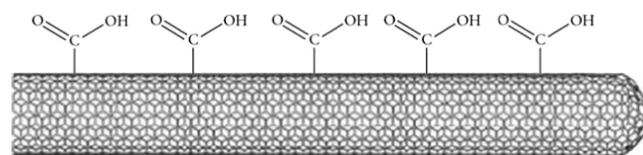


**Figure 14.** Figure depicts -COOH groups covalently attached to the side wall of a CNT. Reproduced (Adapted) with permission.<sup>[137]</sup> Copyright 2009, Hindawi.

**Table 3.** Covalent functionalization of CNTs.

Polymer matrix	Functionalization group	Composite production method	Refs.
TPU	Isocyanate	Melt mixing	[347]
TPU	Polycaprolactone diol (PCL), carboxyl (COOH)	Solution mixing	[348]
TPU	Carboxyl (COOH)	Solution casting	[349]
PC	Carboxyl (COOH), hydroxyl (–OH)	Melt compounding	[191]
TPU	Carboxyl (COOH)	Melt compounding	[350]
TPU	Polytetramethylene ether glycol grafted (PTMEG-g)	Melt compounding	[351]
PC/PLA	Carboxyl (COOH), hydroxyl (–OH), polycarbonate-grafted (PC-g)	Melt compounding	[352]
PC	Poly(methyl methacrylate) (PMMA)-grafted (PMMA-g)	Melt compounding	[353]
PLA	Hydroxyl (–OH)	Melt compounding	[130]
PLA	Hydroxyl (–OH)	Melt compounding	[190]
PLA	Carboxyl (COOH)	Melt blending	[354]
PLA	DO3-functionalized (disperse orange)	Solution mixing/Melt compounding	[355]
PC/PLA	Hydroxyl (–OH), Carboxyl (COOH), polycarbonate-grafted (PC-g)	Melt blending	[352]

like PP<sup>[187]</sup> and PA12.<sup>[188]</sup> The effect of functionalizing CNTs with acids is not removed when melt compounding and therefore this method is suitable for use in FFF filament production. Besides improving the affinity to thermoplastics, chemical side groups such as carboxyl groups (COOH) (shown in **Figure 14**) aid in dispersion in polar solvents.<sup>[189]</sup> This is useful in solvent casting and in situ polymerization techniques because, once ultrasonicated, the CNTs can remain suspended.

Aside from acid functionalization, another method for covalent functionalization is to graft polymers onto the CNTs via in situ polymerization which significantly increases compatibility with thermoplastics (refer to **Table 3**). Polymer-grafted CNTs can also be incorporated into a melt compounding process without compromising the effect of compatibilization.

Some of the various examples of covalent functionalization are summarized in Table 3.

As for the utility of covalent functionalization in FFF, Spinelli et al.<sup>[130]</sup> found that melt compounded masterbatches of PLA/OH-CNTs (CNTs functionalized with OH groups) had higher conductivity compared to unfunctionalized CNTs when mixed with PLA by solvent mixing. However, as the authors used different dispersion methods, it is difficult to separate the effect of dispersion method and surface functionalization. Other authors<sup>[190]</sup> described FFF printed parts made of PLA composites with OH-functionalized CNTs, but the study did not compare conductivity with unfunctionalized CNTs. So, it is still unclear how covalent functionalization directly affects FFF printing and the subsequent conductivity of printed parts. In this regard, it is important to note that, although very useful to ameliorate the dispersion of CNTs and, in case, to improve their interaction with thermoplastic matrices,<sup>[191]</sup> the effect of covalent functionalization does not increase the conductivity of the filler itself.

### 8.1.2. Noncovalent Functionalization

Noncovalent functionalization aims to reduce the strength of the van der Waals forces that act among CNTs. This is expected to prevent CNTs from aggregating without permanently affecting the side walls of the filler. As a matter of fact, although the name might be misleading, “noncovalent functionalization” consists in introducing appropriate additives in the polymer–CNT composite system, rather than in modifying the CNTs themselves. This type of functionalization can be achieved by initially blending the CNTs with a plasticizer that can improve their dispersion in the polymer matrix by attenuating the van der Waals forces. This was shown as an effective way of dispersing CNTs into PVDF with polyvinylpyrrolidone (PVP) being used as the plasticizer.<sup>[192]</sup> Kim et al.<sup>[193]</sup> discovered that, in PP/CNT composites produced by solvent casting, CNTs were positively charged in xylene but, when a polycarboxylate-type superplasticizer was added, the zeta potential became negative. This enabled the superplasticizer to wrap around the CNTs and induce repulsion between CNTs.

An example of noncovalent functionalization of CNTs specifically applied to FFF feedstock is demonstrated by Santillo et al.<sup>[194]</sup> In their study, ionic liquids (ILs) were used as a coupling and dispersing agent as a way to prevent aggregation of CNTs without damaging them. These chemicals are salts that exist in a liquid state with a melting point below 100 °C. An IL such as 1-benzyl-3-methylimidazolium chloride (BenzImCl) is defined as a low-melting point organic salt which has a pair of cationic and anionic chemical groups within its structure. The cation group is able to bond strongly with the CNTs, while the anion group acts as a repelling agent preventing CNT aggregation. Santillo et al.<sup>[194]</sup> produced an FFF composite by initially solvent casting a novel biodegradable polyvinyl alcohol (PVA) known as HAVOH (high amorphous polyvinyl alcohol) with CNTs and the

BenzImCl. This dispersion was then dried, ground, and extruded into a filament which was subsequently printed via FFF. The addition of BenzImCl significantly increased the conductivity of the composites due to the improved dispersion of the conductive filler. Similarly, a substantial improvement in conductivity using ILs for the noncovalent functionalization of CNTs has also been demonstrated in PS/CNT,<sup>[195]</sup> PVDF/CNT<sup>[196]</sup> and PP/CNT<sup>[197]</sup> composites, although these materials have not yet been utilized for FFF.

## 8.2. Graphene

Graphene in its various forms is currently less common in FFF than CNTs, even if graphene (depending on its form) can possess superior conductive properties (both thermal and electrical) and may actually be used as an alternative to CNTs. A commercially available PLA/graphene FFF filament called “BlackMagic3D” has been tested in the design of several objects including anodes of a battery,<sup>[198]</sup> electrodes for nitroaromatic explosives sensing,<sup>[199]</sup> and 3D printed antennas.<sup>[200]</sup> Bustillos et al.<sup>[201]</sup> found that, when printing with “BlackMagic3D,” the FFF printer had to be fit with a 0.6 mm nozzle to prevent clogging, which was attributed to the enhanced thermal conduction of graphene in the material. Bustillos et al.<sup>[201]</sup> also observed that, due to the different thermomechanical properties, there was a mismatch between graphene filler and PLA matrix that led to poor interlayer bonding and voids between the deposited layers. Opposite results have been reported by Sahar and Dadmun,<sup>[202]</sup> who discovered that low levels of graphene ( $\approx 0.5$  wt%) in a PLA filament will assist in the development of interlayer bonds after printing by FFF due to the improved heat transfer between neighboring rasters. As mentioned in Section 3, interlayer bonding in FFF is formed through a polymer sintering and healing. If heat is efficiently transferred from the freshly deposited material to the surrounding beads, which is likely to happen for low amounts of graphene, polymer chain mobility may be retained for a longer period of time and thus stronger interlayer bonds may be developed by effective interdiffusion of polymeric chains. Conversely, if the loading of graphene is relatively high, the filler obstructs the polymer chains from moving and will then impede interlayer bond development. This suggests that there must be a critical loading of graphene above which the hindering effect prevails over the improved interlayer bonding. Working with a graphene loading lower than this critical threshold will be useful in terms of improving interlayer bonding, which may translate to higher electrical conductivity. However, additional studies would be required to identify this critical loading.

Graphene can exist not only as single 2D plates, but also as graphene nanoplatelets (short stacks of ultrathin graphene, GnPs). Dul et al.<sup>[203]</sup> successfully used GnPs to produce ABS/GnP composites for FFF; however, printing was problematic due to the brittleness of the composite filament, which was mitigated by using a spool with a larger diameter than usual.<sup>[203]</sup> Jing et al.<sup>[141]</sup> improved the dispersion of GnPs in LLDPE to obtain FFF filaments by initially preblending the polymer and GnPs together using shear milling to obtain composite powders, which was followed by melt extrusion in a single screw extruder to fabricate the FFF filament. The preblending step was key to improving the dispersion of GnPs in the LLDPE matrix, which made the

filament much easier to print compared to the filament without preblending. On the opposite side of the spectrum, ultralarge-sized GnPs ( $\approx 150$   $\mu\text{m}$  in diameter) have been shown to increase the conductivity in PP composites produced by melt compounding<sup>[204]</sup> due to their increased aspect ratio. However, it is presently unclear if these large GnPs would be useful in FFF printing, as this specific usage has not been tested yet. Also, such a large diameter may cause clogging issues through the standard (400  $\mu\text{m}$ ) nozzle of FFF printers.

Another form of graphene is graphite which is a naturally occurring mineral. Singh et al.<sup>[205]</sup> demonstrated that, in principle, graphite can be compounded into an ABS filament suitable for FFF printing, but they did not actually print the filament, which impedes any comparison with the available literature of FFF parts functionalized with graphene.

As already seen for CNTs, graphene, when used as a filler in a thermoplastic matrix, encounters similar agglomeration issues, which may cause difficulty in printing at high filler loading and hinder conductivity. To enhance the dispersion, like CNTs, graphene may receive covalent or noncovalent functionalization treatments to improve compatibility with a thermoplastic matrix.

### 8.2.1. Covalent Functionalization

Graphene can be changed into graphene oxide or into reduced graphene oxide by introducing oxygen-containing groups (such as carbonyl, hydroxyl, epoxide, and carboxyl groups) on the edges of the graphene hexagons (Figure 15). This can be achieved in several ways including mechanical exfoliation and chemical oxidation.<sup>[206]</sup>

The functional groups on the surface of graphene impart a charge on the filler, and this prevents graphene from agglomerating and enhances dispersion.<sup>[207]</sup> Generally, improved dispersion of graphene results in high electrical conductivity. Nonetheless, although useful to improve the interaction of graphene with the polymer matrix, covalent functionalization introduces oxidized defects that reduce the intrinsic electrical conductivity of graphene.<sup>[208]</sup> This was demonstrated, for example, in PP nanocomposites where graphene was functionalized with polypropylene-graft-maleic anhydride (PP-MA).<sup>[209]</sup> Interestingly, the authors stated that the functionalized graphene had a lower conductivity ( $60 \text{ S cm}^{-1}$ ) compared to the pristine graphene ( $137 \text{ S cm}^{-1}$ ), but the electrical conductivity of the PP/graphene composites was slightly higher with the functionalized filler. This was attributed to the improved dispersion of the functionalized filler, which enabled the precocious development of a percolation pathway despite its reduced conductivity. Methods for covalent functionalization can vary greatly depending on the polymer matrix and the specific kind of graphene in use. Several examples of this variability are listed in Table 4 with the corresponding graphene forms.

### 8.2.2. Noncovalent Functionalization

Similarly, to what already observed for noncovalent functionalization of CNTs (Section 8.1.2), the aim of noncovalent functionalization of graphene is to mitigate the attractive forces that are

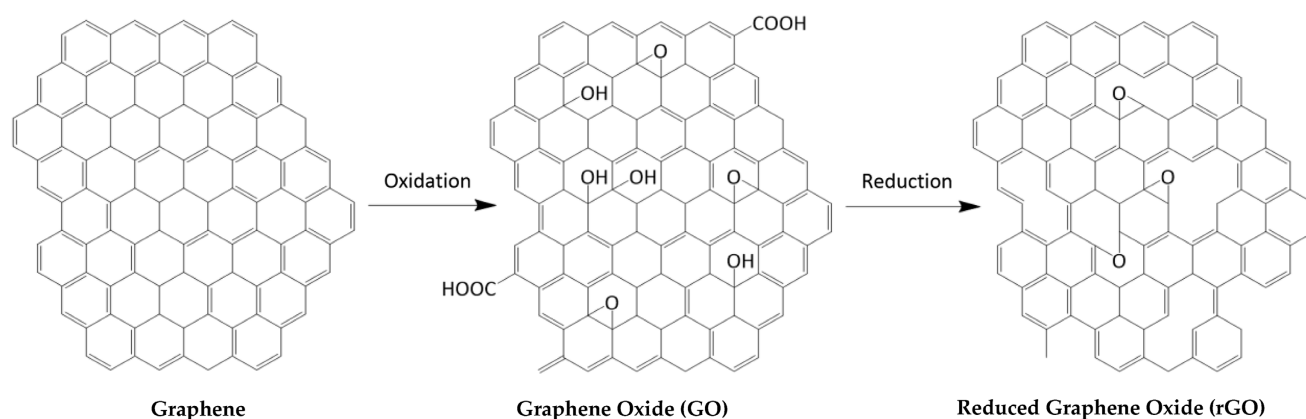


**Figure 15.** Showing the molecular structure of graphene, graphene oxide, and reduce graphene oxide. Reproduced (Adapted) with permission.<sup>[206]</sup> Copyright 2021, MDPI.

responsible for aggregation in a thermoplastic matrix while avoiding structural change or damage to graphene. An example of noncovalent functionalization in graphene for FFF is reported in the study by Pei et al.<sup>[210]</sup> who solution cast GnPs in PVA with the aid of ultrasonication and used glycerol as a plasticizer. As a result of the addition of the plasticizer that also reduced the interparticle attraction among GnPs, the processability of PVA improved and the conductivity of the composite was increased from  $7.8 \times 10^{-7} \text{ S m}^{-1}$  to  $2.4 \times 10^{-4} \text{ S m}^{-1}$  with only 1.0 wt% of GnPs. In addition, Pei et al.<sup>[210]</sup> postulated that the GnPs, which have hydroxyl groups on their surface, were able to form hydrogen bonds with the modified PVA matrix and this improved the matrix-filler compatibility. As summarized by Perumal et al.<sup>[211]</sup> surfactants can be introduced instead of plasticizers to overcome graphene aggregation in a solution, which may be particularly useful for solution casting and in situ polymerization.

### 8.3. CB

Unlike CNTs, which are elongated fillers with a high aspect ratio, and graphene, which is composed of monolayers or ultrathin platelets, CB is roundish. In terms of filler loading, due to the roundish shape of CB and hence due its reduced aspect ratio compared to CNTs or graphene, this filler generally requires a higher filler loading to achieve a similar conductivity. In addition, the diameter of CB particles can range from 2 nm to several hundred nanometers, with aggregation potentially increasing the filler size to a few micrometers.<sup>[212]</sup> Kwok et al.<sup>[213]</sup> found that PP/CB composite filaments for FFF had low conductivity for filler loadings below 15 wt%, so very high weight fractions of CB may be required for targeting good conductive properties. Similarly, in a direct comparison between CNTs and CB, it was demonstrated that PP composites achieved percolation at 8 wt% for PP/CNT and at 9.5 wt% for PP/CB,<sup>[214]</sup> which was attributed to the higher

**Table 4.** Covalent functionalization of graphene/ graphene structures.

Polymer matrix	Type of graphene	Composite production method	Refs.
TPU/PP with (MA-g-PP)	rGO	Melt blending	[356]
PA6/PA6,6	Amino and O <sub>2</sub> GnPs	Melt blending	[357]
PLA	GnP functionalized with sodium dodecylbenzene sulfonate (SDBS)	Melt blending	[358].
Biobased PA	GO (functionalized with hexamethylenediamine)	In situ polymerization	[359]
PLA/PCL	Thermally exfoliated reduced graphene oxide (f-TERGO)	Melt blending	[360]
ABS	In situ (ABS-GO)	In situ polymerization	[361]
PVDF	Slightly oxidized graphene nanoplatelets (GNPs) were functionalized using 3-hydroxytyramine hydrobromide	Solution blending/ melt blending	[362]
PVDF	Polybenzimidazole functionalized graphene oxide (GBI)	In-situ polymerization	[363]
PP	Graphene that had been modified with low molecular weight polypropylene brushes (G-PP)	Solution blending and melt extrusion	[209]
TPU	Hyperbranched aromatic polyamide functionalized graphene sheets (GS-HBA)	Solution blending	[364]

aspect ratio of CNTs over CB. In addition, when combined with PLA, CB has been shown to encourage brittle failure in FFF printed parts.<sup>[215]</sup>

In spite of these drawbacks, CB does offer some advantages for the development of conductive feedstock for FFF. A key value of CB is that its effect on viscosity is less obvious than the effect observed when CNTs are combined into a thermoplastic composite. For example, incorporation of CB was shown to have a smaller effect on viscosity compared to CNTs in ABS/PC blends.<sup>[128]</sup> As printability by FFF is significantly affected by the melt viscosity of the feedstock material, CB is a useful filler to incorporate either on its own or together in a multifiller system (Section 8.4) in an effort to improve printing and retain conductivity of the composite. Another advantage is that CB is an affordable filler because it is formed as a by-product of thermal decomposition of heavy petroleum products.<sup>[216]</sup>

A commercially available conductive filament known as Palmiga PI-ETPU (TPU/CB filament) was successfully used in the production of a 3D printed sensor array.<sup>[217]</sup> Joao et al.<sup>[218]</sup> also investigated this filament to develop an electrode that was able to detect copper ions in ethanol using a method known as square-wave anodic-stripping voltammetry (SWASV). In this specific example, CB was leveraged to transport electrons through the 3D printed electrode, which enabled electroplating of copper ions onto the electrode.

Thus far, there are no covalent functionalization methods which are applicable to CB for FFF conductive composites. This is because most studies focus on the covalent functionalization of CNTs or graphene, which are nanostructured fillers having high surface areas and better conductive properties than CB.

As for the noncovalent functionalization of CB, an option is to use plasticizers which enable dispersion of CB by reducing the viscosity of the polymer matrix to enable better dispersion under shear stress. Palmitamide (a fatty acid amide), as an example, has been used to improve CB dispersion in styrene-butadiene nanocomposites.<sup>[219]</sup> The printability of a lithium-terephthalate PLA/CB filament was increased when poly(ethylene glycol) dimethyl ether was added as plasticizer.<sup>[220]</sup> To the best of our knowledge, this is the only example of CB-filled nanocomposite filament for FFF that uses a plasticizer. In principle, another option is to use ILs to improve the conductivity of the composite as demonstrated in the study by Xing et al.<sup>[221]</sup> who increased the conductivity of a PVDF/CB composite by melt-blending with 1-vinyl-3-ethylimidazolium tetrafluoroborate (an unsaturated IL). The add-on of the IL improved the conductivity owing to the enhanced distribution of CB. However, the contribution by Xing et al.<sup>[221]</sup> was not specifically addressed to AM and, in spite of the positive results in terms of electrical conductivity, to the best of our knowledge ILs have not been utilized in any FFF studies yet.

As a concluding remark, it is important to note that it is often difficult to achieve a low percolation threshold with only CB (mainly due to its spherical shape and relatively large size) and for this reason many researchers utilize instead multifiller conductive systems (Section 8.4) or induce a double percolated structure (as already discussed in Section 7.2) to enhance conductivity of CB composites.

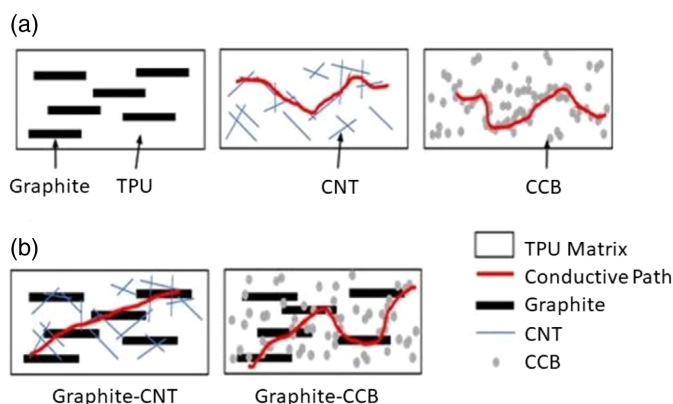


**Figure 16.** Showing the advantage of binary conductive filler systems in a CCB (conductive carbon black), CNT (carbon nanotube), and thermoplastic polyurethane matrix (TPU). Reproduced (Adapted) with permission.<sup>[223]</sup> Copyright 2020, MDPI.

#### 8.4. Multifiller Systems

Carbonaceous multifiller systems are composites that use a combination of different carbon-based fillers. They are often employed to address the limitations of CNTs, graphene forms, and CB when used alone and to attain a balance between viscosity and conductivity. For example, the addition of a secondary conductive filler such as CB in a TPU/CNT composite greatly assists in achieving percolation.<sup>[222]</sup> In a study by Kim,<sup>[223]</sup> the addition of CB or CNTs was shown to induce percolation in a TPU/graphite blend that otherwise remained nonconductive in spite of increasing the graphite loading up to 50 wt% (**Figure 16**). Indeed, a successfully conductive blend was obtained with 20 wt% graphite and 5 wt% CB or 5 wt% CNTs. Zhang et al.<sup>[224]</sup> discovered that, when PP is used as matrix, CB can actively work as a “bridge” between CNTs, thus leading to a low percolation threshold in CB-CNTs systems. This hybrid system could achieve percolation with 0.25 wt% CNTs and 0.25 wt% CB, whereas a system containing only CNTs needed 2 wt% of filler to achieve conductivity. A decreased percolation threshold with the addition of a secondary conductive filler has been attributed to improved electron pathways being formed, as well as to ameliorated dispersion or to volume confinement.<sup>[222]</sup> Therefore, it is manifest that using a multifiller system in conductive thermoplastics can be very advantageous to develop the percolation threshold at smaller filler loadings.

Combinations of various conductive fillers can also enhance printability of the thermoplastic-matrix composite, which is useful to prevent print defects that may be responsible for reduced conductivity in printed parts. One example is seen in the study by Kotsilkova et al.<sup>[225]</sup> who discovered that GnPs can have a lubricant effect and thus can reduce the viscosity and improve the printability of a PLA/CNT composite. Dul et al.<sup>[226]</sup> also combined equal amounts of GnPs and CNTs into ABS to find a good compromise between conductivity and printability. This is because the addition of GnPs improved the printability, but reduced the conductivity, whereas the addition of CNTs had

exactly the opposite effects. An optimal “middle ground” was identified to be 6 wt% total filler loading, with equal amounts of each filler. A similar result was found for high performance polymers, where nearly equal proportions of CNTs and GnP (4 wt% CNTs and 3 wt% GnP) improved the printability of PEEK composites, with conductivity of the filaments being measured at  $7 \pm 2 \text{ S m}^{-1}$ .<sup>[227]</sup> As pointed out by Spinelli et al.<sup>[228]</sup> a potential issue with multifiller systems is that, if one or both fillers are relatively large (as it may happen with graphene or, even more so, with CB), multifiller systems may cause clogging, particularly at high filler loadings (>5 wt%). Despite these printing issues, multifiller systems in FFF have been proven useful in the manufacturing of advanced electronic devices such as electrodes for electro sensing applications.<sup>[229]</sup>

### 8.5. Continuous Carbon Fiber

An emerging field of research that may open new horizons for the obtainment of conductive parts is the FFF of continuous fiber-reinforced polymers. Discontinuous carbon fibers have been used in energy absorption applications but require a high filler loading (up to 30%) for piezoelectric sensing.<sup>[230]</sup> More commonly, continuous carbon fiber is used to take advantage of its favorable aspect ratio as an uninterrupted pathway for electrical current and has been utilized in FFF under commercially available products from MarkForged.<sup>[231]</sup> A special printing equipment is required to this aim.<sup>[232]</sup> According to the “in nozzle impregnation method,” the continuous fibers are fed into the liquefier, where they are impregnated by the molten polymer, and then extruded through the print nozzle. According to the “dual nozzle” method, instead, the polymer matrix filament and the preimpregnated fibers are fed into and printed through two separate nozzles. 3D printing with continuous carbon fibers has been demonstrated with several thermoplastics like polyetherimide (PEI)<sup>[233]</sup> and PLA.<sup>[234]</sup> In an article by Ye et al.,<sup>[235]</sup> it is mentioned that using a low viscosity thermoplastic polymer improves the likelihood of success in printing with continuous carbon fibers.

Printing with continuous fibers poses several technological challenges, such as the potential deposition mismatch between the fiber and the polymer, the difficult control of the g-code to ensure impregnation of the fiber within the polymer, as well as the accurate consideration of the free travel of the nozzle (which is when the print head moves around the build platform without depositing material). Also, printing with continuous fibers requires an inbuilt cutting mechanism.<sup>[236]</sup> The achievement of reliable parts largely depends on specific improvements to the g-code, such as increasing the print temperature and reducing the print speed in order to improve the quality of the print and also increase the interlayer strength.<sup>[237]</sup>

Despite these technological requirements, the use of a continuous carbon fiber completely eliminates the direct dependence on the filler aspect ratio because the conductive element is continuous and laid down in an uninterrupted pathway. This paves the way for new self-monitoring structures because any damage to the printed part leads to a discontinuity within the fibers that can be easily detected as a local change in resistivity.<sup>[238,239]</sup> Luan et al.<sup>[240]</sup> demonstrated this capability of continuous carbon fiber

to sense large-scale deformation and damage by monitoring resistance changes in a 3D printed part where continuous carbon fibers were arranged in transverse and longitudinal directions to create a grid-like structure. The sensing grid integrated within the thermoplastic matrix was also responsible for accurate detection of the loading location. More recently, composite materials combining continuous carbon fiber, CNTs, and a TPU/PLA matrix have been shown to have excellent conductive capabilities in shape memory applications.<sup>[241]</sup> Certainly, with the correct hardware and careful control of the reinforcement placement, continuous carbon fibers are a good option for manufacturing FFF conductive parts.

## 9. Metallic Fillers

Metallic fillers such as tin alloys, silver, or copper have higher conductivity than carbonaceous fillers, but there are several limitations to their use in conductive composites. Unless noble metals are considered such as silver, thermal oxidation is often responsible for the growth of a passive oxide layer that acts as an insulator on the surface of metallic fillers and drastically reduces their conductivity. Also, the dispersion of metallic fillers in a thermoplastic matrix can be problematic because metal fillers have a high density and need high mixing energy to be dispersed without precipitating. This high density will also increase the weight of the final composite and may even cause damage to a FFF printer. Moreover, most metallic fillers need to be purified and dried before melt-compounding, which may promote their agglomeration.<sup>[242]</sup> In addition, similar to what happens with carbon-based fillers, there are limits to the size of metallic fillers because excessively large particles may render the composite unprintable.<sup>[243]</sup>

### 9.1. Low Melting Point Alloys

Low melting point alloys (LMPAs) are metals with a processing temperature comparable to thermoplastics and can be used in melt-processed conductive composites.<sup>[244]</sup> Under melt processing, LMPAs have a low viscosity, which means that they can reduce the overall viscosity of a thermoplastic once melt-blended together. These LMPAs have the additional advantage of being highly conductive and able to form cocontinuous structures in thermoplastics (similar to the way cocontinuous structures are formed between blended immiscible polymers, Section 7.2). Li et al.<sup>[245]</sup> demonstrated that, by varying the relative fractions of tin (low melting point metal) and copper (high melting point metal) in PA6 composites, the composite can change from a “sea-island” morphology to a cocontinuous structure.

Articles discussing LMPAs in FFF are still limited. LMPAs that are commonly combined with thermoplastics include  $\text{Sn}_{60}\text{Bi}_{40}$ ,  $\text{Sn}_{96.5}\text{Ag}_{3.5}$ , or  $\text{Bi}_{58}\text{Sn}_{42}$ . However, these LMPAs have difficulty being processed through an FFF printer due to their tendency to agglomerate within the print head and require some trial and error to find the optimal printing parameters.<sup>[246,247]</sup> A way to mitigate agglomeration was demonstrated by Tan and Low,<sup>[248]</sup> who obtained a highly conductive filament using nickel and a tin-based LMPA ( $\text{Sn}_{95}\text{Ag}_4\text{Cu}_1$ ) which, at 30 wt% LMPA loading, had a conductivity of  $31\,000 \text{ S m}^{-1}$ . Nickel was used

to prevent coalescence of the LMPA in both PA6 and HDPE matrixes and percolation was achieved at 25 vol% loading in both. The same  $\text{Sn}_{95}\text{Ag}_4\text{Cu}_1$  LMPA was also combined with copper particles and dispersed in a LDPE matrix. After printing, the conductivity of the printed parts retained 55% of the initial conductivity of the filament, which was still an impressive value of  $1050 \text{ S m}^{-1}$ .<sup>[249]</sup> Other studies propose to use solder-based alloys in FFF; however, they do not account for the conductivity of the printed parts. In this regard, it is important to note that many solder-based alloys contain tin and therefore have a high tendency to form an insulating oxide skin which limits electrical conductivity.

Given that aggregation is a significant problem, in addition to the presence of nickel or copper as mentioned above, there are some other ways to prevent LMPA particles from attracting each other. In one example, a good distribution of an LMPA ( $\text{SnBi}_{58}$ ) within a PP matrix was achieved by melt-blending nanomontmorillonite (nano-MMT), which improved the dispersion of the alloy into the thermoplastic.<sup>[250]</sup> This composite was drawn into fibers via melt spinning, which resulted in PP/LMPA/nano-MMT fibers having a very good dispersion of the LMPA. This was due to the polar charge of the nano-MMT that could attract the LMPA particles more strongly than the nonpolar PP matrix could do, and thus prevented the LMPA particles from attracting each other. Another study found similar improvements in dispersion of LMPAs into PE when combined with nano-MMT and CNTs. Also, running multiple drawing cycles reduced the size of the alloy particles and ultimately improved the conductivity.<sup>[251]</sup> So, there are several ways to prevent aggregation of LMPAs in a thermoplastic composite. However, further studies would be required to assess the viability of these methods to produce composite filaments for FFF. A deeper understanding of the potential deagglomeration strategies of LMPAs would certainly be advantageous to prevent clogging of the nozzle and increase the print quality of the final parts.

## 9.2. Silver

Silver (Ag) metal boasts high electrical conductivity ( $6.3 \times 10^7 \text{ S m}^{-1}$ ) compared to other metals (like copper) and has slow oxide formation,<sup>[252]</sup> which makes it useful in those production techniques of conductive composites that require heating, like melt extrusion of a filament or the printing process itself. Silver nanostructures with high aspect ratios (such as silver nanowires, AgNWs) are advantageous to attain conductive thermoplastic composites with strain sensing abilities<sup>[253,254]</sup> or self-healing abilities, where conductivity can be fully recovered after healing.<sup>[255]</sup> However, as discussed in Section 3, conductivity and the development of the percolation threshold are highly dependent on the filler's aspect ratio and the polymer matrix. For example, in a thermoset matrix (epoxy), AgNWs (100  $\mu\text{m}$  length, 390 nm diameter) were able to achieve percolation at 10 wt% AgNWs,<sup>[256]</sup> but Zhong et al.<sup>[257]</sup> needed approximately 20 wt% of AgNWs (20  $\mu\text{m}$  length, 60 nm diameter) in a TPU matrix to induce percolation.

Silver fillers can be purchased from suppliers or can be directly manufactured by reducing silver nitrate via the polyol process<sup>[258]</sup> or working in an aqueous solution.<sup>[259]</sup> As a result,

significant agglomeration can occur unless measures are taken (i.e., ultrasonication). Also, the obtained silver fillers require additional purification steps to remove solvents or aqueous liquids before they can be used in melt extrusion. One way to prevent aggregation of silver nanostructures upon solution casting is to synthesize them directly into the polymer solution, rather than reducing silver ions in a separate solution first and adding them to the polymer solution to obtain a composite. In one example, TPU was dissolved into DMF and silver ions (in the form of silver nitrate) were directly reduced in this polymer solution to induce the formation of silver nanoparticles connected in chain-like structures or AgNWs.<sup>[260]</sup> Lu et al.<sup>[261]</sup> treated the AgNWs with a polyethylene glycol derivative that improved surface contact with the TPU matrix and improved dispersion into this thermoplastic matrix. Other structures of silver (e.g., in the form of flakes) have also been shown to be effective conductive fillers in a polyester binder.<sup>[262]</sup>

Due to the relatively high cost of silver and the large amounts that would be needed to produce commercial quantities of FFF filament, silver nanostructures are rarely explored in FFF studies in terms of conductivity. Most development of silver FFF composites is currently related to biomedical applications with a high added value, where silver is explored due to its superior antibacterial properties. An effective antibacterial action can be easily achieved with very low levels of silver, typically below the filler loading that would be required for the electrical percolation threshold.<sup>[263]</sup> For conductivity purposes, high filler loadings are necessary and, in order to reduce the cost of the conductive filler, silver can be deposited onto the surface of other, more affordable fillers. The contribution from Basir and Khan<sup>[264]</sup> showed that silver-coated glass particles could be incorporated into a HDPE/CNT matrix and percolation was achieved with 20 wt% of silver-coated glass particles and 1 wt% of CNTs. However, percolation with just CNTs in HDPE was reported with approximately 2.8 wt% of filler, so using large glass particles may not be so advantageous and perhaps using a glass nanostructure would be more beneficial. Sharifabad et al.<sup>[265]</sup> coated hydroxyapatite nanoparticles with silver and incorporated them into a PLA-matrix filament for FFF for biomedical applications; however, they did not test for electrical conductivity. Another way to tackle the expensiveness of silver-based conductive materials consists in using silver just as a secondary filler to increase electrical conductivity. For example, Zeraati et al.<sup>[266]</sup> used a variety of metallic fillers including silver nanoparticles and wires to achieve high conductivity of a PVDF/CNT composite at 3.0 wt% of CNTs and 10.0 wt% of PVDF/AgNWs. Other forms of silver-based fillers have been explored in the literature. For example, Lei et al.<sup>[267]</sup> combined the thin-film transition technique and melt extrusion-drawing method to produce polyvinyl butyral filaments for FFF loaded with silver flakes having nanoscale thickness, but measuring on average 5.4  $\mu\text{m}$  in diameter. The composite filaments with 55 wt% (11.08 vol%) of filler loading developed a low volume resistivity of  $7.02 \times 10^{-4} \text{ S cm}^{-1}$ .

## 9.3. Copper

Copper is a popular metal in electronic devices and circuitry due to its drawability and high conductivity. However, copper

undergoes thermal oxidation over a broad range of temperatures. Thermally induced oxidation tests proved that, under low-temperature heating (100 and 150 °C), only a thin copper oxide layer is formed over the surface of Cu, which has negligible consequences on electrical conductivity. Conversely, heating at 300 °C induced the growth of a passivating oxide layer composed by CuO and Cu<sub>2</sub>O.<sup>[268]</sup> This suggests that the ideal temperature range to maintain the conductivity of copper during printing would be largely below 180 °C, which is the lower bound of the operational range for common FFF printers. Also, a limited number of thermoplastics feature such a low melting temperature. A commercial grade of conductive copper-filled filament known as Electrifi has been demonstrated to be printable with low resistance values<sup>[269]</sup> compared to CB or graphene composites,<sup>[270]</sup> but the recommended printing temperature is below 150 °C in order to avoid diffused oxidation. Development of the percolation pathway may be affected if this occurs, because this would result in a mixture of unoxidized (conductive) and oxidized (nonconductive) copper imbedded within the filament.

Coating the surface of copper with a protective polymer agent is a method to prevent oxidation. Relevant examples are polyethylene glycol, which can protect copper against oxidation for 3 months at room temperature in ethanol,<sup>[271]</sup> and polyvinyl pyrrolidone, which can be used to stabilize copper nanostructures and prevent their aggregation during synthesis.<sup>[272]</sup> Whereas both of these materials are currently used as plasticizers in thermoplastic composites for FFF due to their ability to reduce the polymer viscosity and improve the filler dispersion, their potential effect on the conductivity of copper-filled composite filaments for FFF has not been investigated yet.

In principle, another way to prevent oxidation and preserve the conductivity of copper upon printing is to coat the surface of copper with a conductive metal that oxidizes at high temperature. A popular core-shell configuration consists in plating silver over a copper substrate.<sup>[273]</sup> As silver has a higher thermal oxidation temperature than copper, it can be extruded and printed while retaining its conductivity. According to this approach, Cruz et al.<sup>[274]</sup> developed a PCL filament functionalized with Cu-Ag core-shell nanowires, but encountered issues upon printing, such as aggregation of the fillers as well as nozzle clogging due to high filler loading. In principle, another potential metal which can coat copper to prevent oxidation is nickel,<sup>[275]</sup> but this has not yet been studied in FFF printing. Carbon can also be used to coat the surface of copper to prevent oxidation,<sup>[276]</sup> but this option seems less favorable than using silver or nickel because the conductivity of carbon is lower than that of copper.

#### 9.4. MXenes

MXenes are an emerging class of 2D materials with excellent conductivity comparable to copper, with the additional advantage that their conductivity can be tailored by etching their surface in a similar manner to graphene. Though very recent, this new class of materials already comprises more 30 members whose composition follows the general formula  $M_{n+1}X_nT_z$  ( $n = 1, 2, \text{ or } 3$ ), where X signifies carbon and/or nitrogen, M represents an early transition metal, and T refers to the various surface terminations

like fluorine, oxygen, chlorine, and/or hydroxyl groups.<sup>[277]</sup> Based on currently available knowledge, these materials are solution processable<sup>[278]</sup> and therefore their usage in AM is limited to those techniques such as solution, paste, or inkjet 3D printing that process a solution-based feedstock. A detailed description of MXene-based inks and their synthesis has been published in the review article by Zhang et al.<sup>[277]</sup>

MXenes such as titanium carbide ( $Ti_3C_2T_x$ ) have been dip coated onto FFF printed electrodes made of a PLA/graphene composite feedstock in order to improve the electrochemical performance with respect to the uncoated electrode.<sup>[279]</sup> It was also demonstrated that the capacitance of the same printed electrode was increased by three times as a result of electrochemical activation followed by MXene functionalization with the archetypal MXene,  $Ti_3C_2$ .<sup>[280]</sup> As an alternative approach, a  $Ti_3C_2T_x$  MXene paste feedstock was formulated to be printed at room temperature to produce microsupercapacitors with ultrahigh energy densities<sup>[281]</sup> of up to 1035 mF cm<sup>-2</sup> areal capacitance.<sup>[282]</sup> As a general rule, MXenes are more compatible with inkjet printing and with solution-based 3D printing if they are dispersed in an organic solvent or in an aqueous medium, respectively. Therefore, incorporating these 2D materials in FFF would require the development of special printers with a syringe/slurry delivery system, instead of the standard filament feeder. Moreover, printing should be completed at room temperature, and particular care should be paid to creating a printable formulation which retains its surface tension in order to prevent drips leading to poor printing.<sup>[283]</sup>

In spite of these difficulties, promising contributions in the literature suggest that MXenes may soon find some potential applicability in the melt extrusion method that is at the heart of FFF. For example, polymeric composites of TPU combined with MXene fillers have been obtained using a melt-based process such as compression molding<sup>[284]</sup> and melt blending,<sup>[281]</sup> and other composites of PVDF/MXene have been produced using solution mixing followed by injection molding at 190 °C in order to fabricate a piezoelectric generator.<sup>[285]</sup>

## 10. Conductive Polymers

Conductive polymers are a class of polymers that can transfer electrons due to their chemical structure. On account of their unique properties, conductive polymers have been used in many applications, including actuators, drug delivery, and energy storage systems.<sup>[178]</sup> However, their peculiar structure that is key for enabling conductivity also limits their processability. In particular, conductive polymers cannot be melted on their own and must be incorporated into another polymer matrix for melt processing. Conductive polymers may need doping to increase their conductivity or improve their processability in order to allow the obtainment of thermoplastic composites. Currently, the most popular conductive polymers in the literature are PANI and polypyrrole (PPy). However, as discussed in the following paragraphs, in spite of the increasing attention being paid to these conductive polymers, there are still several issues and open challenges in terms of their application in FFF.

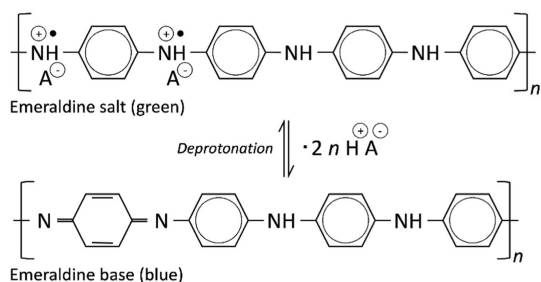


**Figure 17.** Diagram showing chemical structures of PANI in emeraldine base (PANI-EB) and acid (PANI-ES) forms. Protonation of PANI-EB is a reversible reaction that occurs in an acidic solution.<sup>[338]</sup>

### 10.1. PANI

PANI is present in several forms, including leucoemeraldine, emeraldine, and pernigraniline, which represent the three different oxidation states of aniline.<sup>[286]</sup> Among them, the emeraldine form can be formed into an emeraldine base form (PANI-EB) or into an emeraldine salt form (PANI-ES), depending on whether the polymer is polymerized in a basic or acidic solution, respectively (**Figure 17**). Whereas PANI-ES is the most conductive and thermally stable form of PANI, PANI-EB is not conductive. In fact, while PANI-EB has a conductivity of  $10^{-10} \text{ S cm}^{-1}$ , PANI-ES can have a value  $\approx 30 \text{ S cm}^{-1}$ , largely depending on the dopant used to protonate the polymer.<sup>[287]</sup>

There are several ways to produce PANI including in situ electropolymerization, chemical vapor deposition (CVD), dip-coating, and self-organization method.<sup>[288]</sup> The conventional oxidative chemical polymerization method to produce the emeraldine salt form (PANI-ES) involves combining aniline and an acidic medium like strong hydrochloric acid (HCl) and adding ammonium persulfate dropwise (because the reaction is highly exothermic and the temperature needs to be stabilized between 0 and  $5^\circ\text{C}$ ).<sup>[289]</sup>

Another method to obtain the PANI-ES form is to immerse PANI-EB into an appropriate acidic solution as this protonation reaction, if properly conducted, can lead to PANI-ES. Unfortunately, this process is reversible, which also means that PANI-ES can lose its conductivity and revert back to its less conductive form PANI-EB through deprotonation.

Unfortunately, PANI is normally immiscible with other thermoplastics and is difficult to process particularly in its conductive (PANI-ES) form. This is because of its chemical structure, which causes the polymer to have poor solubility in most solvents and also impedes melt processing. Despite this, thermoplastic-PANI blends can be obtained with a good conductivity and improved processability if the compatibilization between the polymers is enhanced by proper strategies as described in the following paragraphs.

#### 10.1.1. PANI–Thermoplastic Blends

The most common way to attain thermoplastic–PANI blends is using in situ polymerization,<sup>[290]</sup> which can synthesize PANI directly within a thermoplastic solution. Alternatively, the

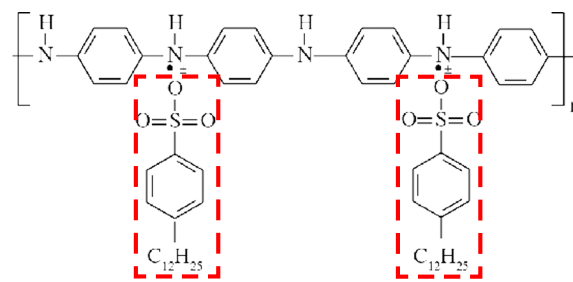


**Figure 18.** Chemical bonding between DBSA (highlighted in red) and the PANI structure (PANI–DBSA). Reproduced (Adapted) with permission.<sup>[339]</sup> Copyright 2017, ResearchGate.

solution casting method can be applied to blend both PANI and thermoplastic within a mutually compatible solvent. However, Vincentini et al.<sup>[291]</sup> found that, when TPU/PANI blends are sought after, in situ polymerization produces a blend with a lower percolation threshold (2.0 wt%) compared to solution casting (2.7 wt%), when the same organic solvent (tetrahydrofuran, THF) is chosen for both procedures. The specific form of in situ polymerization conducted by Vincentini et al.<sup>[291]</sup> is known as emulsion polymerization and leads to better compatibilization of PANI with the TPU matrix compared to solution casting. This study<sup>[291]</sup> enabled solubility and induced conductivity of the emeraldine salt form in THF by doping with a functionalized acid known as dodecylbenzenesulfonic acid (DBSA) instead of HCl and thus obtaining PANI–DBSA (which is a form of PANI-ES). DBSA contains long alkyl groups with a hydroxide ending that attaches to the amine subsections in the PANI structure (**Figure 18**). This can be attributed to site-specific interactions between the carbonyl and amine groups from the TPU and PANI–DBSA, respectively, that are very strong after in situ polymerization, whereas these interactions are less pronounced in solution casting.

DBSA is a popular doping agent to improve the processability of PANI, and acts as both doping agent and surfactant.<sup>[292]</sup> Also, unlike other chemicals such as HCl that can be used to protonate PANI, DBSA is able to preserve the conductivity of PANI in specific thermal cycles,<sup>[293]</sup> which allows PANI to retain its conductivity at higher temperatures as required for melt blending. This is important because, in spite of the thermal stability of the emeraldine salt form, conductivity is lost at relatively low temperatures where most thermoplastics become melt processable. The thermal decomposition occurs in four stages<sup>[294]</sup> 1) first stage—water is lost from the emeraldine salt sample ( $50\text{--}100^\circ\text{C}$ ); 2) second stage—PANI-ES becomes deprotonated and loses conductivity (temperature region where this occurs is highly dependent on the dopant originally used to protonate to the salt form); 3) third stage—decomposition (approximately  $470\text{--}570^\circ\text{C}$ )—amino group breakdown; and 4) fourth stage—decomposition ( $650\text{--}800^\circ\text{C}$ )—degradation of aromatic backbone.

In the research published by Zhang et al.,<sup>[295]</sup> DBSA allowed PANI to be melt processed within a LDPE/EVA copolymer matrix with particular selective localization of the doped PANI polymer (PANI–DBSA) within the EVA matrix.<sup>[295]</sup> As a result, the conductivity of the ternary polymer blend (PANI–DBSA/LDPE/EVA) became one order of magnitude higher than

PANI–DBSA/LDPE. PANI, if doped with DBSA or other chemicals like p-toluene sulfonic acid (PTSA), makes it possible to melt-blend the conductive polymer at above 180 °C without losing conductivity. This has been demonstrated with numerous thermoplastics, including PS,<sup>[296]</sup> ABS,<sup>[297]</sup> LLDPE, copolyamide 6/6,9,<sup>[298,299]</sup> PVC, PETG, and PCL.<sup>[300]</sup> There are several different chemicals other than DBSA which can be used to dope PANI; however, they have varying levels of effectiveness in imbuing PANI with improved processability and/or conductivity.<sup>[301]</sup> PC<sup>[302]</sup> and PS<sup>[303]</sup> blends can be produced with emulsion polymerization using sodium lauryl sulfate as both protonating agent and surfactant.

An alternative method to mitigate the thermal degradation of PANI-ES consists in melt-blending it with low-melting point thermoplastics that require low processing temperatures, preferably below the deprotonation temperature, such as ethylene vinyl acetate (EVA) whose melting point is around 110 °C.<sup>[304]</sup> This strategy is effective especially if combined with the addition of gallate compatibilizers to prevent degradation of PANI–DBSA.<sup>[305]</sup> Sulfonic acid of 3-pentadecylphenoxyacetic acid can also be used to improve the compatibility of PANI with EVA.<sup>[306]</sup>

Although they are very popular, the issue with strong acidic dopants like DBSA, HCl, PTSA, or sodium lauryl sulfate is that they must be removed before melt blending and thus require additional purification steps. As a result, conductivity can be reduced due to removal of the dopant, which can cause subsequent deprotonation, or due to loss of conductive material. For example, Tian et al.<sup>[307]</sup> discussed the risk for reducing conductivity upon washing in the case of electrospun PU (core)/PANI (shell) fibers. Tian et al.<sup>[307]</sup> attributed the observed drop in conductivity to the removal of low molecular weight PANI. So, some loss of conductivity may occur during purification of the doped PANI. Conductivity will likely be degraded further upon melt blending due to thermal degradation. This is an important consideration when developing thermoplastic blends using PANI because specific mitigation strategies must be enforced to preserve the conductivity of PANI-ES.

An important point that emerges from the thermal decomposition stages listed above is that water is already lost during initial heating below 100 °C. This is relevant to the aim of producing conductive feedstock materials for FFF because the loss of water may influence the quality of the filament and ultimately the success of printing. Further, conductivity drops once PANI-ES loses its protonated state and becomes PANI-EB, which is likely to occur upon extruding or printing. Given the fact that the most effective production methods of PANI (either EB or ES form) require in situ polymerization, oftentimes only small laboratory scale amounts can be synthesized, which may be problematic when scaling up for FFF filament production. Additionally, it is still unclear how severe the effect of purification is to FFF filament extrusion and subsequent printing. Due to these limitations, the deployment of new feedstock materials based on thermoplastic–PANI blends in FFF is particularly challenging. However, there are other ways to increase the processability of PANI or to increase its conductivity that may facilitate the future uptake of PANI-based systems in FFF, for example, using PANI as a coating on conductive fillers.

### 10.1.2. Hybrid Fillers with PANI Coating

A list of synthesis methods for PANI nanocomposites up to 2016 can be found in the article written by Sen et al.<sup>[308]</sup> and in a more recent paper published in 2019 by Singh et al.<sup>[309]</sup> As mentioned in the previous section, the main cause for loss in conductivity is the deprotonation of the emeraldine salt form of PANI (PANI-ES)<sup>[310]</sup> and one way to prevent this from occurring is to dope with functionalized acids like DBSA to enhance conductivity and processability. However, another way to improve conductivity of PANI-ES in a thermoplastic blend is to produce a composite by incorporating conductive fillers. PANI is able to be coated onto the surface of carbonaceous fillers and can assist in their dispersion, which facilitates the development of the percolation threshold. PANI-coated CNTs also have improved dispersion in organic solvents compared to uncoated CNTs and this is attributed to PANI weakening the intermolecular forces and thus preventing CNTs from agglomerating.<sup>[311]</sup> Meanwhile, the CNTs can improve the thermal stability of PANI.<sup>[312]</sup> CNTs can be coated with PANI either by polymerizing aniline in the presence of CNTs (in situ polymerization) or by solvent mixing doped PANI with CNTs. Wang et al.<sup>[313]</sup> discovered a clear improvement in the chemical bonding between PANI and CNTs if they were produced via in situ polymerization rather than solvent mixing. However, it is important to note that this study focused on electrospun PANI/CNT fibers and therefore the results of the research by Wang et al.<sup>[313]</sup> may not be strictly applicable to composites that are melt extruded (as it happens for FFF filaments).

The preliminary covalent functionalization of CNTs with carbonyl, carboxyl, and hydroxyl groups can be helpful for subsequent surface coating with PANI.<sup>[314,315]</sup> Aminofunctionalized CNTs have also demonstrated to improve the conductivity of the PANI matrix as well as the dispersion of the PANI/CNT fillers.<sup>[316]</sup> This is attributed to hydrogen bonding between the amino groups of the aniline monomers and the functional groups of the CNTs. This approach has potential to produce PANI–thermoplastic composites with CNTs with low percolation thresholds, such as the TPU/PANI/CNT composite with a very low percolation threshold of 0.58 wt% produced via in situ polymerization by Sohba et al.<sup>[121]</sup> Composites of TPU, PANI, and CNTs functionalized with a carboxyl group can also be produced by solvent mixing in a common solvent such as dimethylformaldehyde (DMF).<sup>[317]</sup>

Other carbon fillers such as graphene can also be coated with PANI via similar methods to CNTs (i.e., via in situ polymerization or solution blending). When added into PANI, graphene has a better dispersion than CNTs,<sup>[318]</sup> however, the effect of graphene on conductivity is still the subject of debate in the literature. For example, when the solution casting method was used, the PANI–graphene composite was unable to reach the percolation threshold. However, Baniasadi et al.<sup>[319]</sup> reported a slight improvement in conductivity (from 2 to 7 S cm<sup>−1</sup>) when less than 1 wt% of graphene was incorporated into a PANI matrix. This improvement of conductivity in PANI in the presence of graphene was attributed to the strong van der Waals interaction that enhances the charge transfer within the composite.<sup>[320]</sup>

In spite of the potential advantages that are disclosed by the improvement strategies discussed so far, producing these hybrid

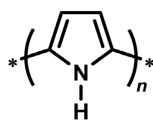


**Figure 19.** Diagram showing the chemical structure of PPy. Reproduced (Adapted) with permission.<sup>[322]</sup> Copyright 2018, MDPI.

fillers (either with solvent mixing or with in situ polymerization) may be time-consuming, especially if they require purification before melt blending. It is still unclear how severely the conductivity of PANI hybrid fillers will be affected with purification and melt blending steps with a thermoplastic matrix to extrude FFF filaments for printing.

## 10.2. PPy

PPy is a conductive polymer produced from an oxidative polymerization reaction of pyrrole using ammonium persulfate as an oxidant<sup>[321]</sup> and can be doped in a similar manner to PANI (Figure 19). It can reach a conductivity of  $100 \text{ S cm}^{-1}$  upon doping,<sup>[322]</sup> but its conductivity is sensitive to pH changes.<sup>[323]</sup> Similar to PANI, the use of PPy is limited due to its poor solubility in most solvents and its inability to be melt processed. Although there are potential uses for PPy in thermoplastic blends, PPy, like PANI, requires doping to enable processability into thermoplastics either via solution- or melt-based methods.

Given the limited processability of PPy, dopants can be utilized to increase its compatibility with thermoplastics. DBSA is shown to be effective, particularly when combined with MMT, (montmorillonite–dodecylbenzenesulfonic acid-doped PPy (MMT–DBSA-PPy)) to enable the melt blending of TPU composites, which results in a composite with a lower percolation threshold (10 wt%) than composites without MMT.<sup>[324]</sup> This can be attributed to improved dispersion of MMT–DBSA-PPy due to the enhanced compatibility with the filler in the presence of MMT and the TPU matrix. In terms of solution-based production methods of conductive composites (i.e., in situ polymerization and solution casting) there are several ways to increase PPy solubility in organic solvents. Although PPy remains insoluble in common organic solvents, it can be made soluble in nonpolar or weakly polar organic solvents when doped with functionalized protonic acids. A way is to combine it with additives that are able to prevent strong interactions between PPy molecules by inserting themselves in between, as summarized in the review published by Sasso et al.<sup>[325]</sup> For example, DBSA is able to penetrate between PPy molecules and act as a spacer. The increased intermolecular distance allows organic solvents to diffuse and dissolve PPy. Also, DBSA may work as a surfactant, promoting the ionic form of the dodecylbenzenesulfonic acid pyrrole salt and ultimately cross-linking, which increases the compatibility with insulating polymers and the solubility in organic solvents. Kotal et al.<sup>[326]</sup> compared the different structures that can be obtained when TPU/DBSA-PPy (PPy doped with DBSA) nanoblends are prepared in the same solvent (THF) either by solvent mixing TPU and DBSA-PPy or by inducing the in situ polymerization of PPy in a solution containing

TPU and DBSA. As a result of the different processing route, Kotal et al.<sup>[326]</sup> found that the solution blended TPU/DBSA-PPy system had higher conductivity than the in situ polymerized counterpart due to the development of a hexagonal segregated structure (similar in Figure 12).

Multicomponent composites containing a combination of PPy and conductive fillers or nanoclay have been proposed in the literature to improve the conductivity over PPy used alone. Bertolini et al.<sup>[327]</sup> melt blended TPU with a mixture of CNTs and CB modified with PPy (PPy-CB) and found the highest conductivity at 3 wt% CNTs and 15 wt% PPy-CB. PPy-CB fillers are produced similar to the hybrid fillers with PANI (Section 10.1.2) and use in situ polymerization to directly polymerize PPy on the filler's surface.<sup>[328]</sup> In another study, upon doping with DBSA, in situ polymerized PPy/MMT fillers led to higher conductivity than neat PPy when dispersed in a TPU matrix.<sup>[329]</sup> Peighambardoust et al.<sup>[330]</sup> prepared a PA6-matrix composite with in situ polymerized PPy/MMT and observed conductivity of  $1.66 \times 10^{-4} \text{ S cm}^{-1}$  at 25 wt% PPy and 5 wt% MMT. Debnath et al.<sup>[331]</sup> melt blended CB and nanoclays to improve the mechanical strength of ABS/PPy and ABS/PANI blends. As CB and nanoclay fillers worked as a heat absorber, the processability of ABS/PPy and ABS/PANI blends was improved, but it is unclear what the effect was on electrical conductivity. Processing of CB in thermoplastics can be improved by coating PANI or PPy onto the CB filler (via in situ polymerization) which has been shown to improve thermal processing of either conductive polymer (PANI or PPy).<sup>[332]</sup> Conductive fillers such as PPy/CNT systems have been prepared via in situ polymerization and, once combined with TPU, have demonstrated significantly higher electromagnetic shield interference (EMI) shielding capability and improved conductivity than PPy alone.<sup>[333]</sup> PPy-conductive filler combinations such as PPy-graphene can also significantly reduce the percolation threshold when blended in either POM, PMMA, or PP matrices, but the final conductivity is largely affected by the nature and inherent properties of the polymer matrix.<sup>[334]</sup>

The applicability of PPy composites in FFF has already been demonstrated by Bertolini et al.,<sup>[335]</sup> who melt blended PVDF/TPU with PPy-coated CB. The conductive PPy-CB filler was shown to preferentially localize in the PVDF matrix. Increasing the relative amount of PVDF lowered the percolation threshold, but the filler loading required to achieve a conductivity of  $4.14 \text{ S m}^{-1}$  was quite high (i.e., 6.77 vol% of CB-PPy) as a consequence of the considerable increase in voids with increasing levels of CB-PPy. However, the elastic modulus remained relatively low (0.43 GPa).

## 11. Conclusions

The development of conductive composites as an alternative to traditional materials like copper and other metals has been driven by factors such as the progressive uptake of thermoplastic-based AM technologies, the deployment of Industry 4.0 innovations and the increasing need for flexible, soft, or noncorrodible materials to be used in emerging fields of robotics, cybernetics, artificial intelligence, and biomedicine. However, the outstanding advancement in conductive capability

of thermoplastic composites that has been observed in the literature over the last 20 years has not yet been fully extended to FFF and significant gaps must be bridged before developers and engineers can take advantage of the new paradigm of FFF of conductive materials.

Limited understanding of the effect of FFF on conductivity. The effect of printing on mechanical properties and mechanical anisotropy of FFF parts is well understood, as well as the influence of voids or other print defects. Conversely, there is only a small portion of literature dedicated to understanding the effect of printing parameters and defects on the conductive properties and anisotropy of printed parts.

Limited selection of studied thermoplastics. The literature on electrical properties is mainly focused on a handful of polymers, especially PLA, ABS, and TPU, which only represent a small portion of feedstock materials available for FFF. Also, due to the lack of data, it is unclear how changes to the chemical nature and structure of the polymer matrix with different monomers or side groups may affect the overall conductivity of the composite material, especially after extruding and printing.

Underutilization of double percolation structures. The intentional localization of the conductive filler within selected areas of a polymeric blend can greatly assist in reducing the filler loading required for the transition between insulating to conductive behavior. There is a tendency for a filler to migrate to a particular polymer region or to the interphase region between the polymers attributed due to surface tension. Some FFF studies have created this double percolation structure unintentionally by blending immiscible polymer blends with conductive fillers. However, research is still missing to arbitrarily cause and control selective localization in FFF. The preferential distribution of conductive fillers within the polymer blend can be predicted with wetting measurements, and therefore this intentional design of double percolation into a thermoplastic nanocomposite may be achieved in FFF to create ultralow percolation thresholds.

Lack of covalent/noncovalent functionalization of carbon-based fillers. As critically discussed in this review, both covalent and noncovalent functionalization of carbonaceous fillers in a thermoplastic matrix can greatly improve distribution and thereby reduce the filler loading required for percolation. An analysis of the available literature regarding the development of conductive thermoplastic composites in FFF shows that there are very few examples that encourage homogenous distribution of carbonaceous fillers either via covalent or noncovalent functionalization. Yet, despite these few occurrences, these methods are still largely underutilized in conductive FFF studies.

Limited use of metallic fillers. Depending on the type of metallic filler, there are significant limitations to using these fillers in conductive FFF composites. LMPAs are mainly tin alloys that can rapidly oxidize and aggregate in thermoplastic blends. Silver, which is highly conductive and resistant to oxidation, is also very expensive. Another downside of silver is that it is difficult to process at nanoscale dimensions. Working with relatively large silver fillers may require 20 wt% to induce percolation and may cause clogging issues upon printing by FFF. Copper needs protection from oxidation when the polymer-matrix composite must be extruded and printed. Although copper can be easily coated with silver or carbon to prevent it from oxidizing and losing conductivity, copper-based core-shell fillers may cause issues with FFF

printing like nozzle clogging or agglomeration. As a result of these factors, metallic fillers are less popular than carbonaceous fillers for the development of FFF materials and additional efforts are needed to enable further research in this area.

Unknown impact of FFF on conductive polymers and their blends. Conductive polymers, while very useful to produce conductive polymer blends, can lose their conductivity upon melt extruding at the typical melting temperatures of thermoplastics used in FFF. This can be mitigated, for example, by choosing a low melting point thermoplastic (like EVA) or doping with various acidic agents that promote a higher deprotonation temperature. However, the main limitation is that the production of these conductive polymers relies on solvent casting or in situ polymerization methods. As a consequence, the amount of obtained polymer is typically small compared to the amount needed to produce a conductive filament for FFF. Also, these polymers require a thorough purification before melt extruding. Owing to these technical hurdles, conductive polymers are rarely seen in FFF and there is a lack of knowledge regarding the effect of printing on the properties, especially the conductivity, of these polymers. If the production and purification steps were successfully scaled up to produce industrial amounts, the usage of conductive polymers in FFF materials with conductive properties would be expanded.

Use of hybrid conductive polymer—conductive fillers. Hybrid fillers with a carbon-based core (such as CNTs or graphene) and a conductive polymer shell are useful in several ways. The polymeric shell prevents aggregation of carbonaceous fillers and the direct polymerization of conductive polymers onto the surface of the filler is an efficient utilization of the polymer without needing to produce large quantities. Thus, these fillers offer several advantages, but they are still severely underutilized in the development of conductive composites for FFF.

## Acknowledgements

Thanks to the Commonwealth Scientific and Industrial Research Organisation (CSIRO) that provided the necessary materials and capability for this review. AS and DPS are supported by the CSIRO Research Office through the 'Science Leader in Active Materials' grant.

## Conflict of Interest

The authors declare no conflict of interest.

## Keywords

additive manufacturing, composite materials, electrical conductivity, fused deposition modeling (FDM), fused filament fabrication (FFF)

Received: October 27, 2021

Revised: March 6, 2022

Published online: April 4, 2022

[1] U. M. Dilberoglu, B. Gharehpapagh, U. Yaman, M. Dolen, *Procedia Manuf.* **2017**, *11*, 545.

[2] Z. Hou, X. Tian, J. Zhang, D. Li, *Compos. Struct.* **2018**, *184*, 1005.

- [3] G. D. Goh, W. Toh, Y. L. Yap, T. Y. Ng, W. Y. Yeong, *Compos. Part B Eng.* **2021**, 216, 108840.
- [4] B. G. Compton, J. A. Lewis, *Adv. Mater.* **2014**, 26, 6043.
- [5] *ISO/ASTM52900-15, ASTM Int.* **2015**.
- [6] M. Mehrali, S. Bagherifard, M. Akbari, A. Thakur, B. Mirani, M. Mehrali, M. Hasany, G. Orive, P. Das, J. Emneus, T. L. Andresen, A. Dolatshahi-Pirouz, *Adv. Sci.* **2018**, 5, 1700931.
- [7] B. C. K. Tee, J. Ouyang, *Adv. Mater.* **2018**, 30, 1802560.
- [8] D. V. Baker, C. Bao, W. S. Kim, *ACS Appl. Electron. Mater.* **2021**, 3, 2423.
- [9] Z. Hou, H. Lu, Y. Li, L. Yang, Y. Gao, *Front. Mater.* **2021**, 8, 91.
- [10] A. Joshi, J. K. Goh, K. E. J. Goh, in *3D and 4D Printing of Polymer Nanocomposite Materials: Processes, Applications, and Challenges*, Elsevier, Amsterdam **2019**, pp. 45–83.
- [11] Conducting polymers forward, *Nat. Mater.* **2020**, 19, 921.
- [12] A. E. Costa, A. Ferreira da Silva, O. Sousa Carneiro, *Rapid Prototyp. J.* **2019**, 25, 555.
- [13] Q. Sun, G. M. Rizvi, C. T. Bellehumeur, P. Gu, *Rapid Prototyp. J.* **2008**, 14, 72.
- [14] L. Lu, O. Ishiyama, *Iron Ore: Mineralogy, Processing and Environmental Sustainability*, Woodhead Publishing, Sawston, United Kingdom **2015**, p. 395.
- [15] Z. Zhang, K. Fu, Y. Li, *Compos. Commun.* **2021**, 27, 100898.
- [16] T. J. Godelier, P. R. Thies, L. Turner, L. Johanning, *Rapid Prototyping J.* **2019**, 25, 953.
- [17] C. C. Shih, M. Burnette, D. Staack, J. Wang, B. L. Tai, *Addit. Manuf.* **2019**, 25, 104.
- [18] M. F. Arif, S. Kumar, K. M. Varadarajan, W. J. Cantwell, *Mater. Des.* **2018**, 146, 249.
- [19] R. M. Mutiso, K. I. Winey, in *Polymer Science: A Comprehensive Reference, 10 Volume Set*, Elsevier, Amsterdam Amsterdam **2012**, pp. 327–344.
- [20] A. B. Oskouyi, U. Sundararaj, P. Mertiny, *Materials* **2014**, 7, 2501.
- [21] A. Malas, in *Progress in Rubber Nanocomposites*, Woodhead Publishing, Sawston **2017**, pp. 179–229.
- [22] N. Johnner, C. Grimaldi, I. Balberg, P. Ryser, *Phys. Rev. B - Condens. Matter Mater. Phys.* **2008**, 77, 174204.
- [23] W. Bauhofer, J. Z. Kovacs, *Compos. Sci. Technol.* **2009**, 69, 1486.
- [24] S. Cano, T. Lube, P. Huber, A. Gallego, J. A. Naranjo, C. Berges, S. Schuschnigg, G. Herranz, C. Kukla, C. Holzer, J. Gonzalez-Gutierrez, *Materials* **2020**, 13, 3158.
- [25] X. Gao, D. Zhang, S. Qi, X. Wen, Y. Su, *J. Appl. Polym. Sci.* **2019**, 136, 47824.
- [26] P. Olesik, M. Godzierz, M. Koziol, *Materials* **2019**, 12, 2520.
- [27] C. Vălean, L. Marşavina, M. Mărghiţăş, E. Linul, J. Razavi, F. Berto, in *Procedia Struct. Integr.*, Elsevier, Amsterdam **2020**, pp. 313–320.
- [28] M. Ouhsti, B. El Haddadi, S. Belhouideg, *Mech. Mech. Eng.* **2018**, 22, 895.
- [29] G. Ćwikła, C. Grabowik, K. Kalinowski, I. Paprocka, P. Ociepa, *IOP Conf. Ser. Mater. Sci. Eng.* **2017**, 227, 012033.
- [30] L. G. Ecco, S. Dul, D. P. Schmitz, G. M. de O. Barra, B. G. Soares, L. Fambri, A. Pegoretti, *Appl. Sci.* **2018**, 9, 37.
- [31] A. Dorigato, V. Moretti, S. Dul, S. H. Unterberger, A. Pegoretti, *Synth. Met.* **2017**, 226, 7.
- [32] K. Prashantha, F. Roger, J. Macromol. *Sci. Part A Pure Appl. Chem.* **2017**, 54, 24.
- [33] S. J. Leigh, R. J. Bradley, C. P. Purcell, D. R. Billson, D. A. Hutchins, *PLoS One* **2012**, 7, 49365.
- [34] K. Gnanasekaran, T. Heijmans, S. van Bennekom, H. Woldhuis, S. Wijnia, G. de With, H. Friedrich, *Appl. Mater. Today* **2017**, 9, 21.
- [35] I. Tirado-Garcia, D. Garcia-Gonzalez, S. Garzon-Hernandez, A. Rusinek, G. Robles, J. M. Martinez-Tarifa, A. Arias, *Compos. Struct.* **2021**, 265, 113744.
- [36] A. Dijkshoorn, M. Schouten, S. Stramigioli, G. Krijnen, *Sensors* **2021**, 21, 3710.
- [37] J. Zhang, B. Yang, F. Fu, F. You, X. Dong, M. Dai, *Appl. Sci.* **2017**, 7, 20.
- [38] S. Mousavi, D. Howard, F. Zhang, J. Leng, C. H. Wang, *ACS Appl. Mater. Interfaces* **2020**, 12, 15631.
- [39] C. J. Hohimer, G. Petrossian, A. Ameli, C. Mo, P. Pötschke, *Addit. Manuf.* **2020**, 34, 101281.
- [40] C. J. Hohimer, G. Petrossian, A. Ameli, C. Mo, P. Pötschke, in *105960*, International Society for Optics and Photonics, **2018**, p. 15.
- [41] A. Abdalla, H. H. Hamzah, O. Keattch, D. Covill, B. A. Patel, *Electrochim. Acta* **2020**, 354, 136618.
- [42] T. Sathies, P. Senthil, C. Prakash, *Mater. Res. Express* **2019**, 6, 115349.
- [43] A. Dijkshoorn, P. Neuvel, S. Stramigioli, G. Krijnen, in *Proc. IEEE Sensors, Virtual Conference, Institute of Electrical and Electronics Engineers Inc.*, **2020**.
- [44] D. Ravoori, S. Salvi, H. Prajapati, M. Qasaimeh, A. Adnan, A. Jain, *Virtual Phys. Prototyping* **2021**, 16, 146.
- [45] H. K. Sezer, O. Eren, *J. Manuf. Process.* **2019**, 37, 339.
- [46] D. P. Schmitz, S. Dul, S. D. A. S. Ramoa, B. G. Soares, G. M. O. Barra, A. Pegoretti, *J. Manuf. Process.* **2021**, 65, 12.
- [47] D. P. Schmitz, T. I. Silva, S. D. A. S. Ramoa, G. M. O. Barra, A. Pegoretti, B. G. Soares, *J. Appl. Polym. Sci.* **2018**, 135, 46546.
- [48] R. S. Chisena, S. M. Engstrom, A. J. Shih, *Addit. Manuf.* **2020**, 34, 101189.
- [49] J. E. Little, X. Yuan, M. I. Jones, *NDT&E Int.* **2012**, 46, 122.
- [50] S. C. Garcea, Y. Wang, P. J. Withers, *Compos. Sci. Technol.* **2018**, 156, 305.
- [51] R. M. Dunn, K. R. Hart, E. D. Wetzel, *Prog. Addit. Manuf.* **2019**, 4, 233.
- [52] M. Handwerker, J. Wellnitz, H. Marzbani, U. Tetzlaff, *Compos. Part B Eng.* **2021**, 223, 109119.
- [53] R. V. Pazhamannil, N. Krishnan, C. P. Govindan, A. Edacherian, *Adv. Mater. Process. Technol.* **2021**, 1, <https://doi.org/10.1080/2374068X.2021.1946753>.
- [54] J. S. Tate, R. P. Brushaber, E. Danielsen, H. Kallagunta, S. V. Navale, O. Arigbabowo, S. Shree, A. Yaseer, in *Solid Free. Fabr. 2019 Proc. 30th Annu. Int. Solid Free. Fabr. Symp. - An Addit. Manuf. Conf. SFF 2019*, Austin, Texas, USA **2019**, pp. 1008–1021.
- [55] J. R. Nixon, D. I. Bigio, in *ASME Int. Mech. Eng. Congr. Expo. Proc.*, American Society of Mechanical Engineers Digital Collection, Houston, Texas, United States **2015**.
- [56] D. Thaler, N. Aliheidari, A. Ameli, in *ASME 2018 Conf. Smart Mater. Adapt. Struct. Intell. Syst. SMASIS 2018*, American Society of Mechanical Engineers Digital Collection, San Antonio, Texas, United States **2018**.
- [57] S. M. Haque, J. A. A. Rey, A. A. Masúd, Y. Umar, R. Albarracin, in *Properties and Applications of Polymer Dielectrics*, IntechOpen, **2017**.
- [58] J. Pan, in *Modelling Degradation of Bioresorbable Polymeric Medical Devices*, Woodhead Publishing, Sawston **2015**, pp. 53–69.
- [59] M. Gültner, L. Häußler, P. Pötschke, *AIP Conf. Proc.* **2017**, 030022.
- [60] B. A. Alshammari, F. S. Al-Mubaddel, M. R. Karim, M. Hossain, A. S. Al-Mutairi, A. N. Wilkinson, *Polymers* **2019**, 11, 1411.
- [61] K. Kalaitzidou, H. Fukushima, P. Askeland, L. T. Drzal, *J. Mater. Sci.* **2008**, 43, 2895.
- [62] X. He, H. Shou, X. Liu, K. Jia, *Polym. Bull.* **2021**, <https://doi.org/10.1007/s00289-021-03725-7>.
- [63] Y. Shmueli, Y. C. Lin, X. Zuo, Y. Guo, S. Lee, G. Freychet, M. Zhernenkov, T. Kim, R. Tannenbaum, G. Marom, D. Gersappe, M. H. Rafailovich, *Compos. Sci. Technol.* **2020**, 196, 108227.
- [64] H. R. Vanaei, K. Raissi, M. Deligant, M. Shirinbayan, J. Fitoussi, S. Khelladi, A. Tcharkhtchi, *J. Mater. Sci.* **2020**, 55, 14677.

- [65] F. Alam, K. M. Varadarajan, J. H. Koo, B. L. Wardle, S. Kumar, *Adv. Eng. Mater.* **2020**, 22, 2000483.
- [66] M. F. Arif, H. Alhashmi, K. M. Varadarajan, J. H. Koo, A. J. Hart, S. Kumar, *Compos. Part B Eng.* **2020**, 184, 107625.
- [67] J. Wang, Y. Kazemi, S. Wang, M. Hamidinejad, M. B. Mahmud, P. Pötschke, C. B. Park, *Compos. Part B Eng.* **2020**, 183, 107663.
- [68] P. Pan, Z. Liang, B. Zhu, T. Dong, Y. Inoue, *Macromolecules* **2008**, 41, 8011.
- [69] D. Auhl, F. Rohnstock, O. Löschke, K. Schäfer, P. Wang, M. H. Wagner, *AIP Conf. Proc.*, **2019**, 14, 2556.
- [70] B. B. Shahriar, C. France, N. Valerie, C. Arthur, G. Christian, *AIP Conf. Proc.* **2017**, 040008.
- [71] K. P. M. Lee, M. Brandt, R. Shanks, F. Daver, *Polymers* **2020**, 12, 1.
- [72] M. Rinaldi, T. Ghidini, F. Nanni, *Polym. Int.* **2021**, 70, 1080.
- [73] Q. Li, W. Zhao, B. Niu, Y. Wang, X. Wu, J. Ji, Y. Li, T. Zhao, H. Li, G. Wang, *Mater. Des.* **2021**, 198, 109333.
- [74] Y. S. Ko, D. Herrmann, O. Tolar, W. J. Elspass, C. Brändli, *Addit. Manuf.* **2019**, 29, 100815.
- [75] X. Gao, S. Qi, B. Yang, Y. Su, J. Li, D. Wang, *Polymer* **2021**, 215, 123426.
- [76] J. K. Palacios, A. Ben Fekih, C. Yus Argon, S. Irusta, S. Jestin, S. Dagréou, *Polym. Int.* **2021**, 70, 1329.
- [77] K. S. Deepa, S. Kumari Nisha, P. Parameswaran, M. T. Sebastian, J. James, *Appl. Phys. Lett.* **2009**, 94, 142902.
- [78] A. Atashpendar, T. Ingenbrand, T. Schilling, *Phys. Rev. E* **2020**, 101, 032706.
- [79] N. Vidakis, M. Petousis, L. Tzounis, E. Velidakis, N. Mountakis, S. A. Grammatikos, *C* **2021**, 7, 38.
- [80] S. Malekie, F. Ziaie, *5th Int. Congr. Nanosci. Nanotechnol.*, Edinburgh, Scotland **2014**, p. 154.
- [81] S. H. Yao, Z. M. Dang, M. J. Jiang, H. P. Xu, J. Bai, *Appl. Phys. Lett.* **2007**, 91, 212901.
- [82] R. Ram, M. Rahaman, A. Aldalbahi, D. Khastgir, *Polym. Int.* **2017**, 66, 573.
- [83] B. Shin, S. Mondal, M. Lee, S. Kim, Y. Il Huh, C. Nah, *Chem. Eng. J.* **2021**, 418, 129282.
- [84] T. Schilling, M. A. Miller, P. Van Der Schoot, *EPL* **2015**, 111, 56004.
- [85] J. Sethi, E. Sarlin, S. S. Meysami, R. Suihkonen, A. R. S. Santha Kumar, M. Honkanen, P. Keinänen, N. Grobert, J. Vuorinen, *Compos. Part A Appl. Sci. Manuf.* **2017**, 102, 305.
- [86] Y. Zare, K. Y. Rhee, *Polymers* **2020**, 12, 182.
- [87] D. Zhang, B. Chi, B. Li, Z. Gao, Y. Du, J. Guo, J. Wei, *Synth. Met.* **2016**, 217, 79.
- [88] X. Lu, J. Yvonnet, F. Detrez, J. Bai, *J. Compos. Mater.* **2018**, 52, 2767.
- [89] G. Ambrosetti, N. Johner, C. Grimaldi, A. Danani, P. Ryser, *Phys. Rev. E - Stat. Nonlinear, Soft Matter Phys.* **2008**, 78, 061126.
- [90] H. P. Wu, X. J. Wu, M. Y. Ge, Q. Q. Zhang, Y. W. Wang, J. Z. Jiang, *Compos. Sci. Technol.* **2007**, 67, 1116.
- [91] V. Nienhaus, K. Smith, D. Spiehl, E. Dörsam, *Addit. Manuf.* **2019**, 28, 711.
- [92] T. Beran, T. Mulholland, F. Henning, N. Rudolph, T. A. Osswald, *Addit. Manuf.* **2018**, 23, 206.
- [93] M. A. Azad, D. Olawuni, G. Kimbell, A. Z. M. Badruddoza, M. S. Hossain, T. Sultana, *Pharmaceutics* **2020**, 12, 124.
- [94] A. Alexandre, F. A. Cruz Sanchez, H. Boudaoud, M. Camargo, J. M. Pearce, *3D Print. Addit. Manuf.* **2020**, 7, 237.
- [95] Y. P. Shaik, J. Schuster, A. Shaik, *OALib* **2021**, 8, 1.
- [96] Z. A. A. Ghaleb, M. Jaafar, A. A. Rashid, in *Carbon-Based Nanofillers Their Rubber Nanocomposites Fundam. Appl.*, Elsevier, Amsterdam **2019**, pp. 49–63.
- [97] P. Verma, J. Ubaid, K. M. Varadarajan, B. L. Wardle, S. Kumar, *ACS Appl. Mater. Interfaces* **2022**, 14, 8361.
- [98] Y. Y. Huang, E. M. Terentjev, *Polymers* **2012**, 4, 275.
- [99] G. R. Kasaliwal, S. Pegel, A. Gödel, P. Pötschke Petra, G. Heinrich, *Polymer* **2010**, 51, 2708.
- [100] S. P. Rwei, I. Manas-Zloczower, D. L. Feke, *Polym. Eng. Sci.* **1992**, 32, 130.
- [101] S. P. Rwei, I. Manas-Zloczower, D. L. Feke, *Polym. Eng. Sci.* **1990**, 30, 701.
- [102] T. Wang, B. Song, K. Qiao, Y. Huang, L. Wang, *Nanomaterials* **2018**, 8, 996.
- [103] T. Feuerbach, S. Callau-Mendoza, M. Thommes, *Pharm. Dev. Technol.* **2019**, 24, 487.
- [104] E. T. Thostenson, T. W. Chou, *Carbon N. Y.* **2006**, 44, 3022.
- [105] A. Caradonna, C. Badini, E. Padovano, M. Pietroluongo, *Materials* **2019**, 12, 1522.
- [106] M. A. Raza, A. V. K. Westwood, A. P. Brown, C. Stirling, *Compos. Sci. Technol.* **2012**, 72, 467.
- [107] L. Li, H. Shi, Z. Liu, L. Mi, G. Zheng, C. Liu, K. Dai, C. Shen, *ACS Appl. Nano Mater.* **2019**, 2, 3636.
- [108] W. Tang, B. Liu, Z. Liu, J. Tang, H. Yuan, *J. Appl. Polym. Sci.* **2012**, 123, 1032.
- [109] A. Shrivastava, *Introduction to Plastics Engineering*, William Andrew Publishing, Norwich, New York, United States **2018**, p. 143.
- [110] E. M. Mount, in *Applied Plastics Engineering Handbook: Processing, Materials, and Applications*, 2nd ed., William Andrew Publishing, **2017**, pp. 217–264.
- [111] M. Micusík, M. Ormastoja, I. Krupa, J. Prokes, P. Pissis, E. Logakis, C. Pandis, P. Pötschke, J. Pionteck, *J. Appl. Polym. Sci.* **2009**, 113, 2536.
- [112] T. Villmow, P. Pötschke, S. Pegel, L. Häussler, B. Kretzschmar, *Polymer* **2008**, 49, 3500.
- [113] S. Besco, A. Lorenzetti, D. Hrelja, C. Boaretti, M. Roso, D. Ferri, M. Modesti, *Macromol. Mater. Eng.* **2014**, 299, 814.
- [114] B. Krause, P. Pötschke, L. Häußler, *Compos. Sci. Technol.* **2009**, 69, 1505.
- [115] G. Kasaliwal, A. Gödel, P. Pötschke, *J. Appl. Polym. Sci.* **2009**, 112, 3494.
- [116] C. McClory, P. Pötschke, T. McNally, *Macromol. Mater. Eng.* **2011**, 296, 59.
- [117] R. Socher, B. Krause, M. T. Müller, R. Boldt, P. Pötschke, *Polymer* **2012**, 53, 495.
- [118] L. E. Solorio-Rodríguez, A. Vega-Rios, *Appl. Sci.* **2019**, 9, 5153.
- [119] K. L. Lu, R. M. Lago, Y. K. Chen, M. L. H. Green, P. J. F. Harris, S. C. Tsang, *Carbon N. Y.* **1996**, 34, 814.
- [120] H. Renhofer, B. Zanghellini, *Nanomaterials* **2021**, 11, 1469.
- [121] A. P. Sobha, P. S. Sreekala, S. K. Narayanankutty, *Prog. Org. Coatings* **2017**, 113, 168.
- [122] A. P. Sobha, S. K. Narayanankutty, *Sens. Actuators, A Phys.* **2015**, 233, 98.
- [123] H. Abdali, A. Ajji, in *Carbon Nanostructures*, Springer, Singapore, **2019**, pp. 127–156.
- [124] N. Parveen, N. Mahato, M. O. Ansari, M. H. Cho, *Compos. Part B Eng.* **2016**, 87, 281.
- [125] J. Abraham, M. Arif, S. Thomas, in *2016 Young Res. Vac. Micro/Nano Electron. VMNE-YR 2016 - Proc.*, Institute of Electrical and Electronics Engineers Inc., **2017**.
- [126] G. S. Sandhu, R. Singh, in *Addit. Manuf. Emerg. Mater.*, Springer, Cham, **2018**, pp. 279–297.
- [127] B. S. Talwar, S. Guo, K. Chizari, D. Theriault, in *ASME Int. Mech. Eng. Congr. Expo. Proc.*, American Society Of Mechanical Engineers (ASME), Columbus, Ohio, United States **2014**.
- [128] E. Dal Lago, E. Cagnin, C. Boaretti, M. Roso, A. Lorenzetti, M. Modesti, *Polymers* **2020**, 12, 29.

- [129] K. Ke, Y. Wang, X. Q. Liu, J. Cao, Y. Luo, W. Yang, B. H. Xie, M. B. Yang, *Compos. Part B Eng.* **2012**, 43, 1425.
- [130] G. Spinelli, P. Lamberti, V. Tucci, R. Kotsilkova, S. Tabakova, R. Ivanova, P. Angelova, V. Angelov, E. Ivanov, R. Di Maio, C. Silvestre, D. Meisak, A. Paddubskaya, P. Kuzhir, *Materials* **2018**, 11, 2256.
- [131] R. Adami, P. Lamberti, D. Bychanok, P. Kuzhir, V. Tucci, *Chem. Eng. Trans.* **2021**, 84, 109.
- [132] K. Sakunphokesup, P. Kongkengkri, A. Pongwisuthiruchte, C. Aumnate, P. Potiyaraj, *IOP Conf. Ser. Mater. Sci. Eng.* **2019**, 600, 012001.
- [133] G. Gorrasí, A. Sorrentino, *Green Chem.* **2015**, 17, 2610.
- [134] F. Delogu, G. Gorrasí, A. Sorrentino, *Prog. Mater. Sci.* **2017**, 86, 75.
- [135] Y. Park, J. Ko, T. K. Ahn, S. Choe, *J. Polym. Sci. Part B Polym. Phys.* **1997**, 35, 807.
- [136] BASF, **2015**, p. 20.
- [137] K. Pontes, T. Indrasiak, B. G. Soares, *J. Appl. Polym. Sci.* **2021**, 138, 49705.
- [138] R. Dweiri, H. Suherman, A. B. Sulong, J. F. Al-Sharab, *Sci. Eng. Compos. Mater.* **2018**, 25, 1177.
- [139] H. Wu, B. Rook, L. T. Drzal, *Polym. Compos.* **2013**, 34, 426.
- [140] B. Wei, S. Yang, Q. Wang, *Polym. Adv. Technol.* **2021**, 32, 2576.
- [141] J. Jing, Y. Chen, S. Shi, L. Yang, P. Lambin, *Chem. Eng. J.* **2020**, 402, 126218.
- [142] H. J. Park, A. Badakhsh, I. T. Im, M. S. Kim, C. W. Park, *Appl. Therm. Eng.* **2016**, 107, 907.
- [143] P. C. Ma, J. K. Kim, B. Z. Tang, in *2006 Int. Conf. Electron. Mater. Packag. EMAP*, Hong Kong, China **2006**.
- [144] D. X. Yan, H. D. Huang, J. F. Gao, K. Dai, W. Q. Zhang, Z. M. Li, *J. Macromol. Sci. Part B Phys.* **2013**, 52, 167.
- [145] J. P. Soares da Silva, B. G. Soares, A. A. Silva, S. Livi, *Front. Mater.* **2019**, 6, 191.
- [146] J. Urquijo, S. Dagréou, G. Guerrica-Echevarría, J. I. Eguiazabal, *J. Appl. Polym. Sci.* **2017**, 134, 45265.
- [147] L. Zhou, Y. Tian, P. Xu, H. Wei, Y. Li, H. X. Peng, F. Qin, *Compos. Sci. Technol.* **2021**, 213, 108919.
- [148] M. Sumita, K. Sakata, S. Asai, K. Miyasaka, H. Nakagawa, *Polym. Bull.* **1991**, 25, 265.
- [149] J. Huang, C. Mao, Y. Zhu, W. Jiang, X. Yang, *Carbon N. Y.* **2014**, 73, 267.
- [150] M. Liebscher, M. O. Blais, P. Pötschke, G. Heinrich, *Polymer* **2013**, 54, 5875.
- [151] M. Gültner, A. Gödel, P. Pötschke, *Compos. Sci. Technol.* **2011**, 72, 41.
- [152] H. Bizhani, H. Nazockdast, V. Nayyeri, in *2017 IEEE MTT-S Int. Microw. Work. Ser. Adv. Mater. Process. RF THz Appl. IMWS-AMP 2017*, Institute of Electrical And Electronics Engineers Inc., Pavia, Italy **2018**, pp. 1–3.
- [153] M. H. Al-Saleh, *Polym. Bull.* **2016**, 73, 975.
- [154] M. H. Al-Saleh, U. Sundararaj, *Compos. Part A Appl. Sci. Manuf.* **2008**, 39, 284.
- [155] H. Pang, L. Xu, D. X. Yan, Z. M. Li, *Prog. Polym. Sci.* **2014**, 39, 1908.
- [156] G. Zitzenbacher, H. Dirnberger, M. Längauer, C. Holzer, *Polymers* **2017**, 10, 38.
- [157] A. Cayla, C. Campagne, M. Rochery, E. Devaux, *Synth. Met.* **2011**, 161, 1034.
- [158] D. Wu, Y. Zhang, M. Zhang, W. Yu, *Biomacromolecules* **2009**, 10, 417.
- [159] M. Sumita, K. Sakata, Y. Hayakawa, S. Asai, K. Miyasaka, M. Tanemura, *Colloid Polym. Sci.* **1992**, 270, 134.
- [160] Y. D. Shi, M. Lei, Y. F. Chen, K. Zhang, J. B. Zeng, M. Wang, *J. Phys. Chem. C* **2017**, 121, 3087.
- [161] C. Su, L. Xu, C. Zhang, J. Zhu, *Compos. Sci. Technol.* **2011**, 71, 1016.
- [162] I. González, J. I. Eguiazabal, J. Nazabal, *Compos. Part A Appl. Sci. Manuf.* **2012**, 43, 1482.
- [163] A. C. Baudouin, C. Bailly, J. Devaux, *Polym. Degrad. Stab.* **2010**, 95, 389.
- [164] K. Zhang, G. H. Li, L. M. Feng, N. Wang, J. Guo, K. Sun, K. X. Yu, J. B. Zeng, T. Li, Z. Guo, M. Wang, *J. Mater. Chem. C* **2017**, 5, 9359.
- [165] Y. Xu, H. Duan, Y. Liu, Y. Yang, G. Zhao, *Gaofenzi Cailiao Kexue Yu Gongcheng/Polymeric Mater. Sci. Eng.* **2017**, 33, 147.
- [166] R. Ravindren, S. Mondal, K. Nath, N. C. Das, *Compos. Part B Eng.* **2019**, 164, 559.
- [167] M. Zilberman, A. Siegmann, M. Narkis, *J. Macromol. Sci. Phys.* **2000**, 39, 333.
- [168] D. Mi, X. Li, Z. Zhao, Z. Jia, W. Zhu, *Polym. Compos.* **2021**, 42, 4277.
- [169] X. Q. Liu, W. Yang, B. H. Xie, M. B. Yang, *Mater. Des.* **2012**, 34, 355.
- [170] S. Zhang, H. Deng, Q. Zhang, Q. Fu, *ACS Appl. Mater. Interfaces*, **2014**, 6, 6835.
- [171] K. Kalaitzidou, H. Fukushima, L. T. Drzal, *Compos. Sci. Technol.* **2007**, 67, 2045.
- [172] K. Kalaitzidou, *Exfoliated Graphite Nanoplatelets as Reinforcement for Multifunctional Polypropylene Nanocomposites*, Michigan State University, Michigan, United States **2006**.
- [173] S. Shi, Z. Peng, J. Jing, L. Yang, Y. Chen, *ACS Sustainable Chem. Eng.* **2020**, 8, 7962.
- [174] P. A. Eutonnat-Diffo, A. Cayla, Y. Chen, J. Guan, V. Nierstraszc, C. Campagne, *Polymers* **2020**, 12, 1.
- [175] Z. Li, Z. Wang, X. Gan, D. Fu, G. Fei, H. Xia, *Macromol. Mater. Eng.* **2017**, 302, 1700211.
- [176] R. Hong, Z. Zhao, J. Leng, J. Wu, J. Zhang, *Compos. Part B Eng.* **2019**, 176, 107214.
- [177] S. Shi, Y. Chen, J. Jing, L. Yang, *RSC Adv.* **2019**, 9, 29980.
- [178] T. K. Das, S. Prusty, *Polym. Plast. Technol. Eng.* **2012**, 51, 1487.
- [179] S. Agarwala, G. L. Goh, G. D. Goh, V. Dikshit, W. Y. Yeong, in *3D 4D Print. Polym. Nanocomposite Mater. Process. Appl. Challenges*, Elsevier, Amsterdam **2019**, pp. 297–324.
- [180] A. Mora, P. Verma, S. Kumar, *Compos. Part B Eng.* **2020**, 183, 107600.
- [181] A. Almazrouei, R. A. Susantyoko, C. H. Wu, I. Mustafa, A. Alhammadi, S. Almheiri, *Sci. Rep.* **2019**, 9, 1.
- [182] B. Podsiadły, P. Matuszewski, A. Skalski, M. Stoma, *Appl. Sci.* **2021**, 11, 1.
- [183] J. Y. Han, T. Chen, D. G. Baird, *Polym. Compos.* **2021**, 42, 4328.
- [184] T. Feng, N. Liu, S. Wang, C. Qin, S. Shi, X. Zeng, G. Liu, T. Feng, N. Liu, S. Wang, C. Qin, S. Shi, X. Zeng, G. Liu, *Adv. Nano Res.* **2021**, 10, 559.
- [185] L. Lavagna, R. Nisticò, S. Musso, M. Pavese, *Mater. Today Chem.* **2021**, 20, 100477.
- [186] M. Raja, A. M. Shanmugharaj, S. H. Ryu, *Soft Mater.* **2008**, 6, 65.
- [187] C. Li, Q. Zhao, H. Deng, C. Chen, K. Wang, Q. Zhang, F. Chen, Q. Fu, *Polym. Int.* **2011**, 60, 1629.
- [188] M. Kwiatkowska, R. Pelech, A. Jedrzejewska, D. Moszyński, I. Pelech, *Polymers* **2020**, 12, 308.
- [189] J. Lee, M. Kim, C. K. Hong, S. E. Shim, *Meas. Sci. Technol.* **2007**, 18, 3707.
- [190] R. Ivanova, R. Kotsilkova, *Appl. Rheol.* **2018**, 28, 201854014.
- [191] M. Liebscher, T. Gärtner, L. Tzounis, M. Mičušik, P. Pötschke, M. Stamm, G. Heinrich, B. Voit, *Compos. Sci. Technol.* **2014**, 101, 133.
- [192] M. Namasivayam, M. R. Andersson, J. G. Shapter, *Polymers* **2021**, 13, 2447.
- [193] G. M. Kim, T. Kil, H. K. Lee, *Compos. Struct.* **2021**, 258, 113377.

- [194] C. Santillo, A. P. Godoy, R. K. Donato, R. J. Espanhol Andrade, G. G. Buonocore, H. Xia, M. Lavorgna, A. Sorrentino, *Compos. Sci. Technol.* **2021**, 207, 108742.
- [195] J. P. Soares da Silva, B. G. Soares, S. Livi, G. M. O. Barra, *Mater. Chem. Phys.* **2017**, 189, 162.
- [196] C. Xing, L. Zhao, J. You, W. Dong, X. Cao, Y. Li, *J. Phys. Chem. B* **2012**, 116, 8312.
- [197] P. Xu, H. Gui, Y. Hu, A. Bahader, Y. Ding, *J. Electron. Mater.* **2014**, 43, 2754.
- [198] C. W. Foster, M. P. Down, Y. Zhang, X. Ji, S. J. Rowley-Neale, G. C. Smith, P. J. Kelly, C. E. Banks, *Sci. Rep.* **2017**, 7, 1.
- [199] F. Novotný, V. Urbanová, J. Plutnar, M. Pumera, *ACS Appl. Mater. Interfaces* **2019**, 11, 35371.
- [200] I. Piekarczyk, J. Sorocki, I. Slomian, K. Wincza, S. Gruszczyński, in *Proc. 2018 8th IEEE-APS Top. Conf. Antennas Propag. Wirel. Commun. APWC 2018*, Institute of Electrical And Electronics Engineers Inc., Cartagena de Indias, Colombia **2018**, pp. 780–782.
- [201] J. Bustillos, D. Montero, P. Nautiyal, A. Loganathan, B. Boesl, A. Agarwal, *Polym. Compos.* **2018**, 39, 3877.
- [202] S. Rostom, M. D. Dadmun, *Polym. Chem.* **2019**, 10, 5967.
- [203] S. Dul, L. Fambri, A. Pegoretti, *Compos. Part A Appl. Sci. Manuf.* **2016**, 85, 181.
- [204] Y. S. Jun, J. G. Um, G. Jiang, G. Lui, A. Yu, *Compos. Part B Eng.* **2018**, 133, 218.
- [205] R. Singh, G. S. Sandhu, R. Penna, I. Farina, *Materials* **2017**, 10, 881.
- [206] C. Sainz-urruela, S. Vera-lópez, M. P. S. Andrés, A. M. Díez-pascual, *Int. J. Mol. Sci.* **2021**, 22, 3316.
- [207] S. Gomari, P. E. Namin, I. Ghasemi, *Iran. J. Polym. Sci. Technol.* **2019**, 32, 101.
- [208] T. S. Sreepasad, V. Berry, *Small* **2013**, 9, 341.
- [209] S. Quiles-Díaz, P. Enrique-Jimenez, D. G. Papageorgiou, F. Ania, A. Flores, I. A. Kinloch, M. A. Gómez-Fatou, R. J. Young, H. J. Salavagione, *Compos. Part A Appl. Sci. Manuf.* **2017**, 100, 31.
- [210] H. Pei, L. Yang, Y. Xiong, Y. Chen, S. Shi, J. Jing, *Plast. Rubber Compos.* **2021**, 50, 263.
- [211] S. Perumal, R. Atchudan, I. W. Cheong, *Polymers* **2021**, 13, 2375.
- [212] A. Mohammed, G. P. Simon, *Polym. Nanocomposites* **2006**, 297.
- [213] S. W. Kwok, K. H. H. Goh, Z. D. Tan, S. T. M. Tan, W. W. Tjiu, J. Y. Soh, Z. J. G. Ng, Y. Z. Chan, H. K. Hui, K. E. J. Goh, *Appl. Mater. Today* **2017**, 9, 167.
- [214] Z. Zhou, S. Wang, Y. Zhang, Y. Zhang, *J. Appl. Polym. Sci.* **2006**, 102, 4823.
- [215] P. Kumar Mishra, P. Senthil, *Mater. Today Commun.* **2020**, 23, 100955.
- [216] M. A. Tofighy, T. Mohammadi, in *Carbon-Based Nanofillers and Their Rubber Nanocomposites: Fundamentals and Applications*, Elsevier, Amsterdam **2019**, pp. 253–285.
- [217] L. Y. W. Loh, U. Gupta, Y. Wang, C. C. Foo, J. Zhu, W. F. Lu, *Adv. Eng. Mater.* **2021**, 23, 2001082.
- [218] A. F. João, A. L. Squizzato, E. M. Richter, R. A. A. Muñoz, *Anal. Bioanal. Chem.* **2020**, 412, 2755.
- [219] H. Khosman, K. N. Hafni, I. Surya, *IOP Conf. Ser. Earth Environ. Sci.* **2021**, 782, 022064.
- [220] A. Maurel, R. Russo, S. Grugeon, S. Panier, L. Dupont, *ECS J. Solid State Sci. Technol.* **2021**, 10, 037004.
- [221] C. Xing, Y. Wang, X. Huang, Y. Li, J. Li, *Macromolecules* **2016**, 49, 1026.
- [222] E. Bilotti, H. Zhang, H. Deng, R. Zhang, Q. Fu, T. Peijs, *Compos. Sci. Technol.* **2013**, 74, 85.
- [223] N. P. Kim, *Polymers* **2020**, 12, 1224.
- [224] S. M. Zhang, L. Lin, H. Deng, X. Gao, E. Bilotti, T. Peijs, Q. Zhang, Q. Fu, *Express Polym. Lett.* **2012**, 6, 159.
- [225] R. Kotsilkova, S. Tabakova, R. Ivanova, *Mech. Time-Dependent Mater.* **2021**, 2021, 1.
- [226] S. Dul, L. G. Ecco, A. Pegoretti, L. Fambri, *Polymers* **2020**, 12, 101.
- [227] J. Gonçalves, P. Lima, B. Krause, P. Pötschke, U. Lafont, J. R. Gomes, C. S. Abreu, M. C. Paiva, J. A. Covas, *Polymers* **2018**, 10, 925.
- [228] G. Spinelli, P. Lamberti, V. Tucci, R. Ivanova, S. Tabakova, E. Ivanov, R. Kotsilkova, S. Cimmino, R. Di Maio, C. Silvestre, *Compos. Part B Eng.* **2019**, 167, 467.
- [229] J. E. Contreras-Naranjo, V. H. Perez-Gonzalez, M. A. Mata-Gómez, O. Aguilar, *Electrochem. commun.* **2021**, 130, 107098.
- [230] J. J. Andrew, H. Alhashmi, A. Schiffer, S. Kumar, V. S. Deshpande, *Mater. Des.* **2021**, 208, 109863.
- [231] J. Galos, Y. Hu, A. R. Ravindran, R. B. Ladani, A. P. Mouritz, *Compos. Part A Appl. Sci. Manuf.* **2021**, 151, 106661.
- [232] S. M. F. Kabir, K. Mathur, A. F. M. Seyam, *Compos. Struct.* **2020**, 232, 111476.
- [233] J. M. Gardner, G. Sauti, J. W. Kim, R. J. Cano, R. A. Wincheski, C. J. Stelter, B. W. Grimsley, D. C. Working, E. J. Siochi, *Addit. Manuf.* **2016**, 12, 38.
- [234] C. Luan, X. Yao, C. Liu, L. Lan, J. Fu, *Carbon N. Y.* **2018**, 140, 100.
- [235] W. Ye, G. Lin, W. Wu, P. Geng, X. Hu, Z. Gao, J. Zhao, *Compos. Part A Appl. Sci. Manuf.* **2019**, 121, 457.
- [236] P. Bettini, G. Alitta, G. Sala, L. Di Landro, *J. Mater. Eng. Perform.* **2017**, 26, 843.
- [237] G. D. Goh, W. Y. Yeong, in *Proc. Int. Conf. Prog. Addit. Manuf.*, Pro-AM, **2018**, p. 505.
- [238] J. C. Abry, S. Bochar, A. Chateauminois, M. Salvia, G. Giraud, *Compos. Sci. Technol.* **1999**, 59, 925.
- [239] S. Wang, D. D. L. Chung, J. H. Chung, *J. Mater. Sci.* **2005**, 40, 6463.
- [240] C. Luan, X. Yao, C. Zhang, B. Wang, J. Fu, *Compos. Struct.* **2019**, 212, 552.
- [241] K. Dong, M. Panahi-Sarmad, Z. Cui, X. Huang, X. Xiao, *Compos. Part B Eng.* **2021**, 220, 108994.
- [242] A. T. Odularu, *Bioinorg. Chem. Appl.* **2018**, 9354708.
- [243] C. Kukla, J. Gonzalez-Gutierrez, I. Duretek, S. Schuschnigg, C. Holzer, *AIP Conf. Proc.* **2017**, 190006.
- [244] D. Amoabeng, S. S. Velankar, *Polym. Eng. Sci.* **2018**, 58, 1010.
- [245] G. Li, H. Xia, Y. Lei, W. Bin Yang, T. Liu, J. P. He, *J. Appl. Polym. Sci.* **2020**, 137, 48820.
- [246] N. Warriar, K. H. Kate, *Prog. Addit. Manuf.* **2018**, 3, 51.
- [247] J. Mireles, H. C. Kim, I. H. Lee, D. Espalin, F. Medina, E. Macdonald, R. Wicker, *J. Electron. Packag. Trans.* **2013**, 135, 011008.
- [248] J. C. Tan, H. Y. Low, *Addit. Manuf.* **2018**, 23, 294.
- [249] J. C. Tan, H. Y. Low, *Addit. Manuf.* **2020**, 36, 101551.
- [250] Y. Zhu, Y. Zhao, X. Zhang, L. Wang, X. Wang, J. Zhang, P. Han, J. Qiao, *Mater. Lett.* **2016**, 173, 26.
- [251] G. Chen, X. Hong Zhang, J. Liang Qiao, *Chinese J. Polym. Sci.* **2015**, 33, 371.
- [252] Y. Sun, *Nanoscale* **2010**, 2, 1626.
- [253] M. Mohammed Ali, D. Maddipatla, B. B. Narakathu, A. A. Chliahiawi, S. Emamian, F. Janabi, B. J. Bazuin, M. Z. Atashbar, *Sens. Actuators, A Phys.* **2018**, 274, 109.
- [254] R. Wang, W. Xu, W. Shen, X. Shi, J. Huang, W. Song, *Inorg. Chem. Front.* **2019**, 6, 3119.
- [255] D. Jiang, Y. Wang, B. Li, C. Sun, Z. Wu, H. Yan, L. Xing, S. Qi, Y. Li, H. Liu, W. Xie, X. Wang, T. Ding, Z. Guo, *Macromol. Mater. Eng.* **2019**, 304, 1900074.
- [256] Y. H. Wang, A. Huang, H. Xie, J. Z. Liu, Y. Z. Zhao, J. Z. Li, *J. Mater. Sci. Mater. Electron.* **2017**, 28, 10.
- [257] J. Zhong, Z. Zhou, J. Zhang, J. Tang, P. Wu, Y. Wang, *J. Mater. Sci. Mater. Electron.* **2020**, 31, 15038.

- [258] S. Coskun, B. Aksoy, H. E. Unalan, *Cryst. Growth Des.* **2011**, 11, 4963.
- [259] X. L. Liu, S. Han, S. B. Zhang, S. S. Zhou, N. Jiao, H. Y. Zhao, J. Li, *Mater. Res. Express* **2020**, 7, 095001.
- [260] J. Gao, R. Qu, B. Tang, C. Wang, Q. Ma, C. Sun, *J. Nanoparticle Res.* **2011**, 13, 5289.
- [261] Y. Lu, J. Jiang, S. Yoon, K. S. Kim, J. H. Kim, S. Park, S. H. Kim, L. Piao, *ACS Appl. Mater. Interfaces* **2018**, 10, 2093.
- [262] J. Y. Park, W. J. Lee, B. S. Kwon, S. Y. Nam, S. H. Choa, *Microelectron. Eng.* **2018**, 199, 16.
- [263] P. Maróti, B. Kocsis, A. Ferencz, M. Nyitrai, D. Lőrinczy, *J. Therm. Anal. Calorim.* **2020**, 139, 367.
- [264] A. Basir, M. I. Khan, in *2016 3rd Int. Conf. Electr. Eng. Inf. Commun. Technol. ICEEICT 2016*, Institute of Electrical and Electronics Engineers Inc., Dhaka, Bangladesh **2017**.
- [265] S. S. Sharifabad, H. A. Derazkola, M. Esfandyar, M. Elyasi, F. Khodabakhshi, *J. Mech. Behav. Biomed. Mater.* **2021**, 118, 104455.
- [266] A. Shayesteh Zeraati, A. Mende Anjaneyalu, S. P. Pawar, A. Abouelmagd, U. Sundararaj, *Polym. Eng. Sci.* **2021**, 61, 959.
- [267] Z. Lei, Z. Chen, H. Peng, Y. Shen, W. Feng, Y. Liu, Z. Zhang, Y. Chen, *J. Mater. Sci.* **2018**, 53, 14495.
- [268] V. H. Castrejón-Sánchez, A. C. Solis, R. López, C. Encarnación-Gomez, F. M. Morales, O. S. Vargas, J. E. Mastache-Mastache, G. V. Sánchez, *Mater. Res. Express* **2019**, 6, 075909.
- [269] N. Lazarus, S. S. Bedair, S. H. Hawasli, M. J. Kim, B. J. Wiley, G. L. Smith, *Adv. Mater. Technol.* **2019**, 4, 1900126.
- [270] P. F. Flowers, C. Reyes, S. Ye, M. J. Kim, B. J. Wiley, *Addit. Manuf.* **2017**, 18, 156.
- [271] C. Cheng, J. Li, T. Shi, X. Yu, J. Fan, G. Liao, X. Li, S. Cheng, Y. Zhong, Z. Tang, *J. Mater. Sci. Mater. Electron.* **2017**, 28, 13556.
- [272] N. Toshima, T. Yonezawa, *New J. Chem.* **1998**, 22, 1179.
- [273] M. Grouchko, A. Kamyshny, S. Magdassi, *J. Mater. Chem.* **2009**, 19, 3057.
- [274] M. A. Cruz, S. Ye, M. J. Kim, C. Reyes, F. Yang, P. F. Flowers, B. J. Wiley, *Part. Part. Syst. Charact.* **2018**, 35, 1700385.
- [275] T. G. Kim, H. J. Park, K. Woo, S. Jeong, Y. Choi, S. Y. Lee, *ACS Appl. Mater. Interfaces* **2018**, 10, 1059.
- [276] C. Kim, G. Lee, C. Rhee, M. Lee, *Nanoscale* **2015**, 7, 6627.
- [277] Y. Z. Zhang, Y. Wang, Q. Jiang, J. K. El-Demellawi, H. Kim, H. N. Alshareef, *Adv. Mater.* **2020**, 32, 1908486.
- [278] M. Alhabeb, K. Maleski, B. Anasori, P. Lelyukh, L. Clark, S. Sin, Y. Gogotsi, *Chem. Mater.* **2017**, 29, 7633.
- [279] K. P. Akshay Kumar, K. Ghosh, O. Alduhaish, M. Pumera, *Electrochem. commun.* **2021**, 122, 106890.
- [280] E. Redondo, M. Pumera, *Electrochem. commun.* **2021**, 124, 106920.
- [281] X. Sheng, Y. Zhao, L. Zhang, X. Lu, *Compos. Sci. Technol.* **2019**, 181, 107710.
- [282] J. Orangi, F. Hamade, V. A. Davis, M. Beidaghi, *ACS Nano* **2020**, 14, 640.
- [283] B. Zazoum, A. Bachri, J. Nayfeh, *Materials* **2021**, 14, 6603.
- [284] L. He, J. Wang, B. Wang, X. Wang, X. Zhou, W. Cai, X. Mu, Y. Hou, Y. Hu, L. Song, *Compos. Part B Eng.* **2019**, 179, 107486.
- [285] R. Han, L. Zheng, G. Li, G. Chen, S. Ma, S. Cai, Y. Li, *ACS Appl. Mater. Interfaces* **2021**, 13, 46738.
- [286] K. Namsheer, C. S. Rout, *RSC Adv.* **2021**, 11, 5659.
- [287] K. Deshmukh, M. Basheer Ahamed, R. R. Deshmukh, S. K. Khadheer Pasha, P. R. Bhagat, K. Chidambaram, in *Biopolymer Composites in Electronics*, Elsevier, Amsterdam **2017**, pp. 27–128.
- [288] M. Dawoud, I. Taha, S. J. Ebeid, *J. Manuf. Process.* **2018**, 35, 337.
- [289] K. A. Thomas, S. Nair, R. Rajeswari, A. V. Ramesh Kumar, V. Natarajan, T. Mukundan, R. John, *Prog. Org. Coatings*, **2015**, 89, 267.
- [290] F.-X. Perrin, C. Oueiny, in *Polyaniline Blends, Composites Nanocomposites*, Elsevier, Amsterdam **2018**, pp. 117–147.
- [291] D. S. Vicentini, G. M. O. Barra, J. R. Bertolino, A. T. N. Pires, *Eur. Polym. J.* **2007**, 43, 4565.
- [292] O. A. Araújo, M. A. De Paoli, *Synth. Met.* **2009**, 159, 1968.
- [293] L. Horta-Romaris, M. J. Abad, M. V. González-Rodríguez, A. Lasagabáster, P. Costa, S. Lanceros-Méndez, *Mater. Des.* **2017**, 114, 288.
- [294] J. Ruiz, B. Gonzalo, J. R. Dios, J. M. Laza, J. L. Vilas, L. M. León, *Adv. Polym. Technol.* **2013**, 32, E180.
- [295] Q. H. Zhang, X. H. Wang, D. J. Chen, X. Bin Jing, *J. Polym. Sci. Part B Polym. Phys.* **2004**, 42, 3750.
- [296] S. K. Dhawan, N. Singh, D. Rodrigues, *Sci. Technol. Adv. Mater.* **2003**, 4, 105.
- [297] S. Koul, R. Chandra, S. K. Dhawan, *Polymer* **2000**, 41, 9305.
- [298] M. Zilberman, G. I. Titelman, A. Siegmman, Y. Haba, M. Narkis, D. Alperstein, *J. Appl. Polym. Sci.* **1997**, 66, 243.
- [299] M. Zilberman, A. Siegmman, M. Narkis, *J. Macromol. Sci. Part B Phys.* **1998**, 37, 301.
- [300] L. W. Shacklette, C. C. Han, M. H. Luly, *Synth. Met.* **1993**, 57, 3532.
- [301] S. Sinha, S. Bhadra, D. Khastgir, *J. Appl. Polym. Sci.* **2009**, 112, 3135.
- [302] T. Jeevananda, Siddaramaiah, V. Annadurai, R. Somashekar, *J. Appl. Polym. Sci.* **2001**, 82, 383.
- [303] H. Ghasemi, U. Sundararaj, *Synth. Met.* **2012**, 162, 1177.
- [304] G. M. O. Barra, M. E. Leyva, B. G. Soares, L. H. Mattoso, M. Sens, *J. Appl. Polym. Sci.* **2001**, 82, 114.
- [305] M. S. Dopico-García, A. Ares, A. Lasagabáster-Latorre, X. García, L. Arboleda, M. J. Abad, *Synth. Met.* **2014**, 189, 193.
- [306] R. K. Paul, C. K. S. Pillai, *J. Appl. Polym. Sci.* **2002**, 84, 1438.
- [307] M. Tian, Y. Wang, L. Qu, S. Zhu, G. Han, X. Zhang, Q. Zhou, M. Du, S. Chi, *Synth. Met.* **2016**, 219, 11.
- [308] T. Sen, S. Mishra, N. G. Shimpi, *RSC Adv.* **2016**, 6, 42196.
- [309] P. Singh, S. K. Shukla, *J. Mater. Sci.* **2020**, 55, 1331.
- [310] J. Prokeš, M. Trchová, D. Hlavatá, J. Stejskal, *Polym. Degrad. Stab.* **2002**, 78, 393.
- [311] W. Xu, Y. Ding, Y. Yu, S. Jiang, L. Chen, H. Hou, *Mater. Lett.* **2017**, 192, 25.
- [312] M. Ginic-Markovic, J. G. Matisons, R. Cervini, G. P. Simon, P. M. Fredericks, *Chem. Mater.* **2006**, 18, 6258.
- [313] Q. Wang, Q. Yao, J. Chang, L. Chen, *J. Mater. Chem.* **2012**, 22, 17612.
- [314] L. Nikzad, M. R. Vaezi, B. Yazdani, *Int. J. Mod. Phys. Conf. Ser.* **2012**, 05, 527.
- [315] A. Kumar, V. Kumar, M. Kumar, K. Awasthi, *Polym. Compos.* **2018**, 39, 3858.
- [316] L. Cui, J. Yu, Y. Lv, G. Li, S. Zhou, *Polym. Compos.* **2013**, 34, 1119.
- [317] K. Dash, N. K. Hota, B. P. Sahoo, *J. Mater. Sci.* **2020**, 55, 12568.
- [318] M. O. Ansari, S. K. Yadav, J. W. Cho, F. Mohammad, *Compos. Part B Eng.* **2013**, 47, 155.
- [319] H. Baniasadi, S. A. Ramazani, S. Mashayekhan, F. Ghaderinezhad, *Synth. Met.* **2014**, 196, 199.
- [320] R.-X. Wang, L.-F. Huang, X.-Y. Tian, *J. Phys. Chem. C* **2012**, 116, 13120.
- [321] A. T. Mane, V. B. Patil, in *Spectroscopy of Polymer Nanocomposites*, William Andrew Publishing, Norwich, New York, United States **2016**, pp. 452–467.
- [322] B. Piro, G. Mattana, S. Zrig, G. Anquetin, N. Battaglini, D. Capitao, A. Maurin, S. Reisberg, *Appl. Sci.* **2018**, 8, 928.
- [323] M. Nishizawa, T. Matsue, I. Uchida, *Sens. Actuators B. Chem.* **1993**, 13, 53.
- [324] S. D. A. S. Ramoa, G. M. O. Barra, C. Merlini, S. Livi, B. G. Soares, A. Pegoretti, *Express Polym. Lett.* **2015**, 9, 945.

- [325] C. Sasso, D. Beneventi, E. Zeno, D. Chaussy, M. Petit-Conil, N. Belgacem, *BioResources* **2011**, 6, 3585.
- [326] M. Kotal, S. K. Srivastava, B. Paramanik, *J. Phys. Chem. C* **2011**, 115, 1496.
- [327] M. C. Bertolini, S. D. A. S. Ramoa, C. Merlini, G. M. O. Barra, B. G. Soares, A. Pegoretti, *Front. Mater.* **2020**, 7, 174.
- [328] C. Yang, P. Liu, T. Wang, *ACS Appl. Mater. Interfaces* **2011**, 3, 1109.
- [329] A. M. dos Santos, C. Merlini, S. D. A. S. Ramôa, G. M. O. Barra, *Polym. Compos.* **2020**, 41, 2003.
- [330] S. J. Peighambaroust, B. Pourabbas, *J. Appl. Polym. Sci.* **2007**, 106, 697.
- [331] N. Debnath, V. Panwar, S. Bag, M. Saha, K. Pal, *J. Appl. Polym. Sci.* **2015**, 132, 42577.
- [332] J. K. Avlyanov, S. Dahman, *ACS Symp. Ser.* **1999**, 735, 270.
- [333] P. Gahlout, V. Choudhary, *Synth. Met.* **2020**, 266, 116414.
- [334] V. B. Mohan, K. Jayaraman, D. Bhattacharyya, *Int. J. Smart Nano Mater.* **2016**, 7, 179.
- [335] M. C. Bertolini, S. Dul, G. M. O. Barra, A. Pegoretti, *J. Appl. Polym. Sci.* **2021**, 138, 50305.
- [336] A. Elkaseer, S. Schneider, S. G. Scholz, *Appl. Sci.* **2020**, 10, 2899.
- [337] J. T. W. Yeow, Y. Wang, *J. Sens.* **2009**, 493904.
- [338] M. A. Abd El-Ghaffar, A. M. Youssef, A. A. Abd El-Hakim, *Arab. J. Chem.* **2015**, 8, 771.
- [339] M. A. C. Mazzeu, L. K. Faria, A. D. M. Cardoso, A. M. Gama, M. R. Baldan, E. S. Gonçalves, *J. Aerosp. Technol. Manag.* **2017**, 9, 39.
- [340] R. Guo, Z. Ren, H. Bi, M. Xu, L. Cai, *Polymers* **2019**, 11, 549.
- [341] S. Dul, L. Fambri, C. Merlini, G. M. O. Barra, M. Bersani, L. Vanzetti, A. Pegoretti, *Polym. Compos.* **2019**, 40, E285.
- [342] A. R. Blythe, *Polym. Test.* **1984**, 4, 195.
- [343] L. K. Massey, in *Permeability Properties of Plastics and Elastomers*, Elsevier Science, Amsterdam, Netherlands **2003**, pp. 315–316.
- [344] *Electrical Properties of Plastics*, <https://www.professionalplastics.com/professionalplastics/ElectricalPropertiesofPlastics.pdf>, **2019**.
- [345] *PVDF Material Properties Data Sheet*, <https://www.allplastics.com.au/engineering-plastics/pvdf>, **2021**.
- [346] P. C. Ma, N. A. Siddiqui, G. Marom, J. K. Kim, *Compos. Part A Appl. Sci. Manuf.* **2010**, 41, 1345.
- [347] E. Y. Choi, S. W. Kim, J. Y. Lee, J. H. Ha, C. K. Kim, *Polym.* **2017**, 41, 490.
- [348] Q. Jing, J. Y. Law, L. P. Tan, V. V. Silberschmidt, L. Li, Z. L. Dong, *Compos. Part A Appl. Sci. Manuf.* **2015**, 70, 8.
- [349] K. Wongtimnoi, B. Guiffard, A. Bogner-Van de Moortèle, L. Seveyrat, J. Y. Cavaillé, *Compos. Sci. Technol.* **2013**, 85, 23.
- [350] A. K. Barick, D. K. Tripathy, *Mater. Sci. Eng. B* **2011**, 176, 1435.
- [351] Y. H. Zhan, R. Patel, M. Lavorgna, F. Piscitelli, A. Khan, H. S. Xia, H. Benkreira, P. Coates, *Plast. Rubber Compos.* **2010**, 39, 400.
- [352] G. Urtekin, A. Aytac, *J. Polym. Res.* **2021**, 28, 1.
- [353] E. Y. Choi, J. U. Nam, S. H. Hong, C. K. Kim, *Macromol. Res.* **2018**, 26, 107.
- [354] T. Bai, B. Zhu, H. Liu, Y. Wang, G. Song, C. Liu, C. Shen, *Int. J. Biol. Macromol.* **2020**, 151, 628.
- [355] T. Vu, P. Nikaeen, M. Akobi, D. Depan, W. Chirdon, *Polym. Adv. Technol.* **2020**, 31, 415.
- [356] Y. Lan, H. Liu, X. Cao, S. Zhao, K. Dai, X. Yan, G. Zheng, C. Liu, C. Shen, Z. Guo, *Polymer* **2016**, 97, 11.
- [357] F. Korkees, A. Aldrees, I. Barsoum, D. Alshammari, *J. Compos. Mater.* **2021**, 55, 2211.
- [358] R. Guo, Z. Ren, X. Jia, H. Bi, H. Yang, T. Ji, M. Xu, L. Cai, *Polymers* **2019**, 11, 1589.
- [359] H. Baniyadi, S. Borandeh, J. Seppälä, *Macromol. Mater. Eng.* **2021**, 306, 2100255.
- [360] O. J. Botlhoko, S. S. Ray, J. Ramontja, *Eur. Polym. J.* **2018**, 102, 130.
- [361] C. Gao, S. Zhang, F. Wang, B. Wen, C. Han, Y. Ding, M. Yang, *ACS Appl. Mater. Interfaces* **2014**, 6, 12252.
- [362] U. O. Uyor, A. P. I. Popoola, O. M. Popoola, V. S. Aigbodion, *J. Test. Eval.* **2019**, 47, 2681.
- [363] N. Maity, A. Mandal, K. Roy, A. K. Nandi, *J. Polym. Sci. Part B Polym. Phys.* **2019**, 57, 189.
- [364] C. Wu, X. Huang, G. Wang, X. Wu, K. Yang, S. Li, P. Jiang, *J. Mater. Chem.* **2012**, 22, 7010.



**Dejana Pejak Simunec** is a postdoctorate at CSIRO working at the Fused Filament Fabrication Facility (4F) in the design and production of composite materials for additive manufacturing. She received her Ph.D. at Royal Melbourne Institute of Technology with a dissertation on the fused filament fabrication of advanced and high-performance polymers. She is currently developing custom-made FFF filaments to produce self-folding structures, metamaterials, and multifunctional parts imbued with properties such as conductivity and flexibility.



**Antonella Sola** is currently acting as science leader in active materials at the Commonwealth Scientific and Industrial Research Organization (CSIRO, Clayton, VIC). She is driving innovation in additive manufacturing and processing technologies for the development of new materials and systems with improved functionalities. At CSIRO, Antonella is leading the Fused Filament Fabrication Facility (4F), a dedicated center for the design and production of bespoke feedstock materials for 3D printing by fused filament fabrication. She has published in more than 100 papers and presented at numerous international conferences, with contributions regarding composite materials, biomaterials, advanced coatings, and additive manufacturing.